STUDIES IN INTERPLANETARY PARTICLES

F. L. WHIPPLE, R. B. SOUTHWORTH and C. S. NILSSON

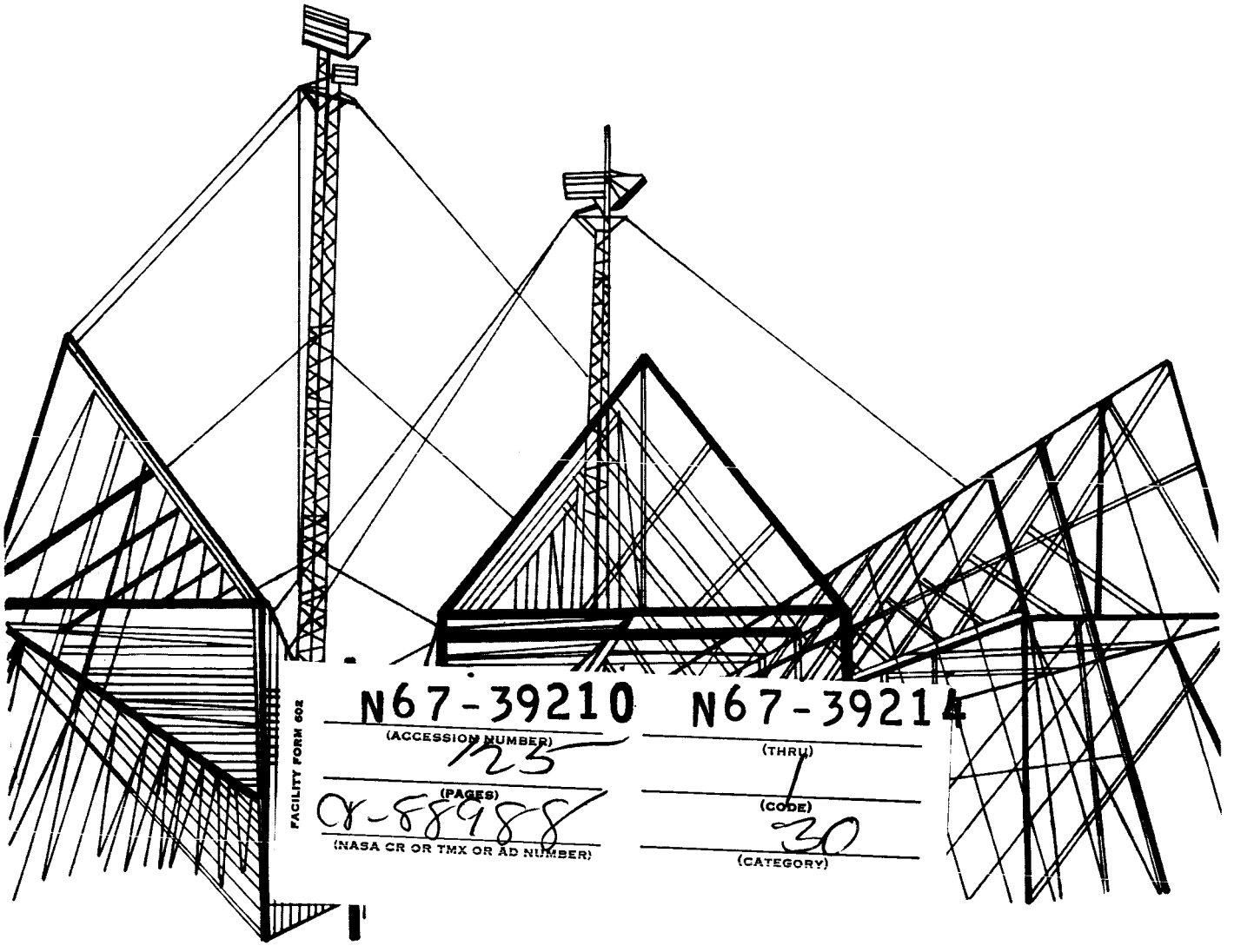

Smithsonian Astrophysical Observatory
SPECIAL REPORT 239

ON MAINTAINING THE METEORITIC COMPLEX

Fred L. Whipple

ABSTRACT

The meteoritic influx on the earth is derived from measurements of penetration of space vehicles, radio and photographic meteors, meteorite falls, Apollo asteroids, lunar craters, and comets. The total flux is some 2×10^{-16} g cm^{-2} sec^{-1} on the surface of a corresponding nongravitating sphere. Such a cloud is self-destructive by collisions. It requires some 10 times the continuous contribution that the Poynting-Robertson effect alone would demand to maintain the zodiacal light and cloud, i. e., some 10 tons per second for quasi-equilibrium.

This observational model is consistent with the etching rates observed on stone and iron meteorites and on photographic meteoroids. Various observational and theoretical facts indicate that the cloud up to masses of about 10^5 g is maintained by "live" comets. "Half-baked" asteroids, however, may compete with comets in contributing to the brightest fireballs. The stony meteorites may be maintained by collisional spallation from earth-crossing asteroids induced by smaller bodies, the Apollo asteroids being derived from the asteroid belt by the gravitational effects of Mars.

The cometary meteoritic complex of smaller particles, carrying most of the mass, has a mean lifetime of some 1.7×10^5 yr. Certain puzzles remain in the orbital properties of the Apollo asteroids and of iron and stone meteorites.

Research in Space Science
SAO Special Report No. 239

STUDIES IN INTERPLANETARY PARTICLES

Fred L. Whipple
Richard B. Southworth
Carl S. Nilsson

May 31, 1967

Smithsonian Institution
Astrophysical Observatory
Cambridge, Massachusetts, 02138

TABLE OF CONTENTS

ON MAINTAINING THE METEORITIC COMPLEX

Fred L. Whipple

1. INTRODUCTION

This paper concerns the "ecology" of the meteoritic material in the solar system, and involves its immediate origin from larger bodies and some details of its dissipation. To date there is no evidence for any meteoritic matter with an immediate origin beyond the gravitational field of the sun, nor is there an indication of any accumulative processes on smaller bodies. The meteoritic complex is self-destructive.

Comets provide a large known source of this small material. We shall accept the icy comet model (Whipple, 1950), in which the comets produce meteoritic material intrinsically by solar radiation, which, via sublimation, releases gas, dust, and finite-sized, low-density meteoritic material into the planetary region of the solar system. Undoubtedly, comets can produce material extrinsically by collisional spallation. It is not yet clear whether larger comets that have somehow attained an aphelion distance within the orbit of Jupiter can, indeed, leave finite inactive nuclei indistinguishable from the smaller asteroids. Öpik (1963, 1966) has strongly supported this suggestion. The possibility is so extremely important from an evolutionary point of view that it needs to be demonstrated as true or false, not lightly accepted as probable. It specifies important factors and processes involved in the original development of the cometary nuclei themselves, presumably

This research has been supported in part by grants NSR-09-015-033 from the U. S. National Aeronautics and Space Administration, AF 19(628)3248 from the U. S. Air Force Cambridge Research Laboratories, and NAS 9-4873 from the NASA Manned Space Flight Center, Houston, Texas.

in the very early stages of solar system development. In other words, we should make a special effort to demonstrate either the existence or the absence of many persistent, inert cometary nuclei.

The asteroids as well as comets are important in the meteoritic complex, acting as a source of smaller bodies, presumably the meteorites, by means of collisional spallation. We have no direct knowledge that the larger satellites or Mercury may not make intrinsic contributions to the meteoritic complex by means of volcanic-type eruptions. Their contributions by collisional spallation are neglected in this discussion, although the moon may be a minor contributor.

Among the outer satellites without atmospheres, the asteroids and the comets, all significant physical processes known to date are dissipative. We are concerned with activities within the orbit of Saturn, and our attention will be concentrated mainly within that of Jupiter. Besides the intrinsic ejection processes and collisional spallation mentioned above, other dissipative processes include the elimination from the system by gravitation, the capture by bodies with atmospheres, and the reduction to gas by various processes, including close approaches to the sun. There is every reason to believe that the solar wind will eliminate gases almost immediately from any part of the inner solar system, while solar light pressure will remove most small particles below a certain size.

This paper will first treat in some detail the numerous dissipative processes. Then follow a quick summary of the factual knowledge concerning the distribution of the meteoritic complex and a detailed discussion of the process rates insofar as they can be ascertained at the present time.

2. DISSIPATIVE PROCESSES OF THE INNER SOLAR SYSTEM

2.1 Solar Radiation

2.1.1 Direct light pressure

Light pressure in the sun on a spherical particle of radius s and density ρ exceeds the solar gravitational attraction when

$$\rho s < 5.8 \times 10^{-5} \theta \text{ cgs} \quad , \tag{1}$$

where θ is the fraction of the incident solar radiation effective in transferring momentum to the particle.

Although equation (1) is satisfied only for submicron-sized particles of reasonable density and the value of θ is highly dependent upon their electrical characteristics, the process is responsible for eliminating considerably larger particles when they are injected into fairly eccentric orbits, e.g., comet orbits. A slight reduction in the effective gravity because of light pressure throws them into hyperbolic orbits. This matter has been discussed by Harwit (1963), who shows that the smallest particles remaining in the solar system after ejection at low velocities from Comet Encke would have radii of the order of a few microns, and for Comet Halley a few tens of microns. Thus, we should expect contributions from comets to be confined to those in short-period orbits and for particles greater than a few microns. The comets of longer period, for other reasons (Whipple, 1955), should not be able to contribute significantly to the zodiacal light. Because of the effect of light pressure it is not surprising that the zodiacal light and the influx rate of particles on the earth become less significant at low masses of the order of 10^{-10} to 10^{-12} g, as is shown, for example, in Figure 1 and discussed by Southworth (1964) and Biermann (1967).

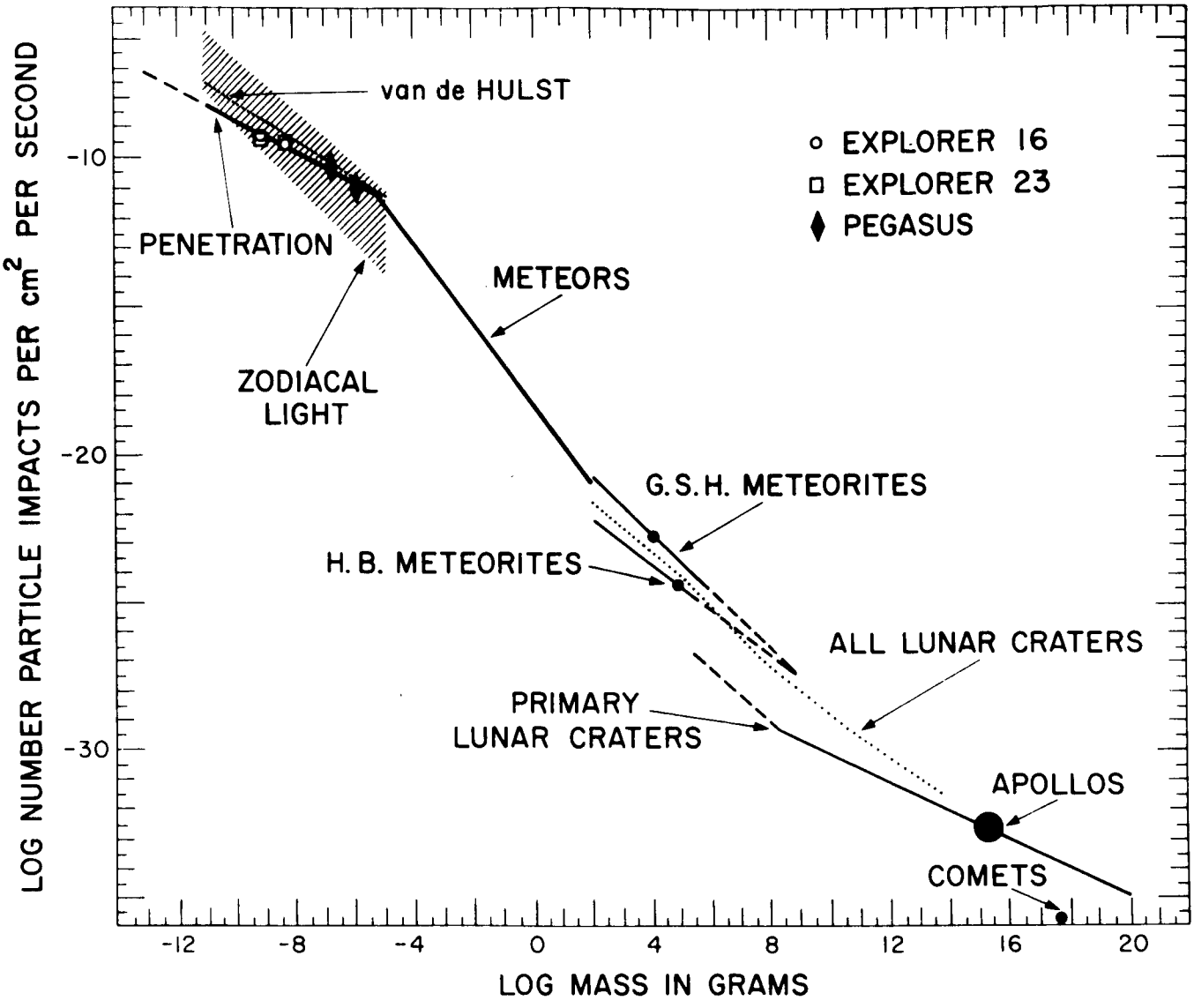

Figure 1. Cumulative impact rates of meteoritic material on a sphere near the earth's orbit.

2.1.2 The Poynting-Robertson effect

Because of the momentum of light, its reradiation or general reflection from a particle in orbit about the sun produces a retarding force on the motion, as described by Robertson (1937) in relativistic terms, based upon an earlier suggestion by Poynting. Thus, the Poynting-Robertson effect (P-R effect) causes a general reduction in the eccentricity and major axes of small bodies in orbit about the sun until, other circumstances permitting, they spiral near the sun to sublimate. The time of spiraling into the sun for a black, or perfectly reflecting, spherical particle of radius s and density ρ in an orbit of perihelion distance q (in a.u.) is given by the following equation:

$$\text{spiral time} = C(e)\, \rho s\, q^2 \times 10^7 \text{ yr} \quad , \tag{2}$$

where the factor $C(e)$ depends solely upon the orbital eccentricity e. This coefficient is 0.70 for a circular orbit, 1.9 for $e = 0.5$, 7.3 for $e = 0.9$, and 28.9 for $e = 0.99$ (see Wyatt and Whipple, 1950). Öpik (1963) has shown that for earth-crossing orbits the mean lifetime by gravitational perturbations is of the order of 10^8 yr, and for Jupiter it is 10^6 yr. Hence, the P-R effect can be significant only for particles of dimension ≤ 10 cm for earth-crossing orbits, and $< 10^{-1}$ cm for Jupiter-crossing orbits.

2.1.3 Charge on particles

Solar radiation on an isolated particle can, by the photoelectric effect, impart a positive charge of a few electron volts (see Belton, 1967; Rhee, 1967; Singer, 1967). A charged particle then becomes susceptible to other physical forces that may interact with its electrical charge.

2.1.4 Direct material sublimation

Near the sun, sublimation of meteoritic material becomes significant (see Kaiser, 1967).

2.2 The Solar Wind

2.2.1 Sputtering

Wehner, Kenknight, and Rosenburg (1963) show that a solar wind flux of 2×10^8 cm^{-2} sec^{-1} protons, moving with a velocity of 600 km sec^{-1} with a normal solar component of heavier ions, will produce a radial sputtering erosion of 0.4 Å yr^{-1} for iron or stony meteorite surfaces, a smaller effect than earlier estimates (Whipple, 1955). We can evaluate the significance of sputtering by comparing its erosion rate to the P-R spiraling rate. Let us adopt the Allen (1963) approximation for the P-R effect [$C(e)\, q^2 = 0.7\, aq$ in equation (2)] with q taken as constant. We then derive for a sputtering rate of 0.4 Å yr^{-1} in s the relation:

$$\frac{ds}{s} \cong \frac{da}{a} \cdot 0.10 \frac{(1 - e)}{(1 - e^2)^{1/2}} \quad . \tag{3}$$

For e = 0 the sputtering rate of loss in radius is 0.10, the rate of loss in the semimajor axis, while for e = 0.5, 0.99, and $(1 - \delta)$ the factor is reduced to 0.06, 0.007, and $0.07\, \delta^{1/2}$, respectively ($\delta << 1$). Hence, sputtering is not relatively important in small-particle ecology.

2.2.2 An injection process

The solar wind makes a minor contribution of a nondissipative character by injecting heavier atoms into the matrices of solids in space. Because of the relative dearth of heavier atoms compared to hydrogen, this contribution is small compared to the loss produced at the surface through sputtering. Laboratory experiments of such trapping have been conducted by Bühler, Geiss, Meister, Eberhardt, Huneke, and Signer (1966).

2.2.3 Pressure on ions in space

The solar wind by direct interaction and charge exchange with atoms or molecules in space, coupled with the collisionless shock wave of magneto-hydrodynamic origin, can help produce and can force back ions in cometary Type-I tails. Since no free atom or molecule within planetary distances can escape eventual ionization by solar radiation, the solar wind acts as a cleaning agent to eliminate all free gas from within the inner solar system.

2.2.4 Pressure on meteoritic particles

The solar wind, because of its relatively low velocity with respect to light, carries a small radial pressure, about 10^{-3} of that due to solar radiation. The pressure effect of the solar wind can be neglected.

2.2.5 Pseudo Poynting-Robertson effect

For a proton flux of 2×10^{8} protons cm^{-2} sec^{-1} at 1 a.u. radially from the sun, the mass encountering a surface is 0.22 of that contributed by solar radiation. For total bulk interception and isotropic reradiation or ejection, the pseudo P-R effect by the average solar wind is then 0.22 of that induced by solar radiation. Hence, the solar wind increases the normal P-R effect by 22%, or possibly more for charged particles or those for which diffraction reduces the effective area for radiation (see Whipple, 1955, and Biermann, 1967).

2.2.6 Magnetic-field effects

The existence of appreciable magnetic fields carried by the solar wind and solar storms may produce significant forces on small isolated particles positively charged by solar photoionization. Parker (1964) has made this suggestion, and predictions of such effects on the motions of small particles have been made by Belton and by Singer (1967). For extremely small particles ($\leq 1\mu$), there are a number of dissipative effects involving

electric charge and electromagnetic effects. We shall not consider them here because the predictions remain difficult and uncertain.

2.3 Miscellaneous Effects

Öpik (1951, 1956) has discussed a number of dissipative effects on small particles in space, including some depending upon rotation. Rotation can be set up by particle collisions and by solar radiation for asymmetrical bodies. In turn, the rotation can make possible forces normal to the radius vector by interaction with particles and radiation. The latter is called by Öpik the Yarkovsky effect. Also, Öpik shows that a rapid rotation rate, like too great an electrical charge, may explosively destroy a small particle, especially if the particle is of low density and of weak structural strength.

Since no detailed theories suitable for direct application are available for these various processes, they will be ignored in this paper, although it is not impossible that they may be significant in space.

2.4 Collisional Effects

2.4.1 Meteoritic erosion in space

Direct evidence for erosion of stony meteorites in space can be deduced from the low exposure ages, less than some 5×10^7 yr, obtained by measurements of short-lived radioactive elements produced by cosmic-ray spallation. The concept was first presented by Whipple and Fireman (1959) for an iron meteorite. Cosmic-ray spallation can produce stable isotopes such as Ar^{38} and radioactive isotopes such as Ar^{39} (half-life order of $\sim$ 300 yr) from heavier atoms in meteorites; the radioactive isotopes measure the current spallation rate due to cosmic rays, and the stable isotopes the total accumulation. Combined, the rate and the accumulation lead to a calculated exposure age. At first such an exposure age was interpreted as the interval since the meteorite broke off from a much larger body in which it had been protected from cosmic rays. On the erosion hypothesis the

earlier greater size of the meteorite reduced the accumulation rate of the stable isotope in the earlier stages and lead to a shorter measured exposure age. An alternative explanation can be made by assuming that the cosmic-ray intensity increases with time.

Fireman and DeFelice (1961) suggested that stones exhibit much shorter exposure ages ($< 5 \times 10^7$ yr) than do irons because of their greater friability and brittleness; stones are thus eroded more rapidly than irons by collisions with interstellar dust. This thesis has been supported strongly by Fisher (1966). Whipple (1963) noted that erosion is a likely cause of the relatively short lives deduced for bright photographic meteors. Nearly half of these bodies move in identifiable streams, and those with aphelia within the orbit of Jupiter show no alignment of their lines of apsides with that of Jupiter, as is observed for the asteroids and might be expected for bodies with lifetimes greater than 10^4 to 10^5 yr. Perturbations should also cause these orbits to lose their identification with streams over periods of the order of 10^4 yr. Hence, it appears that cometary meteoroids are eroded at a rate of the order of a micron per year in radius.

These conclusions are summarized in Table 1. I assume that the encountering small mass knocks out 200 times its mass in iron, 1000 times in stone, and 3200 times in cometary meteoroids. We can fairly assume that the erosion is caused by impacts with dust particles within Jupiter's orbit moving at an inclination of some 20° to the plane of the ecliptic (see, e.g., Southworth, 1967). At a mean collisional speed of some 10 km sec^{-1} for average encounters in this region, the mean density of small particles ($< 10^2$ g) is of the order of 2×10^{-22} g cm^{-3}, and provides an influx rate of some 1.0×10^{-16} g cm^{-2} sec^{-1} on the surface of a nongravitating sphere. At the earth the space density and influx rates should exceed the average by a small factor. Presumably this dust is the material that produces the scattering and diffraction of sunlight observed in the zodiacal light and the Fraunhofer corona.

Table 1. Erosion in space

	Irons	Stones	Cometary meteors
Exposure age (yr)	$\sim 5 \times 10^{8}$	$< 5 \times 10^{7}$	$\sim 10^{4}$ *
Etching rate (cm yr^{-1})	5×10^{-8}	5×10^{-7}	$2.3/\rho \times 10^{-5}$ **
Etching rate (g cm^{-2} sec^{-1})	1.3×10^{-14}	5×10^{-14}	7×10^{-13}
Impact rate (g cm^{-2} sec^{-1})	6×10^{-17}	5×10^{-17}	20×10^{-17}

*average lifetime
**ρ = density

It must be noted that the calculated and critical erosion rate for stones is proved unless one of two assumptions is made: 1) that no stony meteorites were broken to cross the earth's orbit prior to 50 million years ago, or 2) that cosmic radiation has increased markedly in this period of time.

2.4.2 Larger body collision

Grinding effects due to collisional spallation must occur among the larger bodies of the asteroid belt, including the Mars-crossing and the earth-crossing asteroids. Piotrowski (1953) has shown that within the asteroid belt the continuous grinding should lead to a distribution of particle size giving a population index of S = 2.

The population index S applies to a distribution of particle sizes following an inverse power law of the dimension, where the cumulative number larger than a given radius S, area A, or mass m is given in the forms s^{-S}, $A^{-S/2}$, or $m^{-S/3}$. The distribution of the observable asteroids (Kuiper, Fujita, Gehrels, Groeneveld, Kent, van Biesbroeck and van Houten, 1958) indicates that Piotrowski's Law, although not completely proved theoretically, is not far from observation. For a population index S = 2, the integrated area

of bodies in any logarithmic step in dimension is constant, so that integration to diffraction-limited small-particle sizes does not lead to excessive surface area. Hawkins (1960) shows that this comminution law in ball mills for rock crushing begins at first breakage with S = 2, and proceeds to approximately S = 3 for continued crushing.

In hypervelocity-impact breakage, Gault, Shoemaker, and Moore (1963) measure the distribution of particle sizes resulting for a basalt target. They find that the ratio of the total mass of the crater material to that of the projectile at 14.1 km sec^{-1} is $\phi \approx 10^3$; the inverse ratio of the largest fragment to the total mass ejected is approximately $\zeta = 27$ and a population index $S \approx 2.4$ for the broken fragments. They find that various losses amount to some 30%, due mostly to evaporation. Since these measures are the only ones available to the writer, they will be adopted as applicable to collisional spallation by hypervelocity impact on stony meteoritic bodies in space. Since it appears quite possible that the meteorites falling on the earth have been dislodged from earth-crossing asteroids by hypervelocity impacts, this possibility will be considered in subsequent discussions.

That the moon contributes appreciably to the meteoritic complex in space is doubtful. We (Jacchia and Whipple, 1961) find no significant evidence for a direct lunar contribution to the photographic meteors. On the other hand, Arnold's (1965a, b) discussion of orbital changes produced for such particles by earth perturbations makes a definitive answer somewhat less clear-cut until more precise orbits have been determined for meteorites. Unless more convincing evidence is accumulated, I prefer to ignore this probably small source of material.

2.5 Gravitational Effects

Öpik (1963) has developed a theory showing the gravitational effects that a planet exerts on the orbits of bodies crossing the orbit of the planet in question. Close approaches produce large changes in the orbital elements, which can result in ejection or the shifting of the orbits to cross those of

other planets. Captures by the planets or by the sun are other possible endings to this stochastic process. For objects in orbits crossing those of the earth or Venus, he finds a mean life of the order of 1.0×10^8 yr, which usually results in capture. For Mars, the corresponding mean life is considerably larger, some 6×10^9 yr, again usually resulting in capture; this means that objects in Mars-crossing orbits have not been drastically reduced in number by Mars since the formation of the solar system, some 4.7×10^9 yr ago. For earth-crossing orbits, Arnold (1965a,b) has demonstrated by Monte Carlo calculations the validity of Öpik's theory. For Jupiter, the mean life is of the order of 10^6 yr and is quite likely to result in elimination from the system.

Öpik further shows that objects in purely Mars-crossing orbits have a finite probability of being moved into orbits crossing that of the earth. To maintain a population in earth-crossing orbits with a mean life of 10^8 yr, Öpik finds that some 300 times that many objects must continuously exist in orbits that cross only the orbit of Mars.

It is generally recognized that the comets of short periods (less than 100 yr) are captured from highly eccentric, randomly inclined orbits by planetary perturbations, primarily by Jupiter. These perturbations lead to direct-moving orbits with mean inclinations of the order of 30° to Jupiter's plane of motion; the aphelia tend to be concentrated near and beyond Jupiter's orbit.

3. THE APOLLO ASTEROIDS, COMETS, AND LUNAR CRATERS

3.1 The Apollo Asteroids

To form any judgment as to the asteroidal or cometary origin of the earth-crossing or Apollo asteroids, we must first estimate their numbers. Öpik (1963), on the basis of observational circumstances, estimates 39 of diameter exceeding 1.0 km. Whipple (1966a) notes that none of the 8 discovered Apollo asteroids has been rediscovered by chance. This leads to the probability of 0.50 that the total number does not exceed 43, and 0.75 that there are fewer than 100 in all. Here I shall assume that there are 50 Apollo asteroids of absolute magnitude < 18.2 (apparent magnitude at the hypothetical distances of 1 a.u. from both sun and earth).

The masses of small asteroids can be estimated only from their magnitudes by assuming both albedos and mean specific densities. I adopt with Kuiper et al. (1958) the lunar Bond albedo of 0.07 and a density of 3.5 g cm^{-3}, leading to a radius of 10 km for an absolute magnitude of 12.0, and to a radius of 0.58 km and mass of $10^{15.45}$ g for the lower mass limit of the 50 assumed Apollo asteroids. Enormous uncertainty lies in these values because there are no measures whatsoever for the albedos of small asteroids or the nuclei of small comets. The albedo might lie in the range from 0.03 to 0.30, producing a possible uncertainty in radius by a factor of 3, or in mass by a factor of 30. Possibly the albedo is underestimated because darkening of the surface must occur by solar wind ions. No darkened particles knocked off a small asteroid by collision can be recovered, as is usually the case for the moon. Hence, the darkening process may be less pronounced than for the moon.

Figure 1 depicts the influx rate on the surface of a gravitationless sphere in an earth-like orbit for the assumed 50 Apollo asteroids of mass > $10^{15.45}$ g with an assumed mean life for earth crossing of 10^{8} yr

and a mean encounter velocity of 15 km sec^{-1} (19 km sec^{-1} on the earth). The cumulative influx rate for masses exceeding $10^{15.45}$ g is $10^{-32.7}$ cm^{-2} sec^{-1}. The population index is not well enough known for these objects to provide a flux-mass curve, although Öpik (1963) estimates S = 2.7.

To conclude that the Mars perturbations on Mars-crossing asteroids cannot produce enough Apollo asteroids to maintain the quasi-equilibrium numbers, Öpik extrapolates the observed number of much larger Mars-crossing asteroids to the small asteroids. At Mars, the observations are probably complete to a diameter of 10 to 30 km. Öpik assumes S = 1.6 ($m^{-0.53}$ law) to give the extrapolation in the third row of Table 2. At diameter > 1.05 km, some 300 × 50 = 15,000 Mars-crossing asteroids are required. Table 2 shows the extrapolation for S = 2.0 ($m^{-2/3}$ law in line 4) and for S = 2.4 ($m^{-0.8}$ law in line 5). Kuiper et al.(1958) find 1.6 < S < 3.0 for larger asteroids. At S = 2.7, as assumed by Öpik for the Apollo asteroids, a more than adequate number would be provided. At S = 2, perhaps the best present estimate available, the observed and calculated numbers are in fair agreement.

Table 2. Distribution of Mars asteroids

Minimum diameter (km)	>68	34	17	8.5	4.2	2.1	1.05	0.52
	Cumulative number							
Observed number	1	5	11	22	31	32	33	34
Öpik $m^{-0.53}$	1	5	15	45	135	405	1215	3645
$m^{-2/3}$ law	1	4	16	64	256	1024	4096	16400
$m^{-0.8}$ law	1	5	28	147	776	4100	2×10^4	1×10^5

On the basis of these considerations alone I do not feel that it is necessary to assume that old inactive cometary nuclei must be postulated to supply the observed Apollo asteroids. Other aspects of the problem will be taken up in later sections.

3.2 Cometary Nuclei

The basis for the point comets in Figure 1, the cumulative flux rate for cometary nuclei, has been presented previously (Whipple, 1966a). The evaluation is highly uncertain. I adopt a total rate of 1/3 comet yr^{-1} apparitions of comets with perihelion distance ≤ 1 a.u. and absolute magnitude $H \leq 6.0$ (H = apparent magnitude at 1 a.u. from earth and sun on the basis of an inverse-square law of brightness variation from the earth and an inverse-fourth law from the sun). The corresponding mass is calculated by the relation

$$\log \text{mass} = 21.34 - 0.6\,H \text{ (cgs)} \quad , \tag{4}$$

based on Öpik's (1963) relation for a specific density of 1.3 g cm^{-3}. The rate of influx is based on two crossings per apparition of a comet on a sphere of area 2π (a.u.)^2.

3.3 Lunar Craters

The moon is a "proving ground" for natural interplanetary missiles. The distribution of primary lunar craters (Figure 1) has become available from the remarkable Ranger photographs made by the U.S. National Aeronautics and Space Administration and the Jet Propulsion Laboratory. Here the measures and calculations by Kuiper, Strom, and LePoole (1966) lead to the cumulative number N, corresponding to impacting masses exceeding m grams given by

$$\log N = \sim 25.14 - 0.49 \log m \text{ (cgs)} \quad , \tag{5}$$

on the lunar maria for $m > 10^{8.3}$ g (Figure 1). I assume here an age of 4×10^9 yr for the impacting interval. Kuiper et al. (1958) find a curve for $m < 10^{8.3}$ g with about twice the above slope. Below what mass or crater

size overlapping and destructive crater effects predominate is a matter of opinion, although $m = 10^{8.3}$ g is suggested by the data. A much larger limiting mass is possible.

The dotted curve labeled "All Lunar Craters" in Figure 1 is based on Shoemaker's (1965) crater counts on Ranger 7 photographs of Mars Cognitum, and on Shoemaker, Hackman, and Eggleton's (1961) observation that for high-energy terrestrial explosion craters the crater diameter and explosive energy are fairly well connected by the relation

$$\text{crater diameter} = 0.00230\ W^{1/3}\ (\text{cgs}) \quad , \tag{6}$$

where W is the kinetic energy at a velocity of 15 km sec^{-1}. The resultant cumulative frequency distribution for all craters is

$$\log N = -23.3 - 0.6 \log m\ (\text{cgs}) \quad . \tag{7}$$

The apparently perfect agreement in Figure 1 between the calculated impact rates for lunar craters and the Apollo asteroids is, of course, fortuitous. Uncertainties of more than an order of magnitude exist in the calculated masses, not to mention uncertainties concerning the ages of the lunar maria. Even greater uncertainties apply to the comets point in Figure 1. One may conclude tentatively that "live" comets do not contribute much to the formation of lunar craters, although this conclusion is by no means definitive. Figure 1 tells us nothing about the frequency of "old" comet nuclei, but does suggest that the supply of Apollo asteroids has been fairly stable for a significant astronomical interval. This gives us some confidence that we may be dealing with a quasi-stable distribution of larger bodies in the meteoritic complex.

4. THE METEORITIC POPULATION OF SMALL BODIES

This section has been intentionally curtailed because of the comprehensive coverage of the subject by Millman (1967).

In Figure 1, the impact rates for meteorites of mass > 10^2 g are based on estimates by G. S. Hawkins (1960) (GSH) and by Harrison Brown (1960) (HB), both estimates here being corrected from terrestrial falls to outside the earth's atmosphere by an ablation correction of five times. The cumulative impact rates become

$$\text{(GSH)} \quad \log N = -18.67 - \log m \text{ (cgs)} \quad , \tag{8}$$

$$\text{(HB)} \quad \log N = -20.54 - 0.77 \log m \text{ (cgs)} \quad . \tag{9}$$

For the meteors in the mass range from 10^{-5} to 10^{+2} g, I adopt as the cumulative influx rate

$$\log N = -18.30 - 1.34 \log m \text{ (cgs)} \quad . \tag{10}$$

This equation is taken from a recent compilation (Whipple, 1965) with a correction of a factor of 2 in number to allow for earth shadowing in the original equation, and a factor of 1/1.3 to allow for the effect of the gravitational attraction of the moon as compared to that of the earth (velocity at earth = 22 km sec^{-1}). The coefficient of 1.34 (S = 4) for log m is based upon the photographic meteor studies of Hawkins and Upton (1958), consistent with determinations for visual meteors by Millman and Burland (1957). The luminous efficiency factor for photographic meteors has been determined from artificial meteors and recognized asteroidal meteors by Cook, Jacchia, and McCrosky (1963), leading to a cometary meteoroid density of 0.44 g cm^{-3}.

The mass determination is in fair agreement with more recent determinations by Verniani and Hawkins (1964) based upon radio-meteor observations in the Harvard Meteor Program and from calculations of ionizing efficiency.

Undoubtedly the meteor influx curve is not a straight line in the log N – log m plane, and radar-meteor data generally give a smaller value by about a factor of 10 than that of equation (10) for masses below 10^{-3} to 10^{-2} g. The calibration of the radio-meteor mass scale is particularly difficult, as is the correction at small velocities for the electron-production function and at high velocities for the electron spreading in the high atmosphere. Until the radio-meteor data are well calibrated at faint optical magnitudes, I will have little confidence in the absolute values of the mass flux deduced from radio data. Orbital data are similarly prejudiced by this observational optimization in the middle-velocity range. Temporal and spacial variations over the earth, on the other hand, can generally be well determined from radio data.

In the mass range from 10^{-6} g to 10^{-10} g, the penetration data in space from the NASA Explorer and Pegasus probes are remarkably consistent and apparently more precisely calibrated than any other data used for Figure 1. I have adopted the directly reduced data by Naumann (1966), from the penetration experiments, as the most complete and satisfactory. They are corrected to deep space near the earth's orbit by a factor of 1/1.3 in N for earth attraction, and by a factor of π to correspond to 2π ster of exposure on an open sphere. The Explorer and Pegasus data are fitted by least squares to

$$\log N = -13.85 - 0.51 \log m \quad , \tag{11}$$

and labelled "Penetration" in Figure 1 in the range $10^{-11} < m < 10^{-5.36}$ g.

For comparison, van de Hulst's (1947) original estimate based on his theory of the zodiacal cloud is plotted from the equation

$$\log N = -14.50 - 0.66 \log m \text{ (cgs)} \quad . \qquad (12)$$

The agreement between the "Penetration" and the "van de Hulst" lines is rather striking, if fortuitous. For the much wider range in particle flux from theories of the zodiacal cloud, note Figure 1 and refer to Millman (1967) and Proceedings of the ZLIM Conference (to be published).

I have left out of consideration the near-earth acoustic measures of impacts by rockets and satellites and the collection data, as they are orders of magnitudes greater than the apparently reliable penetration data. The latter and the meteor data lead to a total influx rate of small particles amounting to 1.6×10^{-16} g cm^{-2} $(2\pi \text{ ster})^{-1}$ sec^{-1}. At an impact velocity of 15 km sec^{-1}, this corresponds to a space density $\rho = 4 \times 10^{-22}$ g cm^{-3} near the earth's orbit. This influx and space density are consistent with the erosion rates observed for irons, stones, and cometary meteoroids as indicated above in Section 2.4.1.

For future discussions I shall adopt the "Penetration" and "Meteors" curves (equations (10) and (11)) in Figure 1 for other basic calculations without a specific lower cutoff in mass. Most of the mass is contributed by particle masses in the neighborhood of 10^{-6} to 10^{-3} g, less than 0.1 cm in radius. The discontinuity at $m = 10^{-5.6}$ g cannot be physically significant. The use of straight lines in the log N – log m plane simplifies calculation, and we have inadequate data to produce a proper curve. The flattening of the observed curve near 10^{-10} g suggests a curvature that in Naumann's solution leads to an absence of particles much smaller in mass, consistent with the solar-light pressure theory for the partially opaque dielectric particles that we might expect.

5. MASS INPUT REQUIRED TO MAINTAIN THE ZODIACAL CLOUD

5.1 Classical Viewpoint

We must assume that only very small particles are significant in producing the diffraction, scattering, and reflection of sunlight that provides the zodiacal light, and we have seen that the mass influx to the earth is carried primarily by particles less than 0.1 cm in radius. If all the small particles were undisturbed by sputtering or mutual collisions, they could spiral toward the sun by the P-R effect. This I have shown (Whipple, 1955) requires a continuous contribution of only about 1 ton sec^{-1}, regardless of particle size or density if the necessary particles are somewhat larger than the wavelength of light. In fact, however, collisions and particle breakup will increase the quasi-equilibrium input rate (Whipple, 1955), while the problem is quite complicated by the possible need for submicron particles, which appear to be eliminated rapidly by both light pressure and solar wind.

5.2 Total Mass of the Zodiacal Cloud

Once we have determined the total mass of the zodiacal particulate cloud, we can determine the needed input rate by calculations of the particle lifetimes. If we assume a mean space density of 2×10^{-22} g cm^{-3} over a volume of 3.5 a.u. radius about the sun within $i < 20°$ of the ecliptic, the total mass of the zodiacal cloud becomes 4.5×10^{19} g.

We may make another estimate for those particles with perihelion distance of < 1 a.u. For a mean orbital period of 3 yr, the earth of radius R will intercept a fraction $1.3\,(R)^2/1.5\,(2 \sin i)\,(a.u.)^2$ yr^{-1}, or 7.2×10^{-17} sec^{-1}. At an influx rate of 1.6×10^{-16} g cm^{-2} sec^{-1}, this leads to a total mass of 1.1×10^{19} g for the zodiacal cloud ($q < 1$).

Since the first estimate of 4.5×10^{19} g is probably too high, the outer region probably being less dense, and since the latter estimate of 1.1×10^{19} g is too low as $q > 1$ a.u. for perhaps half the mass, a reasonable estimate is perhaps 2.5×10^{19} g for the entire cloud.

For a mean life of 10^5 yr, this mass corresponds to a total influx rate of 8 tons sec^{-1} for the entire cloud. By the pure P-R effect a particle of density 1 g cm^{-3} in an orbit of $q = 1$ a.u. and $e = 0.5$ [$C(e) = 1.92$] with a life of 10^5 yr would have a radius of some 52 μ. These calculations, based on the measured influx rates of particles on the earth, are encouragingly close to the classical calculation of 1 ton sec^{-1} total input to the zodiacal cloud.

We have noted above that for particles of microns or greater in dimension the solar wind increases the pure P-R effect by some 22%, and solar wind sputtering reduces the radius at a rate 10% or less of the rate of decay in perihelion distance. Other dissipative effects except collisions appear not to be significant. Let us then adopt the P-R effect increased by 30% and compare collisional lifetimes with the P-R lifetimes for small particles. In this manner we can estimate the input mass rate to maintain the zodiacal cloud. Later we can consider likely sources of material and the actual production of the zodiacal light.

5.3 Collisional Loss Rates for Small Particles

When the observed flux of particles at the earth is known, it is relatively straightforward to calculate the rate of collisional destruction as a function of particle size. This combined with the P-R effect provides a mean life for average particles that can then be used to calculate the required input rate for the zodiacal cloud.

The collisional loss rate for small particles must be considered as made up of two parts, erosion and collisional destruction. For bright photographic meteorids, in the mass range 10 to 10^{-1} g, the erosion constitutes

essentially the total effect, as we already assumed earlier. This is because most of the mass is concentrated in much smaller particles, at least if $S > 3$, as we have assumed ($S = 4$). Thus, as we go to smaller particle radii, destructive collisions with particles of mass $> m/\phi$ must be considered separately from the erosion by particles of mass $< m/\phi$. The collisional destruction effect is now considered. Let the cumulative flux rate for mass $> m$ be N cm^{-2} sec^{-1} $(2\pi$ ster$)^{-1}$, where

$$N = \frac{K}{m^{\beta}} \quad \text{(cgs)} \quad , \tag{13}$$

and $\beta = S/3$.

The collisional area of a spherical particle of density ρ is $Am^{2/3}$, where $A = (3\sqrt{\pi}/4\rho)^{2/3}$. I adopt the cross section of the larger particle for completely destructive collision when the mass ratio of the two particles is less than ϕ. For destructive collisions of a particle of mass m, with smaller particles to a lower limit m_0, the integrated flux in cross-sectional area is then

$$\text{flux area} = Am^{2/3} \int_{m_0}^{m} \frac{\beta K}{m^{\beta+1}}\, dm = AKm^{2/3} \left(m_0^{-\beta} - m^{-\beta}\right) \quad . \tag{14}$$

For destructive collisions of larger particles up to mass $= m_L$ (area $= Am_L^{2/3}$) with mass m, the flux area is similarly

$$\text{flux area} = \frac{\beta AK}{(2/3 - \beta)} \left(m_L^{2/3 - \beta} - m^{2/3 - \beta}\right) \quad , \tag{15}$$

so long as $\beta \neq 2/3$.

In the mass range $m < 10^{-5.36}$ g, from Figure 1 and equation (11), I adopt $\beta = 0.51$ and $K(obs) = 10^{-13.85} g^{0.51}$ cm^{-2} sec^{-1} $(2\pi \text{ ster})^{-1}$. However, K(obs) must be corrected by a factor of 1/1.5 from a velocity of 15 km sec^{-1} near the earth's orbit to the adopted mean collisional value of 10 km sec^{-1}, and by a factor of 4 to include 4π ster of flux. For a sphere of radius s, the total 2π ster of flux falls on an area of $4\pi s^2$, but $Am^{2/3}$ corresponds only to πs^2. Also, I correct K by a factor of 1/2 to allow for a lower average space density than near the earth's orbit. Hence, for $m < 10^{-5.36}$ g, $K = 10^{-13.73} g^{0.51}$ cm^{-2} sec^{-1} $(8\pi \text{ ster})^{-1}$ and $\rho = 1$ g cm^{-3}.

For $m > 10^{-5.36}$ g, I adopt $\beta = 1.34$, $\rho = 0.44$ g cm^{-3}, and $\log K = -18.18\, m^{1.34}$ cm^{-2} sec^{-1} $(8\pi \text{ ster})^{-1}$. For all values of m for these low-density particles I adopt $\phi = 3200$, corresponding to destruction by collision with a particle of mass > m/3200 at a velocity of 10 km sec^{-1}. Limiting the encounter area only to the cross section of the larger particle is a compromise, since the area for comparable particles is less than 4 times the adopted value, and the area is overestimated when the radii are highly different. Unfortunately, I have not had sufficient time to include the contribution to the zodiacal cloud of the smaller fragments introduced by collisions. This effect is doubtless significant.

For colliding particles of mass < m/3200, simple erosion is assumed at a rate of 3200 times the integrated mass of the small particles.

5.4 Calculation of Particle Lifetimes

Three different kinds of lifetimes are now involved in our calculation:

A. τ_{PR} = P-R spiraling lifetime (reduced by 30% from equation (2)), where

$$\tau_{PR} = 1.16\, m^{1/3} \cdot 10^7 \text{ yr} \quad \text{for } m < 10^{-5.36} \text{ g} \tag{16a}$$

and

$$\tau_{PR} = 1.52\, m^{1/3} \cdot 10^{7} \text{ yr} \quad \text{for } m > 10^{-5.36} \text{ g} \quad . \tag{16b}$$

B. τ_e = erosional lifetime, where the total mass encountered at individual masses < m/3200 is assumed to erode 3200 times its mass from the larger particle.

C. τ_c = collisional mean life equal to the time required for the flux area (equations (14) and (15)) to equal unity. Hence, $e^{-\tau_c}$ of the particles should survive if $\tau_{PR} = \tau_c = \infty$.

In combining these three types of lifetimes, I have first calculated an intermediary lifetime τ_i from τ_{PR} and τ_e, corresponding to the reduction of τ_{PR} by erosion, where

$$\tau_i = \frac{\tau_{PR}\, \tau_e}{\tau_{PR} + \tau_e} \quad . \tag{17}$$

Finally, the destructive probability given by τ_c is combined with τ_i to give the final mean lifetime τ in the form

$$\tau = \tau_c \left(1 - e^{-\tau_i / \tau_c}\right) \quad . \tag{18}$$

The average lifetime T of the entire zodiacal cloud is then the complete integral ratio

$$T = \frac{\int \tau(m)\, dm}{\int dm} \quad . \tag{19}$$

The results of the calculations are shown in Table 3.

Table 3. Distribution of masses and lifetimes

Particle mass (g) log m	Particle radius (cm) log s	Percent mass $10^{-0.5}$ m to $10^{+0.5}$ m	P-R* log τ_{PR}	Lifetimes (yr) Erosion log τ_e	Lifetimes (yr) Collision mean log τ_c	Mean** log τ
-12.0	-4.21	0.02	3.06?	6.70	5.92	3.06?
-11.0	-3.87	0.04	3.40?	6.54	5.84	3.40?
-10.0	-3.54	0.14	3.73	6.39	5.76	3.73
- 9.0	-3.21	0.44	4.06	6.23	5.65	4.05
- 8.0	-2.87	1.4	4.40	6.07	5.53	4.37
- 7.0	-2.54	4.2	4.73	5.92	5.41	4.66
- 6.0	-2.21	12.9	5.06	5.76	5.28	4.88
- 5.0	-1.76	40.9	5.51	5.61	5.13	5.00
- 4.0	-1.42	21.5	5.85	5.45	4.96	4.91
- 3.0	-1.09	10.0	6.18	5.29	4.77	4.75
- 2.0	-0.76	4.6	6.51	5.14	4.40	4.40
- 1.0	-0.42	2.2	6.85	4.97	5.02	4.79
0.0	-0.09	1.0	7.18	5.17	5.69	5.10
+ 1.0	+0.24	0.5	7.51	5.45	6.36	5.42
+ 2.0	+0.58	0.2	7.85	5.76	7.02	5.75
> 2.0	+0.58	0.2				

Weighted mean life of all particles, $T = 8.3 \times 10^4$ yr.

*From equations (16a, b).

**From equations (17), (18), (19).

An interesting observation from Table 3 is the relatively slow change in the mean lifetimes of the particles, considerably slower than the change in radius for the larger particles and only 5 times over the mass range 1.0 to 10^{-8} g. At the largest particle sizes erosion is the limiting factor. This will hold up to masses of the order of 10^6 g, where earth perturbations

begin to limit the mean life. Destructive collisions control in the middle range 10^{-2} to 10^{-5} g and, finally, the corrected P-R effect controls for the smaller particles. Table 4 omits an important column, viz., the calculated input from breakup of larger particles. A rough calculation leads to a somewhat greater yearly input than output for particles in the mass range 10^{-7} to 10^{-12} g by a factor of 2 to 3. The law for breakup of such low-density particles is not known, however, and the use of the relation found by Gault et al. (1963 Sec. II. C. 2) for stones may not be applicable. A tendency for cometary material to be grainy at mass $\sim 10^{-5}$ g could greatly affect the distribution.

Granted that Table 3 will be considerably modified by a more accurate distribution law of particle flux with mass, particularly by the reduction in concentration near 10^{-5} g, it explains a surprising characteristic of the mass distribution curve, viz., the large value of S or the rapid increase in numbers with decreasing mass. At intermediate and large masses in Table 3, the self-destructive character of the zodiacal cloud controls the lifetimes and, by spallation, undoubtedly causes a large concentration of smaller masses. Finally, the P-R effect controls the loss of very small particles because collisions become less important, and so the distribution curve flattens out (S falls).

The present analysis is too crude (omitting the input factor by collisions) to predict the number of extremely fine particles, $s < 1\ \mu$. If larger particles ($s \gg 2\ \mu$) can indeed produce the polarization as well as the brightness of the zodiacal light, then the present solution is consistent. If submicron particles are the major contributors, as suggested by Powell's theory (1967), then the present solution is not very specific and gives too few very small particles. A more complete theory will be needed.

As noted in Table 3, the mean lifetime of the entire small-particle population is calculated to be $T \sim 8.3 \times 10^4$ yr. However, the contributions from the breakup of larger particles may be taken as one-half the losses, assuming a 30% loss to evaporation and submicron particles. This effectively doubles the mean life of the entire cloud to 1.7×10^5 yr. Hence, the required

total influx rate, previously found to be 8 ton sec^{-1} for T = 10^5 yr, becomes some 4 tons sec^{-1}. With the observed distribution of masses we have failed by a factor of 3, however, to destroy the brighter photographic meteors in 10^4 yr. Similarly, for the stony meteorites our solution is inadequate by a factor of 2. Hence, we apparently need 10 to 20 tons sec^{-1} continuous input to maintain the zodiacal cloud in quasi-stable equilibrium, an estimate very close to the original 1955 estimate. Let us now look to the sources of this material.

6. ON THE SOURCE OF THE ZODIACAL CLOUD

6.1 Orbital Considerations

The general story of the photographic and radio meteors need not be repeated here. The mass range involved is from a few grams down to the order of 10^{-4} to 10^{-6} g. The orbits are indicative of the short-period comets with a large fraction of streams among the brighter photographic meteors, and a lesser stream contribution among the radio meteors. The evidence is conclusive that the particles involved are in large measure highly fragile low-density objects, $\rho \sim 0.44$ g cm^{-3}, as adopted earlier in this paper for the brighter meteors. From the physical characteristics, less than 1% suggest a meteorite type of body of stone or iron. Orbitally, Figure 2 illustrates the distribution of aphelion distances from the precision photographic meteors (Jacchia and Whipple, 1961) and a random sample (Hawkins and Southworth, 1961). The aphelion distances show no strong indication of any concentration near the asteroid belt at $\sim$ 3 a.u., the distribution filling in to Jupiter's orbit near 5 a.u. and falling away at greater aphelion distances in the manner of comets. The Mars asteroids, on the other hand, show the normal asteroid distribution with a maximum of aphelion distances just above 3 a.u. From orbital considerations alone and the inclinations, one would deduce that more than 90% of the photographic meteors have cometary origin and, as noted above, the physical circumstances suggest an even higher percentage.

Among the radio meteors the aphelion distances are somewhat more concentrated within the orbit of Jupiter than among the brighter photographic meteors, but there is no indication of an asteroidal origin. The orbits are suggestive of very short-period comets (see, for example, Millman, 1967). We now have information concerning the much brighter fireballs up to masses of perhaps 10^6 g or more, as presented by McCrosky (1966) from the Prairie Network of observing stations covering more than 10^6 km^2

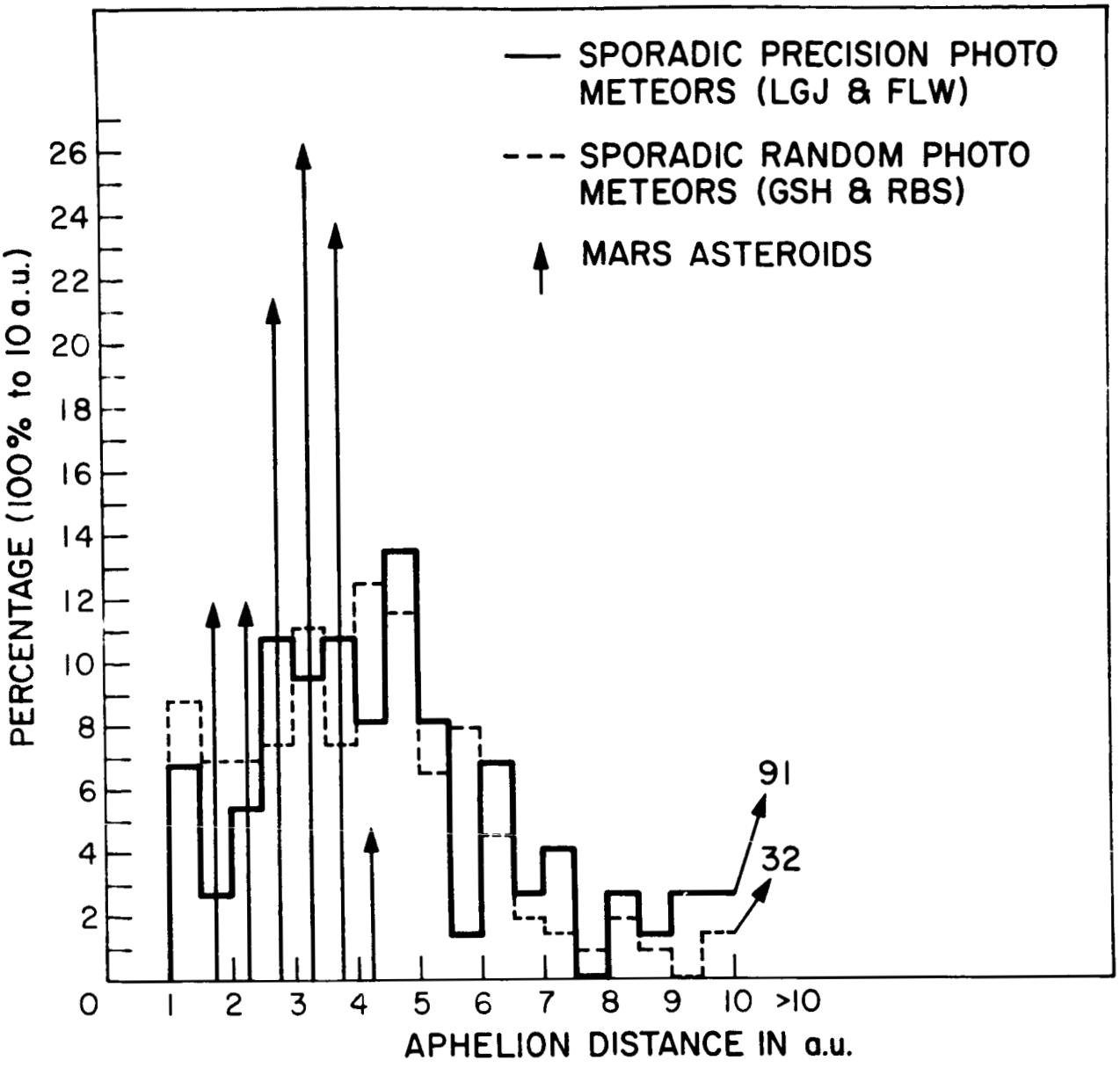

Figure 2. Aphelion distances of precision photographic meteors and of Mars asteroids.

in the U. S. Midwest. The aphelion distances of some three dozen of these orbits reduced by McCrosky are presented in Figure 3. Here we note a striking difference in the distribution of aphelia, a high concentration just within Jupiter's orbit and another concentration between 1 and 2.5 a.u., with a surprising gap in the region 2.5 to 3.0 a.u. The aphelia of the six photographic meteors that are known to be of meteorite physical structure show this same gap. Correspondingly, the eight Apollo asteroids have orbital aphelia distributed similarly. Before the Prairie Network bright fireball program was started, I had expected the meteorite type of body to match the cometary meteoroid in frequency at apparent magnitudes of the order of -6 to -10 visual. McCrosky's result, which comprises much brighter and more massive objects than these, shows a very small percentage of nonfragmenting, apparently solid stones or iron bodies. Thus the evidence is strong that we are dealing among the bright fireballs with incoming bodies of weak physical structure, unless it is indeed possible that the "frothing process" found for melting stones (Allen and Baldwin, 1967) may cause a misinterpretation of meteoritic densities. For bodies with masses of many kilograms, however, this effect should not be important. As an example of extraordinary friability in a very large body, McCrosky (private communication) reports a fireball of approximately a magnitude -18 lasting for only 1 sec and disappearing at an altitude of 70 km. There is no question that a large fraction of bright as well as faint meteoroids are extremely friable and of low density.

I have no explanation for the minimum in the aphelion distribution centered at the middle of the asteroid belt as observed in common by bright fireballs, the photographic meteorites, and the Apollo asteroids. Quite possibly they are closely connected in origin, or perhaps the statistics are inadequate to make the conclusion incontestable. I have suggested (Whipple, 1966b) a further possibility, viz., that these friable bodies may include a considerable membership from the extreme limit of carbonaceous chondrites. If the asteroid belt has suffered only a minor fragmentation by collisions, it is possible that we are dealing with "half-baked" asteroids of small dimension, less than 30 km in diameter, which are similar to the extremely friable and rather low-density carbonaceous chondrites – but even more so. Hence, they

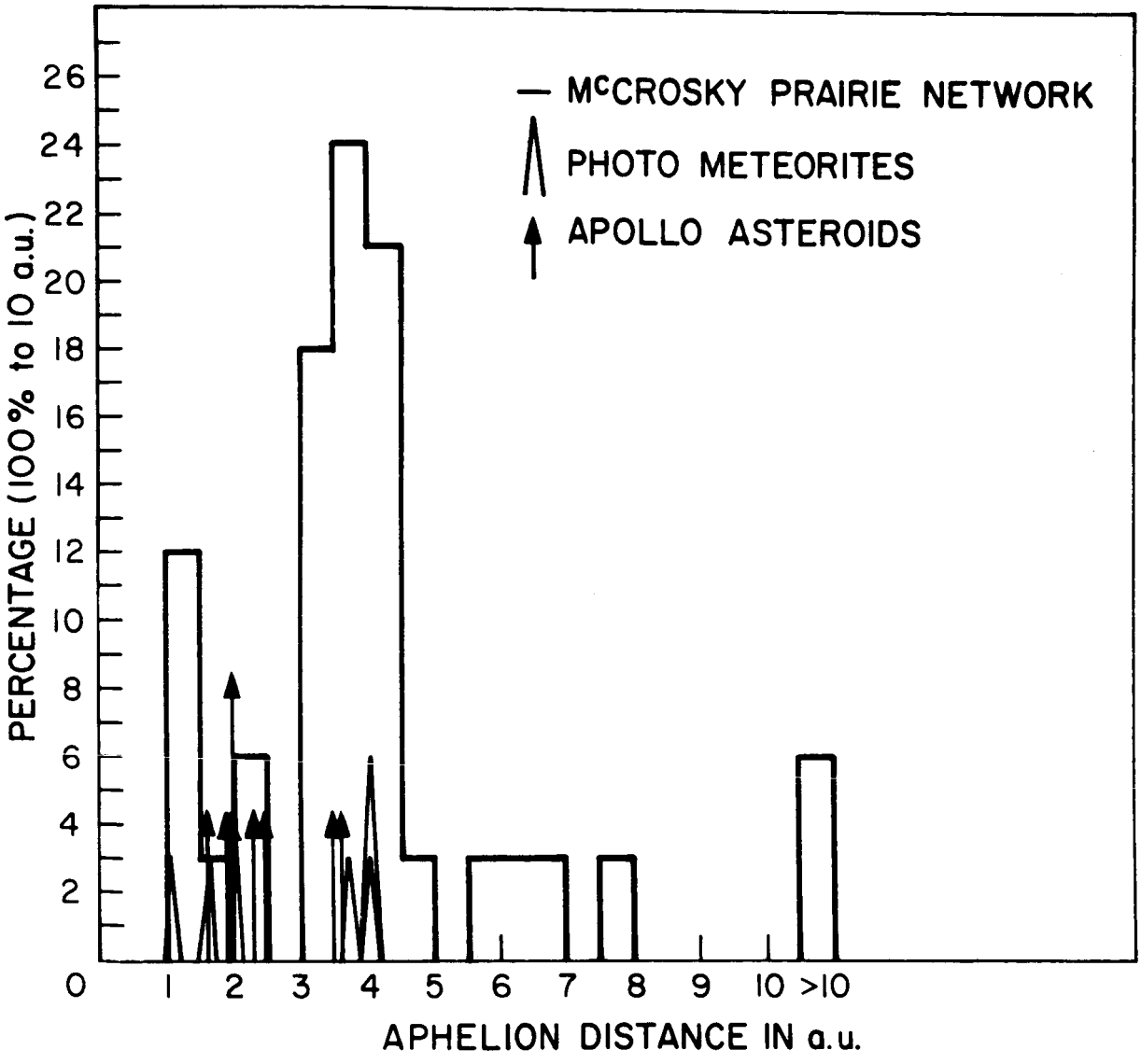

Figure 3. Aphelion distances of fireballs (McCrosky Prairie Network), photographic meteorites, and Apollo asteroids.

could have a structure so weak that we find no examples on the earth because of destruction in atmospheric passage, as is the case for cometary meteoroids.

Anders (1966) suggests that the bodies with aphelia near Mars represent an origin as Mars-crossing asteroids, whereas those with aphelia within the outer limits of the asteroid belt to Jupiter represent old cometary nuclei. This assumption, as mentioned earlier in this paper, is quite possible, but it is one that I prefer not to make until direct proof is available.

In view of the high abundance of highly friable material in the mass ranges from 10^{-5} g to 10^{6} g, the smaller particles being quite clearly of cometary origin, it would be quite surprising if among the still finer material the source should be other than cometary. The mean inclinations of the radio and photographic meteors, the bright fireballs, the Apollo asteroids, and the Mars-crossing asteroids all lie in the range from 11° to 20° as indicated in Table 4, which summarizes the distribution of the aphelion distances. We should note that in all cases except for the Mars-crossing asteroids there is considerable selection toward small inclinations by the higher probability of encounter with the earth. This is true also to some extent for the Apollo asteroids, since their chance of discovery is generally small; hence, those with higher inclinations may tend to be missed because of the still smaller chance of their having a close approach to the earth.

It is interesting to note from Table 4 and Figure 2 that the bright fireballs show a rather small percentage with aphelia beyond Jupiter's orbit. I note, however, that among this group of larger bodies the etching rate gives them lifetimes of the order of 10^{6} yr, which in Jupiter-crossing orbits produces selective elimination by Jupiter perturbations. This, again, allows the possibility that most of the bright fireballs arise from a cometary origin, although some may be of the "half-baked" asteroid type.

Table 4. Distribution of aphelia: Sporadic meteoroids and asteroids

Aphelion (a. u.)	< 2.5 No.	2.5 to 5.2 No.	> 5.2 No.	< 5.2 $i^{\ddagger}$
Photographic meteors*	49	115	121	-
Photographic meteors**	11	42	88	18°
(By cosmic weights)	10	57	74	20°
Asteroidal meteors	3	3	0	15°
Fireballs†	7	24	6	12°
Apollo asteroids	5	3	0	11°
Mars asteroids (mean q = 2.85 a. u.)	4	30	0	15°

*Hawkins and Southworth, 1961.
**Jacchia and Whipple, 1961.
†McCrosky Prairie Network.
‡Mean inclination to the ecliptic.

In view of a cometary origin for the radio and photographic meteors, it is of considerable interest to see whether the expected input rate can indeed match the necessary 10 to 20 tons sec^{-1} required to maintain the zodiacal cloud in quasiequilibrium. The next two sections of this paper will consider this question.

6.2 Physical Characteristics of Comets

In estimates of the meteoritic contribution of cometary nuclei, it is important to have an estimate of the ratio of gas to dust in these bodies. We have little direct evidence as to the numerical value of this ratio. The observations of comets themselves give quite imprecise values since we see neither the parent molecules of the gases nor the meteoroids above micron dimensions. There is no check on the validity of the assumption that the original composition of material that freezes at temperature ~ 30°K

approximates that of the present solar atmosphere. This assumption leads to an ice/meteoritic ratio (I/met) of about 8 (Whipple and Stefanik, 1966), representing a near maximum value, although possibly a high concentration of hydrates (Delsemme, 1966) might give a higher ratio.

It is argued (e.g., Harwit, 1963) that the lack of an observable dust continuum in the spectra of "old" comets, such as P/Encke, compared to relatively weak-band spectra in some "new" comets, means that old comets contain a smaller proportion of meteoritic material than new comets. I believe that the strong meteor contribution by P/Encke indicates possibly even the reverse. The basic idea is that in old large comets, the cores, either by heat or by compression, contain meteoritic material that is more consolidated than the fine dust in the outer regions of "new" comets. There is evidence that the meteoroids from some comets, particularly when observed fairly soon after ejection, are of extremely low density. The best example is the striking Draconid meteor shower from Comet Giacobini-Zinner of 1946. The low-velocity ($\sim$ 21 km sec^{-1}) meteors disappeared nearly 20 km higher in the atmosphere than average meteors of the same velocity (Jacchia, Kopal, and Millman, 1950). Few deceleration measures could be made, but the mean meteoroid density must have been 0.1 g cm^{-3} or possibly much less. Thus, it seems likely that the outer volumes of new comets may contain very friable or even "fluffy" meteoritic material that readily breaks into the fine dust often observed.

Our most direct evidence comes from cometary meteoroids themselves. Suppose the observed density is ρ, for which the compact solid density would be ρ_m. Suppose further that the icy fraction was originally I, by mass, the solid density ρ_i, the fractional volume of void λ, and no losses of earthy material occurred; then the total unit volume was originally made up as follows:

$$\frac{\rho}{\rho_M} + \frac{I}{\rho_i} + \lambda = 1 \quad . \tag{20}$$

Our desired icy mass fraction then becomes

$$I = \rho_i (1 - \lambda - \rho/\rho_M) \quad . \tag{21}$$

We may reasonably adopt $\rho_i = 0.9$ g cm^{-3}, $\rho_M = 3.4$ g cm^{-3}, and $\lambda = 0.1$, or 10% void volume. The solution is not very sensitive to λ for small values, so that Table 5 may be indicative of I and I/ρ = I/met as a function of the observed meteoroid density ρ.

Table 5. The icy component and the I/Met

ρ (g/cm^3)	I	I/Met
0.005	0.81	162
0.05	0.80	16
0.10	0.78	7.8
0.20	0.76	3.8
0.30	0.73	2.4
0.40	0.70	1.7
0.44	0.69	1.58
0.60	0.66	1.10
0.80	0.60	0.75
1.00	0.56	0.56
1.50	0.41	0.27

Although the observed meteoroid density may represent a region of abnormally high concentration of meteoritic material in the comet because the meteoroid has, in fact, stuck together, we see that a typical value, adopted here, of $\rho = 0.44$ g cm^{-3} leads to I/met = 1.58. We may thus be justified in assuming that ices simultaneously eject with them one-half their mass in meteoritic material. I feel that the presence in a comet of highly volatile materials can lead to cracking, breakage, and ejection of considerable water ice, hydrates, and meteoritic material. Generally, this assumption

leads to smaller icy nuclei and relatively more rapid disintegration than would occur if solar heat had to sublimate all the icy mass before it could be released from the nucleus.

6.3 Mass Contributions by Comets

To calculate the meteoritic contributions to the zodiacal cloud by actual comets, let us assume that the solar radiation is 0.9 effective in providing heat for sublimation of ices at a mean value of 450 cal g^{-1}, and that the comet in one perihelion passage receives effectively f yr of radiation at 1 a. u. (see Whipple, 1955). Then for a comet density of 1.3 g cm^{-3}, I/met = 2, and the mass-luminosity relation of equation (4), we find that the meteoritic loss per revolution about the sun, M_{rev}, is

$$M_{rev} = f \times 10^{17.61 - 0.4H} \text{ g} \quad , \tag{22}$$

where H is the absolute magnitude of the comet.

For Halley's comet, H = 4.6 mg, f = 1.5, and period = 76 yr, the meteoritic mass loss becomes 5 ton sec^{-1}, and for Comet Encke with its average H = 9.0 mag for the early 19th century and f = 3.5, the mass loss is 3.5 ton sec^{-1}. The corresponding diameter for Encke's Comet is 3.4 km, whereas Roemer (1966) measures 1.2 km for an albedo of 0.7, and 7.0 km for an albedo of 0.02 from the brightness at large solar distances. We have meteor-stream evidence (Hamid and Whipple, 1951) that Encke's Comet has been in existence for several thousand years. Both from the basic principle of the icy comet model and from brightness observations of Encke's Comet since 1786, we expect the brightness and rate of mass loss to be greater in the past, the rate of the change with time being quite uncertain (see, e. g., Kresák, 1965; Whipple and Douglas-Hamilton, 1966).

The orbit of Encke's Comet is nearly unique, since its aphelion distance is well within Jupiter's orbit (4.10 a. u.). Hence, it is an ideal source for zodiacal cloud material. Only the very faint Comet Wilson-Harrington (1949 III)

(aphelion 2.47 a.u.) and the extinct source of the Geminid meteor shower qualify as astronomically "currently active" sources. Material injected in Jupiter-crossing orbits is rapidly lost by Jupiter perturbations and by orbital velocity effects for very small particles.

Quite probably, then, Encke's Comet over the past several thousand years has been the major support for the zodiacal cloud to maintain quasi-equilibrium. Our evidence is lacking for as much as the mean life of the zodiacal cloud, 1.7×10^5 yr, but the 50×10^6 yr maximum exposure ages for the stony meteorites indicate that erosion, averaged over this longer interval, has been as rapid or more so than at present. Enormous comets have been observed in the past 300 yr; Comet 1729 was a naked-eye object at 4.1 a.u. from the sun. Thus, over 10^5 yr one need not be surprised if the short-period comet supply does not average as well as or, indeed, better than our present sample. Note that a collision-controlled mean life leads to a zodiacal cloud density varying as the square root of the influx rate. Hence, rather large fluctuations of influx rate do not change the cloud mean density so strikingly.

Thus, the consensus suggests that comets are an adequate source. A primarily asteroidal source would probably produce too high a concentration toward the fundamental plan of the solar system. Comets clearly contribute most of the material in the mass range 10^{-2} to 10^5 g, and collisions are clearly a dominating destructive factor. The steepness of the particle population curve in this mass range and the concentration of mass in the 10^{-5} g range suggest not simple collisional spallation but a tendency for some fundamental grain mass to lie in this region, not characteristic of meteorites but quite possibly of friable cometary material.

If a massive population of short-lived submicron particles is finally shown to be necessary in producing polarization, or possibly color, in the zodiacal light, then the present data and this model will require adjustment in the submicron range. Otherwise the model based directly on meteoritic observations appears to be a fair approximation.

7. REFERENCES

ALLEN, C. W.

1963. Astrophysical Quantities. 2nd ed., Athlone Press, Univ. of London, London, 291 pp.

ALLEN, H. J., AND BALDWIN, B. S.

1964. To be published.

ANDERS, E.

1966. Private communication.

ARNOLD, J. R.

1965a. The origin of meteorites as small bodies. II. The model. Astrophys. Journ., vol. 141, pp. 1536-1547.

1965b. The origin of meteorites as small bodies. III. General discussion. Astrophys. Journ., vol. 141, pp. 1548-1556.

BELTON, M. J. S.

1967. Dynamics of interplanetary dust particles near the sun. Paper presented at ZLIM conference in Hawaii, January 1967.

BIERMANN, L.

1967. Survey paper presented at ZLIM conference in Hawaii, January, 1967.

BROWN, H.

1960. The density and mass distribution of meteoritic bodies in the neighborhood of the earth's orbit. Journ. Geophys. Res., vol. 65, pp. 1679-1683.

BÜHLER, F., GEISS, J., MEISTER, J., EBERHARDT, P., HUNEKE, J. C., AND SIGNER, P.

1966. Trapping of the solar wind in solids. Earth Planet. Sci. Letters, vol. 1, pp. 249-255.

COOK, A. F., JACCHIA, L. G., AND McCROSKY, R. E.

1963. Luminous efficiency of iron and stone asteroidal meteors. Smithsonian Contr. Astrophys., vol. 7, pp. 209-220.

DELSEMME, A. H.

1966. Occurrence des hydrates de gaz dans les noyaux cometaires Univ. Liège Inst. Astrophys. Coll. 8°, vol. 21, no. 510, pp. 69-76.

FIREMAN, E. L., AND DEFELICE, J.

1961. Tritium, argon 37, and argon 39 in the Bruderheim meteorite. Journ. Geophys. Res., vol. 66, pp. 3547-3551.

FISHER, D. E.

1966. The origin of meteorites, space erosion and radiation ages. Journ. Geophys. Res., vol. 71, pp. 3251-3259.

GAULT, D. E., SHOEMAKER, E. M., AND MOORE, H. J.

1963. Fragments ejected from the lunar surface by meteoroid impact. NASA Tech. Note D-1767, 39 pp.

HAMID, S., AND WHIPPLE, F. L.

1951. On the origin of the Taurid meteor streams. Helwan Obs. Bull. No. 41, pp. 1-30.

HARWIT, M.

1963. Origins of the zodiacal dust cloud. Journ. Geophys. Res., vol. 69, pp. 2171-2180.

HAWKINS, G. S.

1960. Asteroidal fragments. Astron. Journ., vol. 65, pp. 318-322.

HAWKINS, G. S., AND SOUTHWORTH, R. B.

1961. Orbital elements of meteors. Smithsonian Contr. Astrophys., vol. 4., pp. 85-95.

HAWKINS, G. S. AND UPTON, E. K. L.

1958. The influx rate of meteors in the earth's atmosphere. Astrophys. Journ., vol. 128, pp. 727-735.

JACCHIA, L. G., KOPAL, Z., AND MILLMAN, P. M.

1950. A photographic study of the Draconid meteor shower of 1946. Astrophys. Journ., vol. 111, pp. 104-133.

JACCHIA, L. G., AND WHIPPLE, F. L.

1961. Precision orbits of 413 photographic meteors. Smithsonian Contr. Astrophys., vol. 4, pp. 97-129.

KRESAK, L.

1965. The secular variations in the absolute brightness of periodic comets. Bull. Astron. Inst. Czech., vol. 16, pp. 348-355.

KUIPER, G. P., FUJITA, Y., GEHRELS, T., GROENEVELD, I., KENT, J., VAN BIESBROECK, G., AND VAN HOUTEN, C. J.

1958. Survey of asteroids. Astrophys. Journ. Suppl. 3, no. 32, pp. 289-428.

KUIPER, G. P., STROM, R. G., AND LePOOLE, R. S.

1966. JPL Tech. Rept. No. 32-800, 35 pp.

McCROSKY, R. E.

1966. Meteorite photography and recovery network. NASA Progress Rept. No. 8.

NEWKIRK, G., AND KAISER, C.

1967. Thermodynamics of interplanetary particles. Paper presented at ZLIM conference in Hawaii, January 1967.

MILLMAN, P. M.

1967. Observational evidence of the meteoritic complex. Paper presented at ZLIM conference in Hawaii, January 1967.

MILLMAN, P. M., AND BURLAND, M. S.

1957. Magnitude distribution of visual meteors. Sky and Telescope, vol. 16, p. 222.

NAUMANN, R. J.

1966. The near-earth meteoroid environment. NASA Tech. Note D-3717, 38 pp.

ÖPIK, E. J.

1951. Collision probabilities with the planets and the distribution of interplanetary matter. Proc. Roy. Irish Acad., vol. 54A, pp. 165-199.

1956. Interplanetary dust and terrestrial accretion of meteoritic matter. Irish Astron. Journ., vol. 4, pp. 84-135.

1963. Stray bodies in the solar system. Part I. Survival of cometary nucleii and asteroids. In Adv. in Astron. and Astrophys., vol. 2, ed. by Z. Kopal, Academic Press, Inc., New York, pp. 219-262.

ÖPIK, E. J. (Cont.)

1966. Stray bodies in the solar system. Part II. The cometary origin of meteorites. In Adv. in Astron. and Astrophys., vol. 4., pp. 301-336, ed. by Z. Kopal, Academic Press, Inc., New York.

POWELL, R. S.

1967. Survey paper presented at ZLIM conference in Hawaii, January 1967.

PARKER, E. N.

1964. The perturbation of interplanetary dust grains by the solar wind. Astrophys. Journ., vol. 139, pp. 951-958

PIOTROWSKI, S. L.

1953. The collisions of asteroids. Acta Astron., vol. 5A, pp. 115-136.

RHEE, J. W.

1967. Electrostatic potential of a cosmic dust particle. Paper presented at ZLIM conference in Hawaii, January 1967.

ROBERTSON, H. P.

1937. Dynamical effects of radiation in the solar system. Monthly Notices Roy. Astron. Soc., vol. 97, pp. 423-438.

ROEMER, E.

1966. The dimensions of cometary nuclei. Univ. of Liège Inst. Astrophys. Coll. 8°, vol. 21, no. 510, pp. 23-28.

SHOEMAKER, E. M.

1965. Preliminary analysis of the fine structure of the lunar surface, Ranger VII Part II. Experimenters' Analyses and Interpretations. JPL Tech. Rept. No. 32-700, pp. 75-132.

SHOEMAKER, E. M., HACKMAN, R. J., AND EGGLETON, R. E.

1961. Interplanetary correlation of geologic time. In Adv. in Astronaut. Sci., vol. 8, Plenum Press, New York, pp. 70-89.

SINGER, S. F.

1967. Dust dynamics in the magnetosphere and interplanetary space. Paper presented at ZLIM conference in Hawaii, January 1967.

SOUTHWORTH, R. B.

1964. The size distribution of the zodiacal particles. Ann. N. Y. Acad. Sci., vol. 119, pp. 54-67.

1967a. Phase function of the zodiacal cloud. Paper presented at ZLIM conference in Hawaii, January 1967.

1967b. Space density of meteors. Paper presented at ZLIM conference in Hawaii, January 1967.

VAN DE HULST, H. C.

1947. Zodiacal light in the solar corona. Astrophys. Journ., vol. 105, pp. 471-488.

VERNIANI, F., AND HAWKINS, G. S.

1964. On the ionizing efficiency of meteors. Harvard Radio Meteor Project Res. Rep. No. 5, February 1964.

WEHNER, G. K., KENKNIGHT, C., AND ROSENBURG, D. L.

1963. Sputtering rates under solar-wind bombardment. Planet. Space Sci., vol. 11, pp. 885-895.

WHIPPLE, F. L.

1950. A comet model. I. The acceleration of comet Encke. Astrophys. Journ., vol. 111, pp. 375-394.

1955. A comet model. III. The zodiacal light. Astrophys. Journ., vol. 121, pp. 750-770.

1963. Meteoritic erosion in space. Smithsonian Contr. Astrophys., vol. 7, pp. 239-247.

1965. Meteoroids and dust. Proc. III Intl. Symp. on Biostronaut. and Explor. of Space, ed. by T. C. Bedwell and H. Strughold, Southwest Research Inst., San Antonio, pp. 7-24.

1966a. Before type I carbonaceous chondrites? Paper presented at Met. Soc. Meeting, Washington, D. C., November 1966.

1966b. The meteoritic environment of the moon. Proc. Roy. Soc. (London), vol. 296A, pp. 304-315.

WHIPPLE, F. L., AND DOUGLAS-HAMILTON, D. H.

1966. Brightness changes in periodic comets. Mem. Roy. Soc. Liège, vol. 12, ser. 5, pp. 469-480.

WHIPPLE, F. L., AND FIREMAN, E. L.

1959. Calculation of erosion in space from the cosmic-ray exposure ages of meteorites. Nature, vol. 183, p. 1315.

WHIPPLE, F. L., AND STEFANIK, R. P.

1966. On the physics and splitting of cometary nuclei. Univ. of Liège Inst. Astrophys., Coll. 8°, vol. 21, no. 510, pp. 33-52. Also Smithsonian Astrophys. Obs. Spec. Rept. No. 182, 25 pp.

WYATT, S. P., AND WHIPPLE, F. L.

1950. The Poynting-Robertson effect on meteor orbits. Astrophys. Journ., vol. 111, pp. 134-141.

ZLIM CONFERENCE

1967. Conference on Zodiacal Light and the Interplanetary Medium, Honolulu, Hawaii, proceedings to be published.

PHASE FUNCTION OF THE ZODIACAL CLOUD

Richard B. Southworth

ABSTRACT

Smith, Roach, and Owen's zodiacal-light photometry has been analyzed for the phase function and distribution of the particles. It is assumed that 1) there is a unique phase function, 2) the space density is the product of a distribution in heliocentric latitude and another in radius vector, and 3) all the observed light is scattered by interplanetary particles symmetrically distributed about the sun, except for the enhancement at 65° elongation (possibly this is double scattering by ice in the high atmosphere). Various distributions in radius vector are tried, each yielding a phase function and a latitude distribution, and a predicted zodiacal-light distribution. Good fits to the observations are found with radial density distributions similar to that found from radar meteors; these also yield latitude distributions comparable to the meteor distribution. For scattering angles above 60°, the phase functions resemble a Lambert law, except for an extra peak near 180°, which could be caused by particle roughness.

PHASE FUNCTION OF THE ZODIACAL CLOUD

Richard B. Southworth

1. INTRODUCTION

A complete general account of the relationship between the observed brightness of the zodiacal light and the cloud of interplanetary particles that scatter the sun's light to the earth must consider a particle distribution with several degrees of freedom. The cloud doubtless contains many types of particles, each with a distinct scattering (phase) function, distributed in three dimensions. Time, polarization, and color are other variables that I will not consider here. On the other hand, the observed zodiacal-light brightness (with time, polarization, and color again neglected) has only two dimensions. Thus, the observations alone are not sufficient to specify all the properties of the cloud. Nonetheless, with reasonable simplifications, the observations are enough to deduce some important average properties.

Hapke (1965) has shown that the effect of low-energy proton bombardment on a wide variety of substances is to make their scattering functions nearly similar. Thus, we can expect that all except the newest zodiacal particles in fact have approximately the same scattering function, as a consequence of the solar wind. For this paper, however, it is sufficient to assume that there is a homogeneous mixture of particles. The scattering function to be found here is, then, a mean scattering function.

I will assume here that the zodiacal light is scattered primarily by a heliocentric, and not a geocentric, cloud. It is then clear that the cloud is symmetric about an axis through the sun and the ecliptic poles. Large or small deviations from symmetry must occur, but they will be neglected.

The space-density distribution is thus a two-dimensional one. A point in this distribution will be specified here by its radius vector r and its heliocentric latitude β.

The particles in the cloud spiral toward the sun under the influence of the Poynting-Robertson effect (Whipple, 1955). Figure 1 (from Southworth, 1964) shows the time average of the relative space density of a single particle, as a function of r. Figure 2 shows schematically the relative space density to be expected from many such particles injected into the cloud as cometary debris. These are released near the perihelia of the comets, with nearly parabolic initial orbits (Southworth, 1964). The initial perihelia of the particles are thus the same as those of the comets, roughly half of which (Richter, 1963) lie between 0.5 and 1.5 a.u.

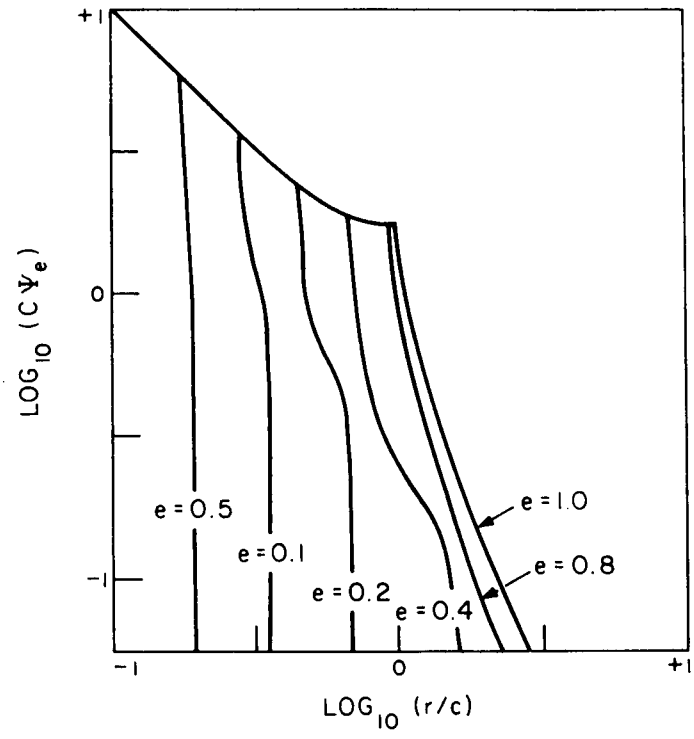

Figure 1. Average space density Ψ_e of particles spiraling toward the sun under the Poynting-Robertson effect, as a function of radius vector r, orbital invariant $C = (a/2)(1 - e^2)e^{-4/5}$, and initial eccentricity e. For any value of e the graph of Ψ_e consists of a nearly vertical curve (interpolated if necessary) marked with the value of e, and also of that part of the upper diagonal curve that lies to the left of the nearly vertical curve. The intersection of the two curves occurs at the perihelion distance of the initial orbit.

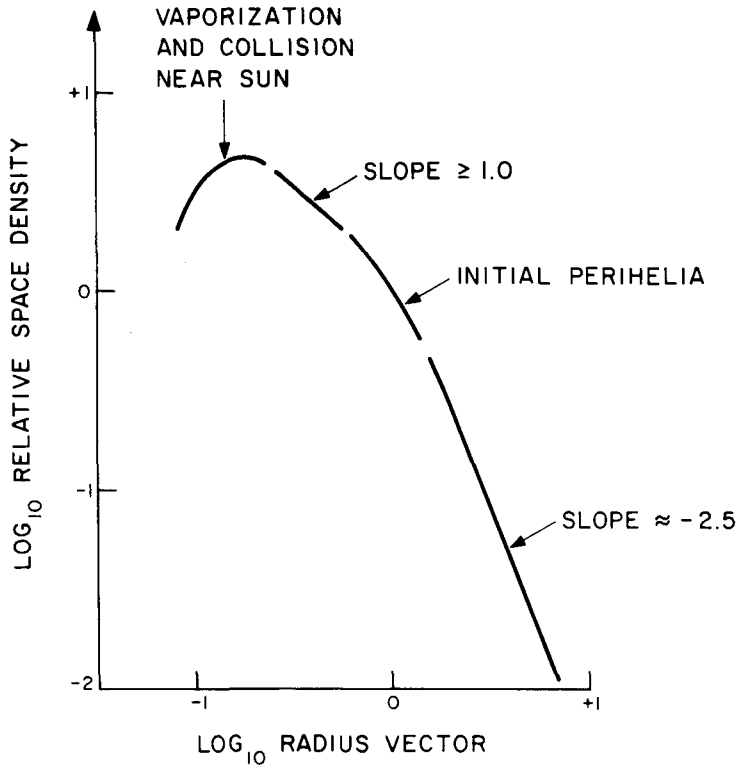

Figure 2. Schematic density distribution under the Poynting-Robertson effect.

The Poynting-Robertson effect does not alter the plane of a particle's orbit, but it gradually alters the distribution of true anomalies in the orbit. Initially, when the orbit is highly eccentric, the particle spends most of its time near aphelion, with true anomaly in the neighborhood of 180°. Later, when the orbit is less eccentric, true anomalies are more uniformly spread. Since this will also change the distribution of heliocentric latitudes, an estimate of the magnitude of the change is needed here. On the hypothesis of a cometary origin for the zodiacal particles (and also on some other hypotheses), it is expected that the initial orbits of the particles will be similar to the orbits of short-period comets. This is because a few of the particles will be released from short-period comets, and many of the rest, released from bright long-period comets, will soon be perturbed by Jupiter into short-period orbits in exactly the same way that the comets themselves are perturbed. Like the comets (Porter, 1963), the particles will have values

of the argument of perihelion clustered near 0° and 180°; i.e., their aphelia and perihelia will tend to be at lower heliocentric latitudes than the intermediate sections of their orbits.

Figure 3 is a contour diagram of the time average of the relative space density of a particle under the Poynting-Robertson effect, as a function of both radius vector and true anomaly, computed by numerical integration. It shows how the space densities in Figure 1 are distributed over true anomaly. To see how the Poynting-Robertson effect will alter the distribution of heliocentric latitudes, we should compare the average of the densities near perihelion and aphelion (which will be at relatively low latitudes) with the densities in the neighborhood of true anomaly 90° (which will be at relatively high latitudes). We find that, at distances more than two to three times the initial perihelion distance, the particles are concentrated toward aphelion, and hence toward low latitudes. At less than twice the initial perihelion distance, however, the distribution of latitudes will not be significantly biased by the distribution of true anomalies. It follows that the zodiacal cloud should be appreciably more concentrated at low latitudes at roughly 2 or more a.u. from the sun than at roughly 1 or less a.u.

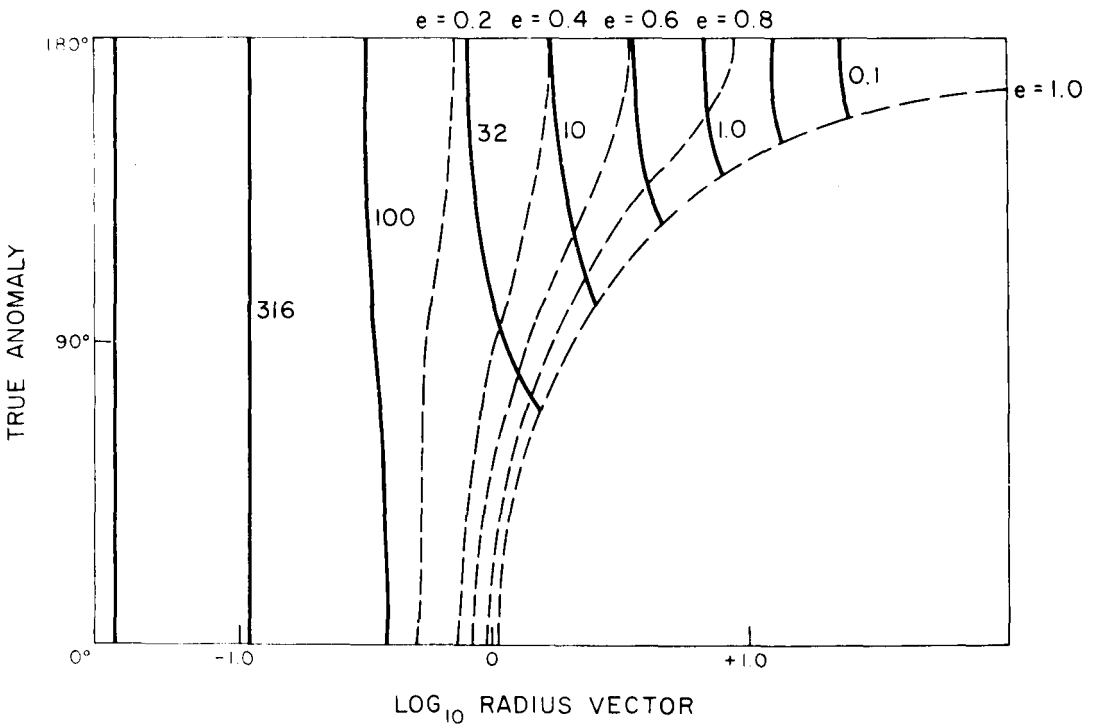

Figure 3. Relative density contours under the Poynting-Robertson effect.

2. MODEL CLOUD

The model of the zodiacal cloud used in the computations to be reported here is defined by three 1-dimensional distributions. The scattering function phase function $T(\theta)$ denotes the light intensity scattered at an angle θ by a unit particle space density, and is assumed to be the same in all parts of the cloud. The light scattered is taken to be proportional to the space density ρ, which is assumed to depend only on r and β and to be of the form

$$\rho(r,\beta) = R(r)\, S(\beta) \quad . \tag{1}$$

Thus, the expected dependence of the latitude distribution on distance from the sun is not included in the model. Since no observations at less than 30° elongation from the sun have been used, and since contributions to the observed zodiacal light from more than about 2 a.u. from the sun are small, the latitude distribution to be found here represents an average over the range 0.5 to 2 a.u.

In order not to spend a disproportionate amount of computing time on the relatively small volume of space at high heliocentric latitudes, the distribution S is treated as a function of $\sin\beta$ rather than of β; equal intervals of $\sin\beta$ represent equal volumes in space.

A variety of distributions $R(r)$, of a form suggested by Figure 2, are assumed. Given R, S, and T, we can formally compute zodiacal-light intensities as

$$I = \int_{\substack{\text{line of} \\ \text{sight}}} R\, S\, T\, ds \quad , \tag{2}$$

where ds is the differential of distance along the line of sight from the earth. Since I is a two-dimensional distribution, it suffices to determine a two-dimensional distribution of S and T. For simplicity and numerical stability, however, S and T were assumed to be independent one-dimensional distributions. They are found by successive approximations, as described below.

3. COMPUTING

The radial density distribution was taken to be of the form

$$\log_{10} R(r) = C_1 \log_{10} r + C_2 (\log_{10} r)^2 \quad . \tag{3}$$

This is smooth (which is essential) and adequately versatile. Table 1 shows the values used for C_1 and C_2.

The functions S and T are each taken to be the sum of seven triangular functions, multiplied by coefficients

$$S(\sin \beta) = \sum_{j}^{7} S_j s_j (\sin \beta) \quad ;$$

$$T(\theta) = \sum_{k}^{7} T_k t_k (\theta) \quad . \tag{4}$$

Figure 4 shows how the sum forms a function defined at seven points whose ordinates are the coefficients S_j or T_k, with straight-line segments joining the points.

The observational equations (2) now become

$$I = \sum_{j} S_j \sum_{k} T_k \int_{\substack{\text{line of} \\ \text{sight}}} s_j t_k R \, ds \quad . \tag{5}$$

Table 1. Numerical results for 11 radial distributions.

Case	Radial distribution coefficients		rms residual in intensity	Latitude-distribution coefficients							Phase-function coefficients						
	C_1	C_2		0.0	0.1	0.3	0.5	0.7	0.9	1.0	30°	54°	79°.2	104°.4	129°.6	154°.8	180°
1	-0.6	-4	0.492	1.0	0.83	0.52	0.35	0.20	0.16	0.18	2.50	0.29	0.42	0.45	0.61	0.77	1.0
2	-0.6	-2	0.499	1.0	0.85	0.54	0.36	0.21	0.17	0.19	2.52	0.31	0.48	0.49	0.69	0.77	1.0
3	-0.6	0	0.540	1.0	0.87	0.57	0.38	0.22	0.19	0.21	2.72	0.35	0.60	0.56	0.76	0.75	1.0
4	-1.2	-4	0.393	1.0	0.83	0.51	0.36	0.22	0.18	0.20	1.59	0.12	0.32	0.41	0.64	0.76	1.0
5	-1.2	-2	0.383	1.0	0.84	0.52	0.37	0.23	0.19	0.21	1.41	0.12	0.36	0.44	0.66	0.76	1.0
6	-1.2	0	0.399	1.0	0.87	0.54	0.39	0.24	0.20	0.23	1.22	0.13	0.42	0.48	0.70	0.76	1.0
7	-1.8	-4	0.313	1.0	0.83	0.50	0.37	0.24	0.20	0.22	0.85	0.00	0.24	0.38	0.63	0.76	1.0
8	-1.8	-2	0.297	1.0	0.84	0.51	0.38	0.25	0.20	0.23	0.52	0.00	0.26	0.40	0.64	0.76	1.0
9	-1.8	0	0.302	1.0	0.86	0.53	0.40	0.27	0.21	0.24	0.10	0.00	0.28	0.44	0.66	0.76	1.0
10	-2.4	-2	0.419	1.0	0.85	0.51	0.38	0.27	0.21	0.23	0.00	0.00	0.13	0.41	0.59	0.75	1.0
11	-2.4	0	0.582	1.0	0.88	0.54	0.39	0.27	0.23	0.26	0.00	0.00	0.11	0.44	0.60	0.76	1.0

The integrals in equation (5) are evaluated numerically. The integration was continued to r = 5 a.u., beyond which contributions are negligible.

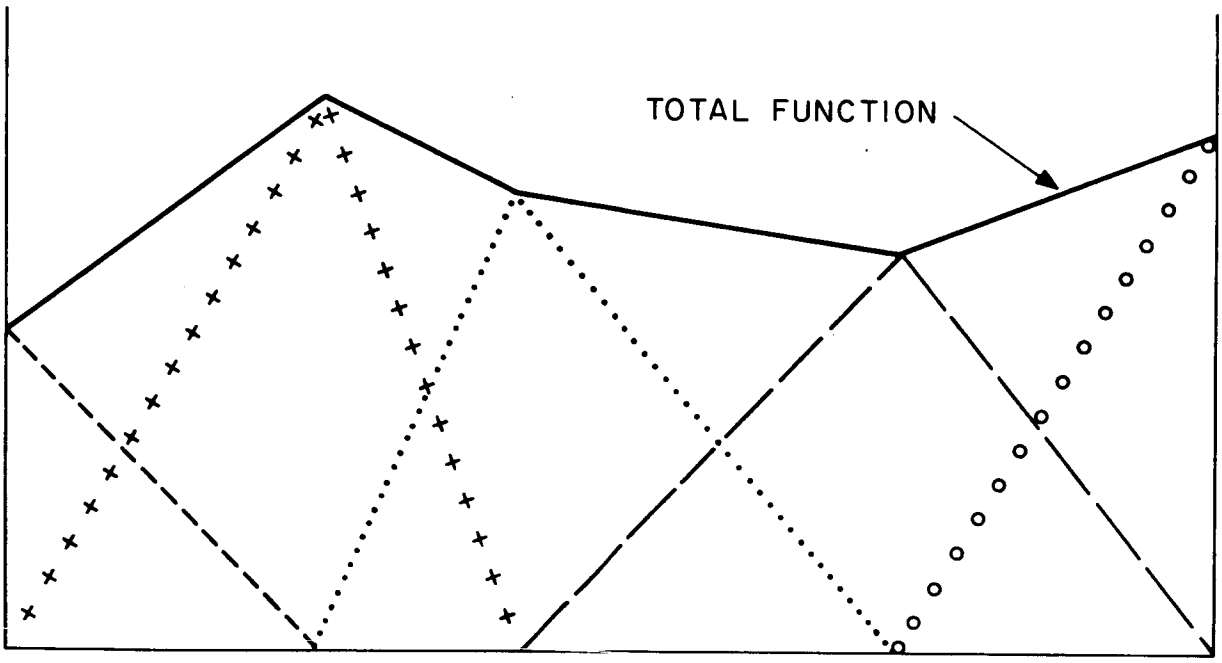

Figure 4. Resolution of a function consisting of n connected straight-line segments into a sum of n + 1 triangular functions.

Initial trial values are assumed for both S_j and T_k, and then equations (5) are solved by least squares for improved values of S_j and T_k, alternately. However, the least-squares solution is not allowed to make any coefficient negative or to make any very large change that might cause unstable iteration. When a coefficient would have exceeded one of these bounds, it is set equal to that bound, and a new least-squares solution is carried out for the remaining variables.

Ten iterations or fewer were sufficient in each case to reach a stable solution.

4. OBSERVATIONS

Smith, Roach, and Owen's (1965) observations have been used. Following their estimates of observational errors, I took the standard error σ of an intensity I to be

$$\sigma = (361 + 0.01\, I^2)^{\frac{1}{2}} \quad . \tag{6}$$

They note an excess brightness in their observations at an elongation of about 65°. This excess was not observed by Wolstencraft and Rose (1967) and cannot be reconciled with a model of zodiacal particles under the Poynting-Robertson effect. Accordingly, I have empirically drawn smooth curves through the observations and have removed this excess. Appendix A describes a possible, but not very probable, cause for the excess brightness. Table 2 contains the observations used, as corrected.

Table 2 presents observations used for all cases, and includes detailed results for case 8. The observations were corrected for the excess brightness observed at 65° elongation from the sun. Three hundred were then chosen to represent the distribution over the whole sky, with comparatively few in the region of small elongation, which was not so well observed as other regions.

The table is arranged in rows by latitude. For each point, the quantities printed are: the longitude measured from the sun, the corrected intensity, the residual from the final fit, and the residual divided by the standard error assigned to the observation.

Table 2. Reticuled results for case 8

LAT																				
0.	LONG	30.	35.	40.	45.	50.	55.	60.	65.	70.	75.	80.	85.	90.	95.	100.	105.	110.	115.	120.	125.
	INT	2330.	1595.	1185.	945.	745.	600.	500.	425.	370.	320.	290.	265.	250.	235.	220.	210.	200.	190.	185.	180.
	O-C	228.7	77.2	51.8	70.2	45.5	19.9	6.7	-2.1	-5.3	-14.1	-10.9	-9.4	-3.4	-1.8	-3.7	-3.8	-5.8	-9.2	-8.4	-8.3
	*/SIG	0.98	0.48	0.43	0.73	0.59	0.32	0.12	-0.04	-0.13	-0.38	-0.31	-0.29	-0.11	-0.06	-0.13	-0.13	-0.21	-0.34	-0.32	-0.32

LONG	130.	135.	140.	150.	160.	170.	180.
INT	175.	175.	175.	170.	175.	185.	205.
O-C	-8.4	-4.1	-1.0	-4.1	-5.3	-5.6	1.4
*/SIG	-0.32	-0.16	-0.04	-0.16	-0.20	-0.21	0.05

LAT																				
5.	LONG	35.	40.	45.	50.	55.	60.	65.	70.	75.	80.	85.	90.	95.	100.	105.	110.	120.	130.	140.	150.
	INT	1145.	870.	735.	610.	505.	425.	370.	335.	300.	275.	255.	235.	215.	205.	200.	190.	180.	175.	170.	165.
	O-C	-41.2	-44.7	9.1	15.9	1.6	-10.7	-12.7	-5.5	-6.4	-3.3	-0.6	-2.5	-8.2	-7.0	-3.4	-6.6	-6.0	-2.0	-0.3	-3.6
	*/SIG	-0.35	-0.50	0.12	0.25	0.03	-0.23	-0.31	-0.14	-0.18	-0.10	-0.02	-0.08	-0.28	-0.25	-0.12	-0.24	-0.23	-0.08	-0.01	-0.14

LONG	160.	170.	180.
INT	170.	175.	195.
O-C	-4.5	-8.8	3.6
*/SIG	-0.18	-0.34	0.13

LAT																				
10.	LONG	35.	40.	45.	50.	55.	60.	65.	70.	75.	80.	85.	90.	95.	100.	105.	150.	180.		
	INT	845.	655.	555.	485.	430.	380.	345.	310.	285.	255.	235.	215.	205.	195.	190.	160.	185.		
	O-C	5.9	-28.2	-11.3	3.7	8.7	5.7	9.4	6.4	8.0	0.8	-0.9	-5.9	-4.0	-4.6	-2.5	-2.6	5.6		
	*/SIG	0.07	-0.41	-0.19	0.07	0.18	0.13	0.24	0.18	0.23	0.02	-0.03	-0.21	-0.14	-0.17	-0.09	-0.11	0.21		

LAT																				
15.	LONG	30.	35.	40.	45.	50.	55.	60.	65.	70.	75.	80.	85.	90.	95.	100.	110.	120.	130.	140.	150.
	INT	905.	690.	505.	425.	370.	330.	305.	285.	265.	245.	230.	215.	200.	190.	185.	175.	170.	165.	160.	155.
	O-C	110.8	53.8	-14.8	-12.1	-10.6	-13.2	-9.1	-4.0	-1.9	-2.5	-0.6	-1.1	-4.3	-4.8	-2.4	-2.4	-0.3	0.9	1.3	-1.7
	*/SIG	1.20	0.75	-0.27	-0.26	-0.25	-0.35	-0.25	-0.12	-0.06	-0.08	-0.02	-0.04	-0.16	-0.18	-0.09	-0.09	-0.01	0.04	0.05	-0.07

LONG	160.	170.	180.
INT	155.	160.	175.
O-C	-4.6	-5.4	6.8
*/SIG	-0.19	-0.22	0.26

LAT																				
20.	LONG	30.	35.	40.	45.	50.	55.	60.	65.	70.	75.	80.	85.	90.	95.	100.	120.	150.	180.	
	INT	545.	450.	390.	345.	315.	290.	270.	255.	240.	225.	210.	195.	185.	180.	175.	165.	150.	165.	
	O-C	-40.9	-40.7	-25.6	-14.3	-5.6	-3.6	-0.9	3.4	5.0	4.4	2.0	-2.1	-3.2	-1.0	-0.2	2.4	-1.0	7.1	
	*/SIG	-0.71	-0.83	-0.59	-0.36	-0.15	-0.10	-0.03	0.11	0.16	0.15	0.07	-0.08	-0.12	-0.04	-0.01	0.10	-0.04	0.28	

LAT																				
25.	LONG	25.	30.	35.	40.	45.	50.	55.	60.	65.	70.	75.	80.	85.	90.	95.	110.	120.	130.	140.	150.
	INT	520.	465.	410.	360.	315.	285.	255.	240.	225.	210.	200.	190.	180.	175.	170.	165.	160.	155.	155.	150.
	O-C	27.1	36.5	33.7	27.9	16.8	10.4	-1.4	0.2	-0.2	-2.2	-0.7	-0.2	-1.6	0.6	1.3	6.3	5.1	3.5	7.5	4.7
	*/SIG	0.49	0.73	0.75	0.68	0.46	0.30	-0.04	0.01	-0.01	-0.08	-0.02	-0.01	-0.06	0.02	0.05	0.25	0.20	0.14	0.31	0.19

LONG	160.	170.	180.
INT	145.	150.	155.
O-C	-0.3	3.1	7.0
*/SIG	-0.01	0.13	0.28

Table 2. (Cont.)

LAT	LONG	30.	40.	50.	60.	70.	80.	90.	100.	120.	150.	180.
30.	INT	300.	250.	230.	200.	180.	160.	155.	155.	145.	145.	150.
	O-C	-24.7	-17.6	-7.6	-14.6	-14.1	-16.5	-8.5	-0.3	-3.3	4.2	9.3
	*/SIG	-0.70	-0.56	-0.26	-0.53	-0.54	-0.67	-0.35	-0.01	-0.14	0.18	0.38

LAT	LONG	25.	30.	35.	40.	45.	50.	55.	60.	65.	70.	75.	80.	85.	90.	95.	110.	120.	130.	140.	150.
35.	INT	245.	230.	225.	215.	205.	200.	195.	185.	180.	175.	170.	170.	165.	160.	155.	150.	150.	145.	145.	140.
	O-C	-37.4	-27.7	-12.2	-7.3	-8.8	-7.7	-5.7	-8.3	-5.9	-3.7	-1.7	5.1	5.8	5.5	4.4	5.7	7.5	4.1	6.2	3.4
	*/SIG	-1.21	-0.93	-0.41	-0.25	-0.31	-0.28	-0.21	-0.31	-0.23	-0.14	-0.07	0.20	0.23	0.22	0.18	0.23	0.31	0.17	0.26	0.14

	LONG	160.	170.	180.
	INT	135.	135.	140.
	O-C	-0.6	-0.4	4.6
	*/SIG	-0.03	-0.02	0.20

LAT	LONG	15.	25.	35.	45.	55.	65.	75.	85.	120.	150.	180.
40.	INT	235.	225.	215.	205.	190.	170.	160.	155.	135.	125.	125.
	O-C	-26.2	0.2	13.7	15.4	9.7	-0.6	-0.1	4.5	-2.3	-8.2	-6.4
	*/SIG	-0.87	0.01	0.48	0.55	0.36	-0.02	-0.00	0.18	-0.10	-0.36	-0.28

LAT	LONG	10.	15.	20.	25.	30.	35.	40.	45.	50.	55.	60.	65.	70.	75.	80.	90.	100.	110.	120.	130.
45.	INT	210.	205.	205.	200.	195.	190.	185.	180.	170.	165.	155.	145.	140.	135.	135.	135.	135.	135.	135.	135.
	O-C	-8.2	-3.9	6.8	11.2	12.8	11.5	9.8	8.2	1.5	-0.1	-6.5	-12.9	-14.1	-15.1	-11.4	-5.0	-0.7	1.5	2.3	2.9
	*/SIG	-0.29	-0.14	0.24	0.40	0.47	0.43	0.37	0.31	0.06	-0.00	-0.26	-0.54	-0.60	-0.65	-0.49	-0.21	-0.03	0.07	0.10	0.12

	LONG	140.	150.	160.	170.	180.
	INT	135.	130.	130.	130.	130.
	O-C	3.5	-0.5	0.7	1.3	1.5
	*/SIG	0.15	-0.02	0.03	0.06	0.06

LAT	LONG	0.	10.	20.	30.	40.	50.	60.	70.	100.	140.	180.
50.	INT	180.	180.	175.	170.	165.	160.	155.	145.	135.	130.	125.
	O-C	-5.2	-1.2	2.4	4.5	4.4	4.1	4.3	0.0	4.1	1.9	-1.4
	*/SIG	-0.20	-0.05	0.09	0.18	0.17	0.16	0.17	0.00	0.18	0.08	-0.06

LAT	LONG	0.	5.	10.	15.	20.	25.	30.	35.	40.	45.	50.	55.	60.	65.	70.	75.	90.	105.	120.	135.
55.	INT	165.	165.	165.	160.	160.	155.	150.	150.	145.	145.	140.	140.	135.	135.	130.	130.	130.	130.	125.	120.
	O-C	1.7	2.1	3.2	-0.1	2.0	-0.8	-3.5	-1.4	-4.5	-2.8	-6.0	-4.0	-7.0	-4.9	-7.5	-5.1	0.7	4.1	0.1	-4.9
	*/SIG	0.07	0.08	0.13	-0.00	0.08	-0.03	-0.15	-0.06	-0.19	-0.12	-0.25	-0.17	-0.30	-0.21	-0.33	-0.22	0.03	0.18	0.00	-0.22

	LONG	150.	165.	180.
	INT	125.	125.	125.
	O-C	0.2	0.4	0.5
	*/SIG	0.01	0.02	0.02

LAT	LONG	0.	15.	30.	45.	60.	75.	100.	140.	180.
60.	INT	155.	150.	145.	140.	135.	125.	125.	125.	125.
	O-C	5.1	1.9	1.0	0.5	-0.1	-4.7	1.8	3.1	3.0
	*/SIG	0.21	0.08	0.04	0.02	-0.00	-0.21	0.08	0.14	0.13

LAT	LONG	0.	10.	20.	30.	40.	50.	60.	70.	80.	90.	100.	110.	120.	130.	140.	150.	160.	170.	180.
65.	INT	150.	150.	145.	140.	140.	135.	130.	130.	125.	125.	120.	120.	125.	125.	125.	125.	125.	125.	125.
	O-C	9.9	10.4	6.7	3.6	5.8	3.2	0.7	3.5	1.0	3.1	-1.4	0.6	6.0	5.9	5.8	5.6	5.5	5.4	5.4
	*/SIG	0.41	0.43	0.28	0.15	0.25	0.14	0.03	0.15	0.04	0.13	-0.02	0.03	0.27	0.26	0.25	0.25	0.24	0.24	0.24

LAT	LONG	0.
70.	INT	145.
	O-C	12.5
	*/SIG	0.52

Table 2. (Cont.)

LAT	LONG	0.	15.	30.	45.	60.	75.	90.	105.	120.	135.	150.	165.	180.
75.	INT	135.	135.	130.	130.	130.	125.	125.	120.	120.	115.	115.	115.	115.
	O-C	8.7	9.0	5.2	7.1	9.0	6.0	7.6	3.8	4.5	-0.2	-0.1	-0.2	-0.3
	*/SIG	0.37	0.39	0.23	0.31	0.39	0.26	0.33	0.17	0.20	-0.01	-0.01	-0.01	-0.01

LAT	LONG	0.	20.	40.	60.	80.	100.	120.	140.	160.	180.
80.	INT	130.	130.	125.	125.	125.	115.	115.	115.	115.	115.
	O-C	8.8	9.2	5.3	6.8	8.3	-0.5	0.4	0.8	1.1	1.1
	*/SIG	0.38	0.40	0.23	0.30	0.37	-0.02	0.02	0.04	0.05	0.05

LAT	LONG	0.	20.	40.	60.	80.
85.	INT	125.	125.	115.	110.	110.
	O-C	7.6	7.8	-1.8	-6.2	-5.6
	*/SIG	0.33	0.34	-0.08	-0.28	-0.25

LAT	LONG	0.
90.	INT	110.
	O-C	-5.0
	*/SIG	-0.23

5. LATITUDE DISTRIBUTION

Table 1 shows the radial-density distributions used and the resulting rms error of an individual observation in units of the expected observational error. All these radial distributions make acceptable fits to the observations, but the best fit is case 8, which is also the best fit to Figure 2. Table 2 includes the individual residuals of each observation for case 8, both in the original units and in terms of the estimated observational error.

Table 1 shows all values found for the latitude coefficients S_j, which are remarkably insensitive to the radial distribution. Figure 5 shows the latitude distribution for case 8; the others hardly differ. The minor maximum at 90° latitude is not likely to be real. It possibly results from inadequate correction of the observations for the peak at elongation 65°, or more probably from the known inadequacy of the assumption expressed in equation (1).

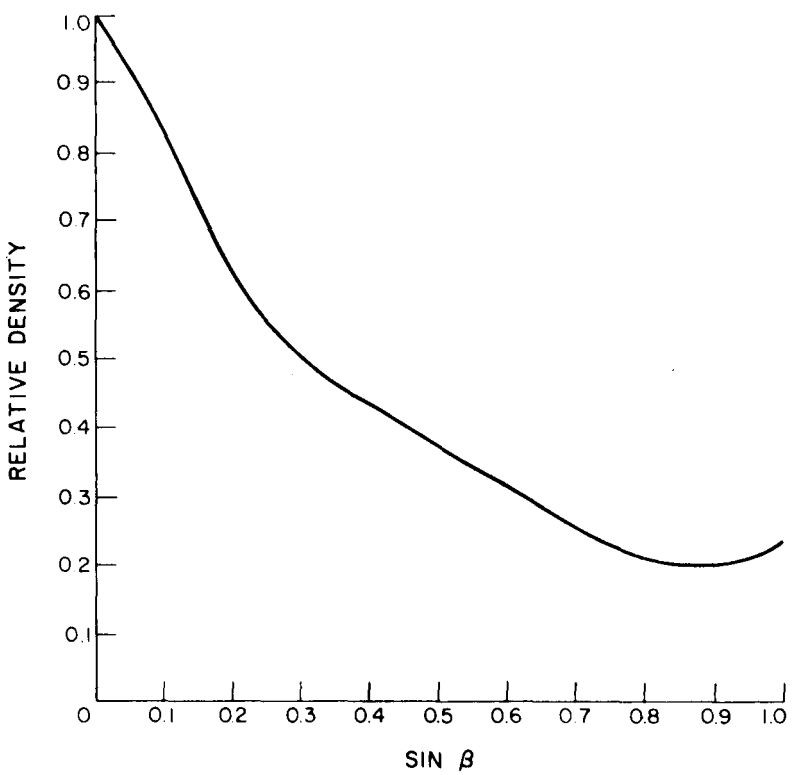

Figure 5. Latitude distribution for case 8.

The width of the latitude distribution is a very satisfactory confirmation that the zodiacal particles are in orbits like those of the short-period comets.

6. PHASE FUNCTION

Table 1 further gives all values for the phase function coefficients T_k; the distributions are plotted in Figure 6, with the scale successively displaced upward 0.1 for each distribution. The distribution found between 30° and 54° depends strongly on the assumed radial density. It is likely that this part of the phase function (if it is real) can be explained by classical diffraction.

The major part of the phase function found here is not very sensitive to the assumed radial-density distribution, and consequently merits some attention. It is doubtless possible to produce a similar curve with several different sorts of particles, especially as this is only an average curve. However, it should be pointed out that the function found is very similar to a Lambert law, which is the phase function in diffuse reflection by smooth spherical particles much larger than a wavelength of light. Figure 6 includes a Lambert-law curve fitted to case 8. Rough particles would be expected to show an extra peak in the phase function at 180° because shadows are then eliminated. The phase function found here, in fact, has just such a peak. It would be expected that particles from comets should be rough, in harmony with the phase function found.

One more confirmation is still available. According to classical theory (van de Hulst, 1957), the luminous intensity at wavelength λ diffracted at an angle θ to a distance r by a spherical particle of radius a under incident intensity I_0 is

$$I_D = \frac{a \lambda I_0}{2\pi^2 r^2 \sin^3 \theta} \quad , \tag{7}$$

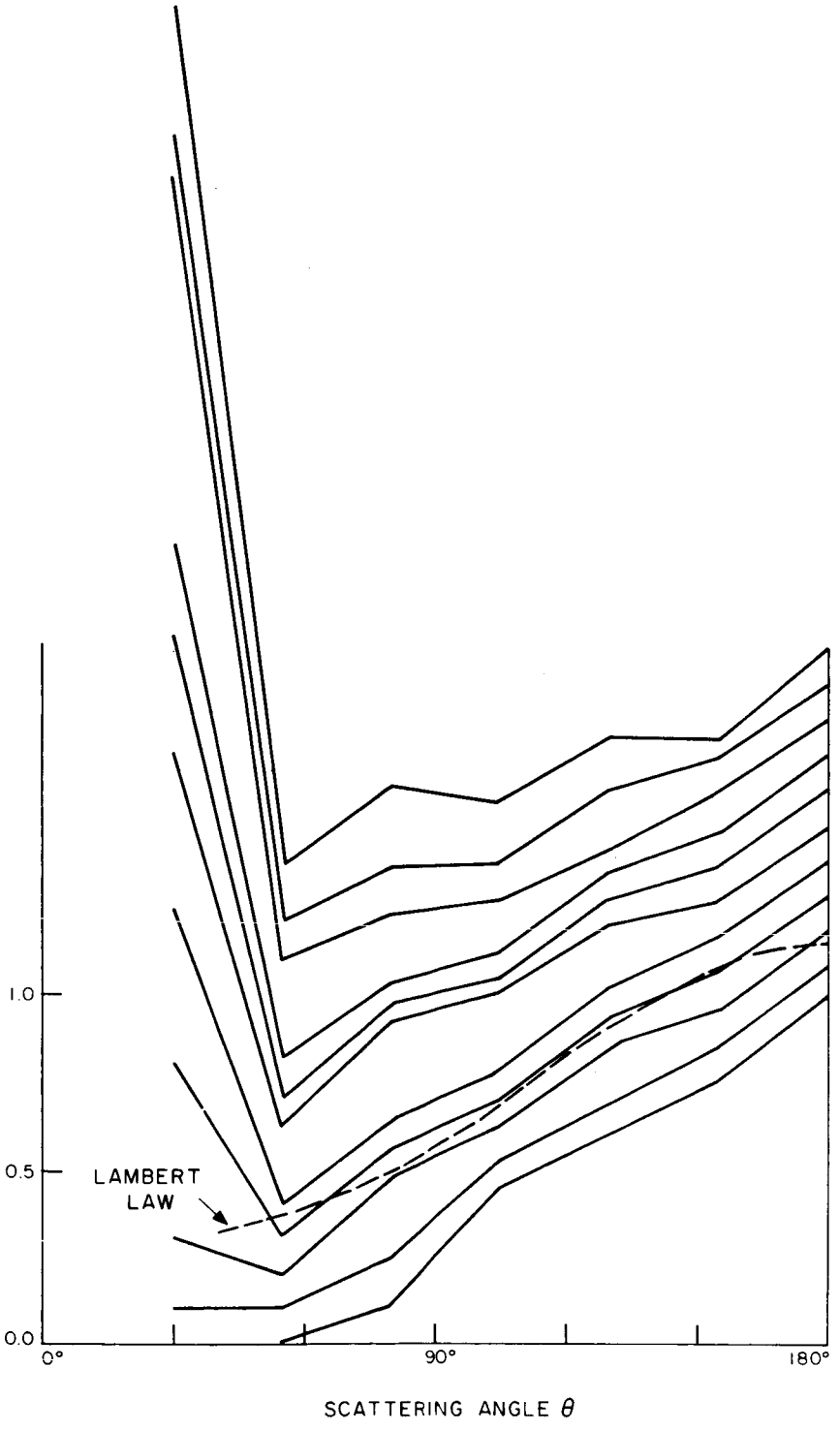

Figure 6. Phase functions.

if θ is outside the first few diffraction rings and if the rings have been smoothed out. The corresponding scattered intensity from a Lambert-law particle that scatters a fraction A of the total light incident on it is

$$I_L = \frac{2a^2 A I_0 (\sin\theta - \theta\cos\theta)}{3\pi r^2} \quad . \tag{8}$$

Evaluating I_D at $\theta = 30°$ and I_L at $\theta = 150°$, with $\lambda = 5300$ Å and $A = 0.07$ as for the moon, and comparing with the results of case 8, we find

$$a \sim 6\,\mu \quad .$$

This value can be no more than an order-of-magnitude estimate, both because we actually must consider distributions of particle sizes and because the phase-function results are uncertain. Nonetheless, it tends to confirm that the zodiacal particles are large compared to the wavelength of light, in harmony with the appearance of a phase function appropriate to large particles.

7. CONCLUSIONS

The latitude and radius-vector distributions deduced here are compared with the meteor space-density distribution (Southworth, 1967). The radius-vector distribution of the meteors is not so steep as case 8, or as the equilibrium Poynting-Robertson distribution. Presumably this difference is caused by collisions of the meteors with zodiacal dust; while collisions would be much less important for the zodiacal dust itself, which spirals in faster. The meteor latitude distribution is similar in character to that of the meteors, although the meteors have a wider distribution in latitude near the sun than far out. This characteristic was also theoretically expected in the zodiacal distribution, but had been omitted from the model for simplicity.

The space distribution of the zodiacal particles as found here is entirely accordant with a cometary origin and with subsequent evolution under planetary perturbations and the Poynting-Robertson effect.

The mean phase function of the zodiacal particles has a broad peak in the backscatter direction. The phase function is consistent with opaque, rough particles much larger than the wavelength of light.

APPENDIX A

The anomalous excess of brightness that Smith, Roach, and Owen (1965) found at approximately 65° elongation off the ecliptic could be explained by double scattering of sunlight in ice crystals at the noctilucent-cloud level. The light would be scattered twice, once into the common 22° halo and once into the 46° halo (see, for example, Minneart, 1954). Figure A-1 is a schematic diagram for the double scattering. Clouds B and D are approximately 82 km above sea level. Sight lines A and C pass above the tropopause (roughly 15 km above sea level), but they do not pass much above it because cloud B must be in sunlight at the same time that the sun is more than 18° below the horizon at F. The maximum depression of the sun at F, when A and C graze the tropopause and when D is 10° above the horizon at F, is 29°. Sight lines A and C are necessarily in different vertical planes. The azimuth difference between the planes is 14° to 19° when the scattering angle at B is 22°, and 43° to 46° when the scattering angle at B is 46°. Sight lines C and E are generally in different vertical planes.

When skew rays are considered, both the 22° and 46° halos are actually a few degrees wide even for monochromatic light. For simplicity, however, their width is neglected in Figure A-2, which is a schematic diagram on the celestial sphere for the case of 22° scattering at B. A comparable diagram for the case of 46° scattering at B can be readily imagined. The sun is depressed 18° to 29° below the horizon at F. Light scattered in the 22° halo at cloud B reaches cloud D only if it is in arc GH (or KL), the exact position depending on the distance from B to D. Point G is 5° nearer the horizon than the sun, and point H is 11° nearer. Light scattered in the 46° halo at cloud D reaches the observer at F anywhere on the arc MNP, but preferentially at low elevation because sight line E then has a longer path in cloud D. The observed excess brightness corresponds to light scattered to points near M or Q. Smith, Roach, and Owen did not observe below 10° elevation.

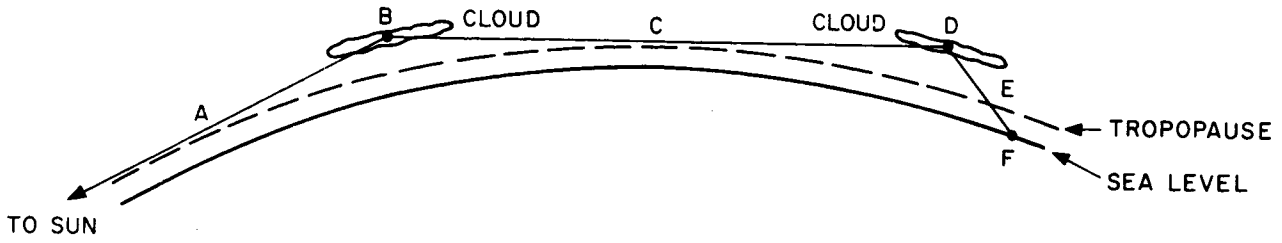

Figure A-1. Schematic model for double scattering of sunlight by ice clouds.

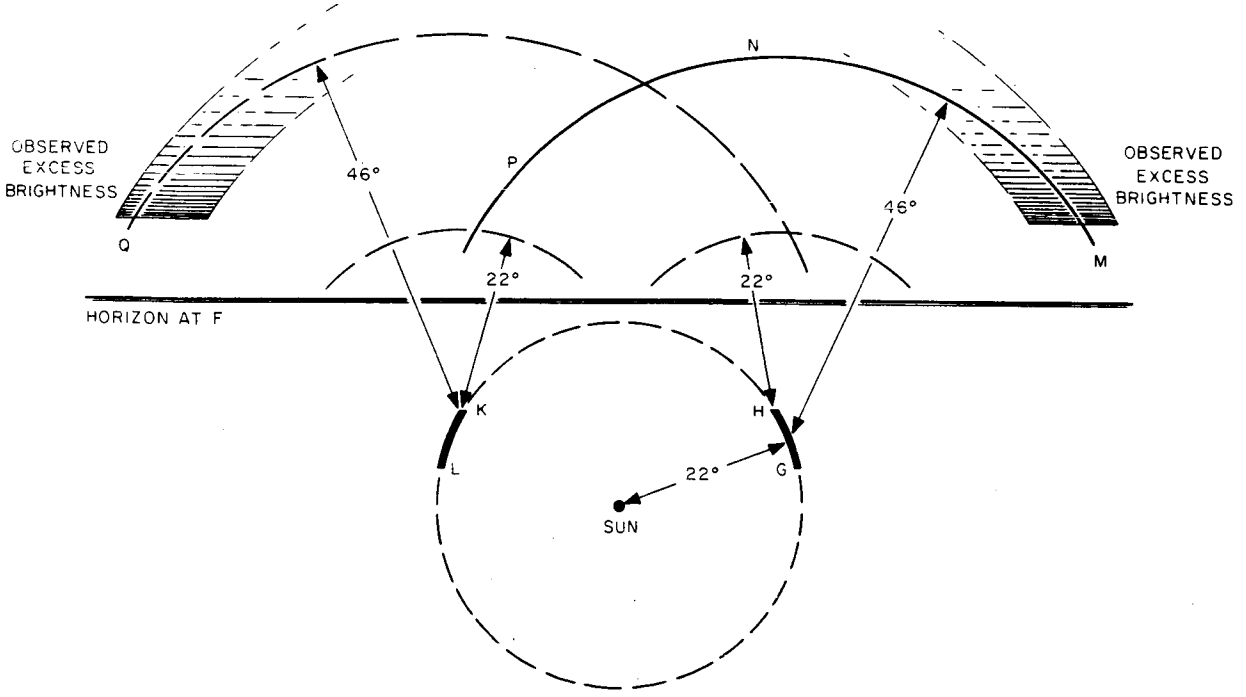

Figure A-2. The relationship between ice-crystal halos and observed excess brightness in the zodiacal light.

Light scattered to P and light scattered in the 22° halo at cloud D form a broad band of excess brightness superposed on the brightest part of the zodiacal light, and will not be readily distinguishable from other light.

The principal merit of this hypothesis of ice clouds is that the scattered light 60° to 70° from the sun would be strong only where it is actually observed – mostly at comparatively low elevation and at a different azimuth from the depressed sun. Under the circumstances of observation, this corresponds to high ecliptic latitude.

Only ice crystals that are large compared to the wavelength of light will form the halos. We can estimate the number density N cm^{-3} of crystals 5 μ in diameter that would reproduce the observed excess brightness, as follows. Let us assume light paths 100 km long in clouds B and D (Figure A-1) and ice-crystal cross sections $2 \times 10^{-7} cm^2$, so that the fraction of light intercepted by ice crystals in each cloud is approximately 2N. Let us estimate that 0.1 of the light incident on a crystal is scattered into the 22° halo, and 0.05 into the 46° halo. Let us further estimate that cloud D subtends a vertical angle of roughly 1° at B; then the fraction of the 22° halo light reaching D is 0.02, and the fraction of 46° halo light is 0.009. When the 46° scattering occurs at D, roughly 0.4 of the light is scattered toward the ground. However, only half this amount contributes to the excess brightness, because the shift at D in the azimuth of the ray must be in the same sense as the shift at B if the final elongation of the ray from the sun is to be about 65°. When the 22° scattering occurs at D, roughly 0.2 of the light is scattered toward the ground and half contributes to the excess brightness. Let us estimate that 0.7 of 5300 Å light is absorbed along each of paths A and C; absorption in path E is accounted for in original data reductions.

The total excess brightness observed by Smith, Roach, and Owen in the whole sky is approximately 1.15×10^5 10th magnitude stars, or 2×10^{-10} of the sun's brightness. Only half of this is actually observed at one time. Thus,

$$(2N)^2 (0.1) (0.05) [(0.02) (0.2) + (0.009) (0.1)] (0.3)^2 = 10^{-10} \quad ,$$

and

$$N = 3 \times 10^{-3} \quad .$$

These ice crystals constitute 1.6×10^{-5} of the atmospheric mass density at 82 km. They may be compared with the noctilucent cloud material collected by Hemenway, Soberman, and Witt (1964). If it is assumed that their "halos" are ice and that the cloud they sampled was near 82 km in height and 3 km thick, then their "halos" contained 1×10^{-5} to 4×10^{-5} of the atmospheric density as ice. The hypothetical cloud of 5-μ particles thus seems comparable in ice content to noctilucent clouds, but it would scatter less sunlight because its total cross section is 0.1 to 0.3 of that of the noctilucent cloud.

The principal fault with the hypothetical clouds is the lack of real noctilucent clouds at the same latitudes. The hypothetical clouds would presumably be formed under conditions similar to noctilucent clouds, except for a much smaller number of condensation nuclei. The first scattering cloud (B) ought to be observable in the Pacific Ocean at 30° to 35° N latitude, but it would be considerably fainter than normal noctilucent clouds. The second cloud (D) would be hard to detect except as the excess brightness found by Smith, Roach, and Owen. It is clear that these clouds might not have been seen previously even if they existed. However, the only noctilucent clouds so far observed at latitudes less than 45° were caused artificially by rocket launchings at Point Magu, California (Fogle and Haurwitz, 1966). I have not investigated whether the artificial clouds themselves might be important here.

From present knowledge of atmospheric temperature at noctilucent cloud heights, it seems unlikely, but not impossible, that the hypothetical ice clouds at 20° to 30° latitude actually exist. The necessary temperature for

persistence of ice depends on the water-vapor content of the atmosphere, which is ill known. If water vapor is as abundant as ice in the hypothetical cloud, i.e., 2×10^{-5} by mass of the atmosphere, then the frost point at 82 km is 159°K. However, for a preliminary measurement of water-vapor pressure at 79 km by Fedynski (quoted by Fogle and Haurwitz, 1966), the frost point is 179° K. According to CIRA (COSPAR Working Group IV, 1965), the mean temperature at 80 km and 30° north latitude is 199° K on September 1, which is a representative date for Smith, Roach, and Owen's excess brightness observations. Mean temperature at 60° N in June and July (representative for noctilucent clouds) are about 170° K. However, since measurements in noctilucent clouds reach down to 135° K (Fogle and Haurwitz, 1966), it is possible that variation from the mean temperature is necessary for the formation of a noctilucent cloud. A comparable variation might then cause one of the low-latitude ice clouds hypothesized here.

8. REFERENCES

COSPAR WORKING GROUP IV

1965. CIRA 1965, COSPAR International Reference Atmosphere 1965. North-Holland Publ. Co., Amsterdam, 313 pp.

FOGLE, B., AND HAURWITZ, B.

1966. Noctilucent clouds. Space Sci. Rev., vol. 6, pp. 278-340.

HAPKE, B.

1965. Effects of a simulated solar wind on the photometric properties of rocks and powders. Ann. N.Y. Acad. Sci., vol. 123, p. 711.

HEMENWAY, C. L., SOBERMAN, R. K., AND WITT, G.

1964. Sampling of noctilucent cloud particles. Tellus, vol. 16, pp. 84-88.

MINNAERT, M. G. J.

1954. The Nature of Light and Color in the Open Air. Transl. by H. M. Kremer-Priest, Dover Publ., New York, 362 pp.

PORTER, J. G.

1963. The statistics of comet orbits. In The Moon, Meteorites, and Comets, ed. by B. M. Middlehurst and G. P. Kuiper, Univ. of Chicago Press, Chicago, Illinois, pp. 550-572.

RICHTER, N. B.

1963. The Nature of Comets. Transl. by A. Beer, Methuen and Co., London, 221 pp.

SMITH, L. L., ROACH, F. E., AND OWEN, R. W.

1965. The absolute photometry of zodiacal light. Planet Space Sci., vol. 13, pp. 207-217.

SOUTHWORTH, R. B.

1964. The size distribution of the zodiacal particles. Ann. N. Y. Acad. Sci., vol. 119, pp. 54-67.

1967. Space density of radio meteors. This Special Report, pp. 75-97.

VAN DE HULST, H. C.

1957. Light Scattering by Small Particles. John Wiley and Sons, New York, 470 pp.

WHIPPLE, F. L.

1955. A comet model. III. The zodiacal light. Astrophys. Journ., vol. 121, pp. 750-770.

WOLSTENCRAFT, R. D., AND ROSE, L. J.

1967. Observations of the zodiacal light from a sounding rocket. Astrophys. Journ., vol. 147, pp. 271-292.

SPACE DENSITY OF RADIO METEORS

Richard B. Southworth

ABSTRACT

The space-density distribution of dust in the solar system is estimated from the orbits of approximately 13,000 radar meteors observed by the Harvard-Smithsonian Radio Meteor Project. Approximate corrections are made for unobservable classes of orbits and for other observational selection effects. Within the limits 0.1 to 10 a.u., the space density decreases monotonically outward from the sun. The distribution in heliocentric latitude has a very broad maximum centered on the ecliptic, and a deep minimum over the ecliptic poles. There is no evidence for any substantial enhancement of density in the asteroid belt. The distribution shows the effects of planetary perturbations and collisional destruction.

SPACE DENSITY OF RADIO METEORS

Richard B. Southworth

1. INTRODUCTION

This report presents the distribution of relative space densities of observed radio meteors, and also a distribution that is approximately corrected for inherent deficiencies in observation. Briggs (1962) computed densities assuming observed photographic meteor orbits as an injection distribution, and then assuming breakup into smaller particles, which would spiral into the sun under the Poynting-Robertson effect. These are the first published space densities of meteors known to me. I believe the present paper gives the first density distributions derived from observed meteors alone.

This work was supported in part by grants NSR 09-015-033 and NSR-158 from the National Aeronautics and Space Administration, grant NAS 9-4875 from NASA Manned Space Flight Center, Houston, Texas, and Contract AF 19(628)-3248 from the U.S. Air Force Cambridge Research Laboratories.

2. METEOR OBSERVATIONS

The data used here comprise 13,672 meteors observed between November 1962 and November 1965 by the six-station radar network of the Radio Meteor Project operated in Havana, Illinois, by the Harvard College and Smithsonian Astrophysical Observatories, and supported by the National Bureau of Standards, the National Science Foundation, and the National Aeronautics and Space Administration. The orbit of each meteor was computed from its observed speed and trajectory in the atmosphere, and its mass from the observed distribution of electrons left behind the meteor. Verniani and Hawkins's (1964) luminous efficiency was used in the latter computation.

Each meteor is assigned a weight proportional to the product of five factors. Factor (1) is the 1.33 power of the observed mass; this is proportional to the total mass of all sizes of particles down to any given limiting mass in a distribution of the form found by Hawkins and Upton (1958) for photographic meteors. Factor (2) depends on the altitude and azimuth of the observed radiant. It is the reciprocal of the probability found by Elford (1964) for observing the radiant, except that radiants with less than 10% relative probability of detection have been assigned zero weight. Such inherently improbable radiants are likely to result from observational or computational errors and should not be given their high theoretical weights. Factor (3) depends upon the declination of the observed radiant. It is inversely proportional to the fraction of the sidereal day during which a point at any given declination remains within the 10% contour of Elford's distribution. Factor (4) is unity for radiants north of the ecliptic and zero for radiants south of it, and thus the incompletely observed southern sky is eliminated from this analysis. Factor (5) is inversely proportional to a slight refinement of Öpik's (1951) probability that a body in an orbit of given semimajor axis a, eccentricity e, and inclination i will collide with the earth during one revolution of the body. This probability is

$$P = R_E^2 \frac{V_c^2}{\pi V_G V_R \sin i} , \qquad (1)$$

where R_E is the earth's radius, V_c is the geocentric velocity outside the atmosphere, V_G is the geocentric velocity after the earth's attraction is deducted, and V_R is the radial component of the heliocentric velocity. The refinement consists in the eccentricity of the earth's orbit not being neglected when computing

$$V_R = \left[\frac{2}{r} - \frac{1}{a} - \frac{a}{r^2} \left(1 - e^2 \right) \right]^{1/2} , \qquad (2)$$

where r is the earth's distance from the sun at the time the meteor is observed. Neglect of the refinement yields imaginary weights on a few meteors. In practice, if the difficulty is not recognized, these meteors may be grotesquely misweighted.

The weighted distribution of radio-meteor orbits represents, as accurately as the data permit us to determine it, the total orbital distribution down to a certain limiting mass of all meteors in orbits that have perihelia at ≥ 1 a. u. and aphelia at ≤ 1 a. u. Figure 1 gives the weighted distribution of the logarithms of observed masses. The optimum limiting mass representing these observations will be in the range $10^{-3.5}$ to 10^{-4} g.

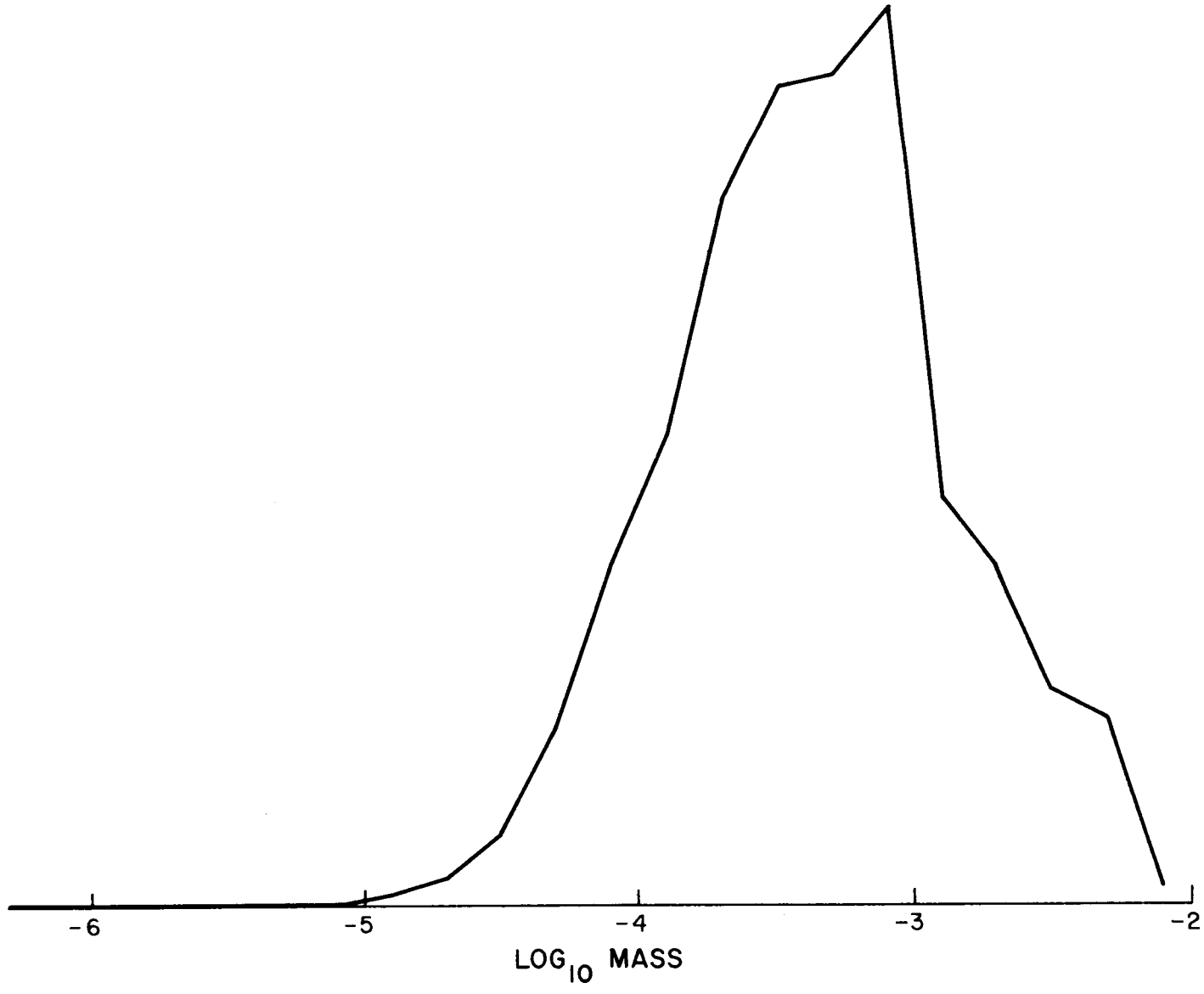

Figure 1. Relative frequency of mass (g) in the weighted sample.

3. UNCORRECTED RELATIVE SPACE DENSITY

Space density will be discussed here as a function of two dimensions in a plane normal to the ecliptic through the sun. Any dependence of space density of ecliptic longitude has been averaged out. The two dimensions used are: r, distance from the sun in astronomical units, and $\sin\beta$, the sine of the heliocentric ecliptic latitude.

For this computation, distance from the sun in the range $0.1 \leq r \leq 10$ is divided into 20 intervals, and sine latitude is also divided into 20 intervals. This yields 200 cells, with boundaries:

$$\left.\begin{matrix} \log_{10} r \\ \\ \sin\beta \end{matrix}\right\} = -1.0,\ -0.9,\ -0.8,\ \ldots\ ,\ +1.0 \quad . \tag{3}$$

The cell volumes are proportional to r_b^3, where r_b is either bounding r.

In each cell the relative space density is computed from the weighted sum of the residence times of all meteors passing through the cell, divided by the volume of the cell. The residence time is the time each meteor spends within a cell in the course of one orbital revolution. The residence times in the intervals of radius vector are computed exactly, but the subdivision into intervals of sine latitude within each radius vector interval is approximate. The approximation used is to apportion the time within each interval of radius vector as if the meteor's sine latitude had varied linearly with time from its value at one boundary of the interval to its value at the other boundary. However, if the meteor passed through perihelion or aphelion in any interval of radius vector, the time was apportioned as if the sine latitude had varied linearly from entering the interval to perhelion or aphelion, and then linearly at a different rate after that. Table 1 presents decimal logarithms of these uncorrected relative space densities.

4. AVERAGES WITH RESPECT TO ARGUMENT OF PERIHELION

All the observed orbits necessarily intersect the earth's orbit, and Table 1 shows a correspondingly large peak in density near the earth's orbit. A much better approximation to reality can be achieved by assuming that the longitudes of the nodes Ω are independent of the arguments of perihelion ω. In the present context, this is equivalent to assuming that ω is uniformly distributed from 0° to 360° independent of a, e, or i. In fact, complete uniformity is not expected, as will be discussed below, but the true distribution of ω cannot be calculated without numerous further assumptions and a great deal of effort.

To compute the space-density average over ω, we implicitly replace each observed meteor by a set of meteors that are similar except for a uniform distribution of ω. Thus each observed meteor will contribute to all cells between its perihelion and aphelion, and between latitudes $\pm$ i. From the well-known relation

$$\sin \beta = \sin i \sin (\omega + v) \quad , \tag{4}$$

where v is true anomaly (invariant under the averaging), it can easily be found that the relative frequency of values of $\sin \beta$ in the range $B_1 \leq \sin \beta \leq B_2$ is

$$F_{12} = \frac{1}{\pi}\left[\arcsin\left(\frac{B_2}{\sin i}\right) - \arcsin\left(\frac{B_1}{\sin i}\right)\right] \quad . \tag{5}$$

Table 2 presents space densities averaged over ω. They were computed without approximations from equation (5). Since these densities are symmetric about the ecliptic, only northern latitudes are presented.

Table 1. Logarithms of uncorrected relative space density

Sine latitude	Radius vector 0.100	0.126	0.158	0.199	0.251	0.316	0.398	0.501	0.631	0.794	1.00	1.26	1.58	1.99	2.51	3.16	3.98	5.01	6.31	7.94	10.0
1.0	4.474	4.506	4.335	4.258	4.166	3.861	3.830	3.802	3.686	3.507	3.418	3.061	2.917	2.853	2.523	2.301	2.039	1.984	1.781	1.400
	4.851	4.823	4.680	4.590	4.652	4.630	4.581	4.517	4.351	4.222	4.047	3.823	3.607	3.298	3.164	2.901	2.412	2.252	2.253	2.124
	5.134	5.121	5.096	5.000	4.931	4.927	4.878	4.734	4.603	4.507	4.356	4.115	3.847	3.661	3.333	3.148	2.988	2.711	2.291	2.018
	5.129	5.102	5.091	5.099	5.084	4.985	4.869	4.861	4.790	4.630	4.482	4.420	4.150	3.898	3.567	3.307	3.016	2.699	2.436	2.153
0.5	5.289	5.185	5.171	5.155	5.140	5.039	4.998	4.945	4.957	4.819	4.660	4.496	4.275	4.028	3.784	3.480	3.043	2.854	2.256	2.133
	5.212	5.312	5.275	5.231	5.241	5.140	5.105	5.048	5.125	4.942	4.772	4.722	4.469	4.194	3.937	3.509	3.237	2.908	2.489	2.365
	5.339	5.200	5.170	5.225	5.323	5.221	5.199	5.239	5.186	5.142	4.983	4.815	4.509	4.289	4.071	3.668	3.340	2.942	2.685	2.145
	5.374	5.193	5.209	5.186	5.264	5.277	5.303	5.320	5.411	5.313	5.204	5.064	4.801	4.452	4.263	3.909	3.600	3.157	2.763	2.507
	5.354	5.185	5.298	5.233	5.320	5.229	5.304	5.359	5.437	5.465	5.328	5.117	4.920	4.632	4.346	4.014	3.687	3.032	2.704	2.169
	5.337	5.245	5.295	5.253	5.291	5.272	5.236	5.291	5.435	5.701	5.618	5.109	4.795	4.422	4.255	3.833	3.545	2.922	2.453	1.973
0.0	5.426	5.305	5.299	5.278	5.357	5.305	5.257	5.395	5.492	5.754	5.580	4.992	4.607	4.431	4.039	3.740	3.418	3.145	2.740	2.501
	5.459	5.414	5.318	5.263	5.355	5.334	5.413	5.485	5.553	5.434	5.310	5.053	4.718	4.449	4.142	3.860	3.459	3.132	2.842	2.544
	5.305	5.478	5.323	5.312	5.328	5.341	5.480	5.431	5.349	5.240	5.075	4.963	4.793	4.479	4.179	3.932	3.549	3.115	2.935	2.872
	5.311	5.433	5.326	5.287	5.300	5.225	5.225	5.210	5.222	5.016	4.974	4.852	4.514	4.212	3.961	3.596	3.228	3.042	2.495	2.224
-0.5	5.400	5.352	5.366	5.269	5.205	5.071	5.238	5.161	5.022	5.013	4.794	4.563	4.391	4.098	3.708	3.433	3.257	2.814	2.460	2.195
	5.316	5.297	5.296	5.253	5.151	5.097	5.083	5.034	4.917	4.853	4.590	4.463	4.230	3.970	3.616	3.340	3.132	2.792	2.488	2.146
	5.284	5.282	5.201	5.101	5.109	5.037	4.921	4.930	4.772	4.652	4.379	4.284	3.990	3.719	3.511	3.180	2.907	2.611	2.045	1.872
	5.095	5.148	5.135	5.191	5.013	4.903	4.790	4.771	4.568	4.430	4.251	4.071	3.735	3.466	3.252	3.055	2.833	2.359	2.172	1.979
	4.722	4.812	4.836	4.749	4.755	4.590	4.563	4.486	4.332	4.067	3.900	3.696	3.561	3.296	3.069	2.775	2.453	2.345	1.919	1.661
-1.0	4.348	4.234	4.203	4.223	4.132	4.069	4.073	3.828	3.775	3.557	3.303	3.176	3.008	2.772	2.592	2.136	2.023	1.846	1.632	1.179

Table 2. Logarithms of relative space density averaged with respect to ω

Sine latitude																					
1.0	4.423	4.290	4.259	4.195	4.106	4.095	4.150	4.114	4.060	4.059	3.892	3.473	3.127	2.806	2.484	2.202	1.994	1.811	1.582	1.263
	4.735	4.708	4.753	4.707	4.631	4.578	4.549	4.524	4.470	4.465	4.314	3.935	3.600	3.308	3.008	2.719	2.457	2.193	1.931	1.668
	5.115	5.036	5.058	4.976	4.884	4.836	4.759	4.775	4.693	4.716	4.574	4.223	3.852	3.524	3.228	2.986	2.732	2.429	2.134	1.903
	5.201	5.081	5.112	5.038	5.003	4.905	4.854	4.846	4.791	4.844	4.691	4.378	4.047	3.744	3.464	3.162	2.929	2.575	2.265	2.038
	5.301	5.215	5.156	5.095	5.127	4.992	4.991	4.949	4.948	4.997	4.838	4.538	4.226	3.919	3.634	3.360	3.057	2.751	2.393	2.115
0.5	5.367	5.329	5.251	5.184	5.183	5.085	5.071	5.032	5.055	5.104	4.947	4.652	4.345	4.082	3.788	3.492	3.175	2.811	2.461	2.167
	5.336	5.387	5.286	5.259	5.290	5.203	5.192	5.167	5.159	5.202	5.057	4.789	4.473	4.195	3.941	3.588	3.259	2.910	2.593	2.191
	5.363	5.364	5.340	5.302	5.335	5.295	5.345	5.345	5.356	5.378	5.254	4.974	4.734	4.418	4.144	3.818	3.449	3.117	2.817	2.595
	5.375	5.357	5.344	5.329	5.382	5.345	5.377	5.401	5.430	5.438	5.306	5.036	4.801	4.531	4.264	3.928	3.585	3.154	2.782	2.559
0.0	5.364	5.351	5.354	5.372	5.401	5.383	5.425	5.482	5.537	5.507	5.370	5.108	4.860	4.587	4.329	3.976	3.652	3.198	2.775	2.542

5. UNOBSERVABLE ORBITS

Orbits with aphelia < 1 a.u., or perihelia > 1 a.u., cannot be observed from the earth. A reasonable correction for these unobservable orbits is essential. The approximation used here is to extrapolate the observed two-dimensional distribution of 1/a and e into the range of unobservable orbits. It is assumed, for this purpose only, that the distribution of angular elements i, ω, and Ω is independent of a and e. Table 3 gives the weighted distribution of the 13,672 meteors with respect to 1/a and e. The relative density D in this array is approximately fitted by the following empirical formulas:

$$D = A\,E\ ,$$

$$A = \begin{cases} 15\,a & \text{if } a < 1 \\ 250 - 800\,a^{-1} + 955\,a^{-2} - 390\,a^{-3}, & \text{if } a > 1 \end{cases}$$

$$E = 4 + 6\,e + 3\,e^{2} - 16\,e^{3} + 4\,e^{4}\ . \qquad (6)$$

Figure 2 shows the region in the (1/a) - e distribution that can be observed at any given value of radius vector. The correction factor for unobservable orbits is computed as a function of radius vector r, and is the ratio of the integral of D over the region observable at r to the integral over the common region observable both at r and at the earth. These ratios were computed by numerical integration for the logarithmic midpoints of the radius vector cells used for computing density. They are printed in Table 4 in logarithmic form. Numerical experiments in fitting formulas other than (6) to the data yielded correction factors whose logarithms agreed with Table 4 to about 10%. They included formulas where the eccentricity distribution was made to depend upon the major axis, giving proportionately more low eccentricities in small orbits and high eccentricities in large orbits.

Table 3. Weighted relative distribution of 1/a and e in the observed sample of meteors

1/a											
2.0										6	
1.9									37	5	
1.8								85	40	21	
1.7							69	93	66	84	
1.6						30	55	91	188	53	
1.5					39	59	60	113	120	37	
1.4				2	38	98	219	50	136	101	46
1.3			5	55	130	99	149	273	148	134	42
1.2			76	161	116	289	309	107	174	137	64
1.1		80	182	142	127	404	62	160	193	98	80
1.0	118	169	264	398	232	206	160	394	171	72	
0.9		202	276	301	308	429	403	164	200	84	
0.8			272	206	372	485	257	197	205	57	
0.7				201	549	375	429	199	267	66	
0.6					319	555	606	431	189	73	
0.5						656	689	376	221	123	
0.4							462	800	291	99	
0.3								403	342	98	
0.2									553	237	
0.1										231	
0.0											118
-∞											
	0.0	0.1	0.2	0.3	0.4	0.5	0.6	0.7	0.8	0.9	1.0 e

Table 4. Correction factors for unobservable eccentricities

$\log_{10} r$	$\log_{10}$ correction	$\log_{10} r$	$\log_{10}$ correction
-1.0		0.0	
	1.099		0.048
-0.9		0.1	
	0.962		0.150
-0.8		0.2	
	0.828		0.260
-0.7		0.3	
	0.695		0.375
-0.6		0.4	
	0.566		0.488
-0.5		0.5	
	0.443		0.597
-0.4		0.6	
	0.326		0.706
-0.3		0.7	
	0.219		0.818
-0.2		0.8	
	0.122		0.935
-0.1		0.9	
	0.038		1.055
0.0		1.0	

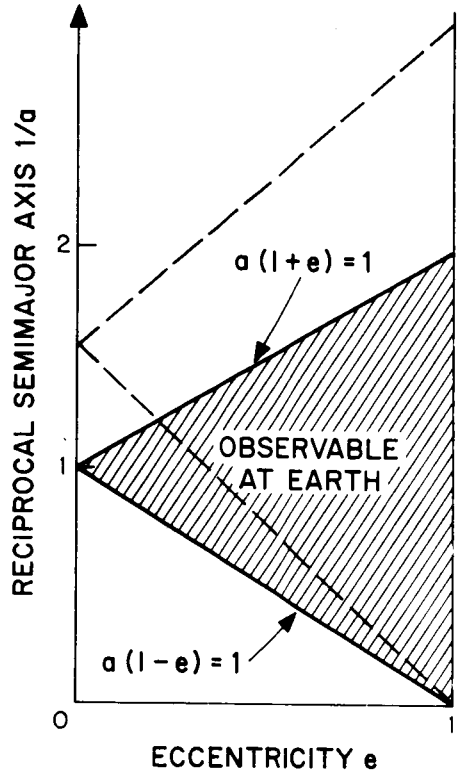

Figure 2. The region in the (1/a) - e distribution that can be observed at a distance r from the sun is a triangle bounded above and below by a(1 + e) = 1/r and a(1 - e) = 1/r, respectively.

6. CORRECTED RELATIVE SPACE DENSITIES

Table 5 presents the logarithms of the final corrected relative space densities computed. Figure 3 shows these as functions of radius vector, in the ecliptic and at latitude $\pm 30°$. Figure 4 shows them as functions of latitude, at three different values of radius vector. Finally, Figure 5 shows contours of space density in a plane normal to the ecliptic, at two different scales. Generally speaking, the neighborhood of the earth is not an exceptional region in any of these figures; this fact may be taken as one qualitative confirmation that appropriate corrections have been made to the observations. One exception to this generalization is the bump appearing in Figure 3 near $r = 1$, on the curve for $\beta = \pm 30°$. This bump is probably to be understood as the result of a correlation between i and e in meteor orbits, contrary to the assumption made when the correction was being made for unobservable orbits. A more exact correction would be expected to raise the rest of the curve so as to eliminate the bump.

Only a very modest relative increase in space density appears in the asteroid region — perhaps 15% over a smooth distribution, and perhaps only a statistical fluctuation. Of course, this does not mean that there is no considerable excess in meteor space density in the asteroid belt, because asteroidal orbits cannot be observed on earth and Table 3 cannot be safely extrapolated to such orbits. The absence of a concentration near the asteroids does mean, however, that less than the order of 5% of the radar meteors originated in the asteroid belt and have also kept nearly their original orbits.

Observed orbits of short-period comets are a most instructive parallel for meteor orbits. Whether the meteors are supplied from long-period or short-period comets, their orbits will tend to resemble those of short-period comets, because "capture" by Jupiter has similar effects either on the comet

Table 5. Logarithms of corrected relative space density

Sine latitude	Radius vector																			
	0.100	0.126	0.158	0.199	0.251	0.316	0.398	0.501	0.631	0.794	1.00	1.26	1.58	1.99	2.51	3.16	3.98	5.01	6.31	7.94	10.0
1.0	5.522	5.252	5.087	4.890	4.672	4.538	4.476	4.333	4.182	4.097	3.940	3.623	3.387	3.181	2.972	2.799	2.700	2.629	2.517	2.324	
0.9	5.834	5.670	5.581	5.402	5.197	5.021	4.875	4.743	4.592	4.503	4.362	4.085	3.860	3.683	3.496	3.316	3.163	3.011	2.866	2.723	
0.8	6.214	5.998	5.886	5.671	5.450	5.279	5.085	4.994	4.815	4.754	4.622	4.373	4.112	3.899	3.716	3.583	3.438	3.238	3.069	2.964	
0.7	6.300	6.043	5.940	5.733	5.569	5.348	5.180	5.065	4.913	4.882	4.739	4.528	4.307	4.119	3.952	3.759	3.635	3.393	3.200	3.093	
0.6	6.400	6.177	5.984	5.790	5.693	5.435	5.317	5.168	5.070	5.035	4.886	4.688	4.486	4.294	4.122	3.957	3.763	3.569	3.318	3.170	
0.5	6.466	6.291	6.079	5.879	5.749	5.528	5.397	5.251	5.177	5.142	4.995	4.802	4.605	4.457	4.276	4.089	3.881	3.629	3.396	3.222	
0.4	6.435	6.349	6.114	5.954	5.856	5.646	5.518	5.386	5.281	5.240	5.105	4.939	4.733	4.570	4.429	4.185	3.956	3.728	3.525	3.246	
0.3	6.462	6.326	6.168	5.997	5.901	5.738	5.671	5.564	5.478	5.416	5.302	5.124	4.994	4.793	4.632	4.415	4.155	3.935	3.752	3.650	
0.2	6.474	6.319	6.172	6.024	5.948	5.788	5.703	5.620	5.552	5.476	5.354	5.186	5.061	4.906	4.752	4.525	4.291	3.972	3.717	3.614	
0.1	6.463	6.313	6.182	6.067	5.967	5.826	5.751	5.701	5.659	5.545	5.418	5.258	5.120	4.962	4.817	4.573	4.358	4.016	3.711	3.595	
0.0																					

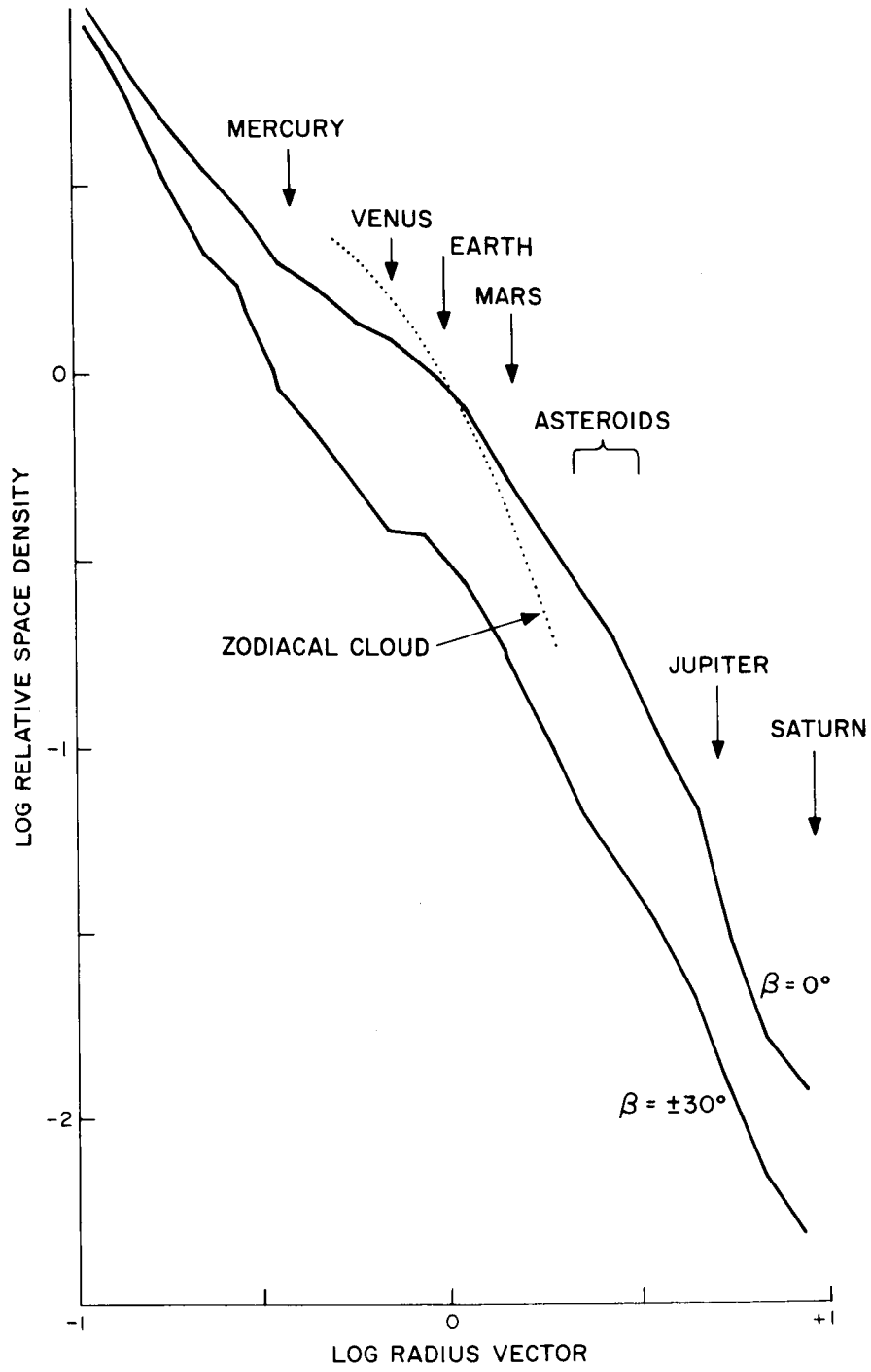

Figure 3. Relative space density of radio meteors as functions of r, and of zodiacal particles (dotted line).

orbits or on the meteor orbits after the meteors have left the comet. The dip in space density that is evident in Figure 3 beyond Jupiter's orbit is readily understood as a concentration of aphelia near Jupiter, just as in Jupiter's "family" of comets.

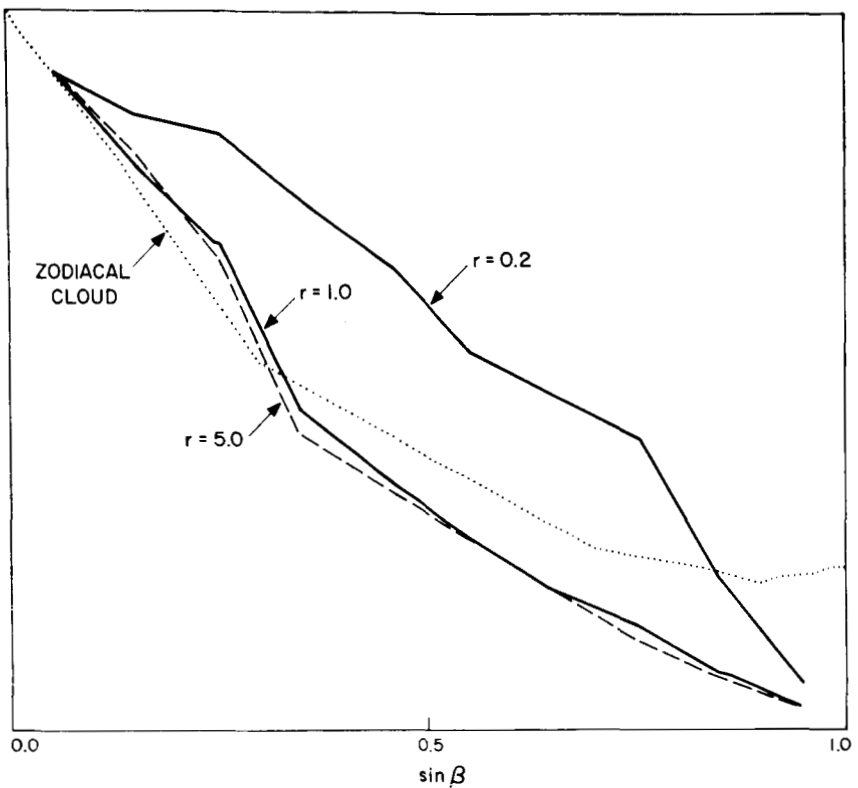

Figure 4. Relative space density of radio meteors as a function of sin β, and zodiacal particles (dotted line).

Outside the initial perihelion distance, a particle spiraling into the sun under the Poynting-Robertson effect has a radial density distribution with a slope at least as steep as -2.5 in Figure 3 (cf., Southworth, 1964). The curves in Figure 3 are appreciably flatter, which strongly suggests that these meteors do not, on the average, persist long enough to spiral in. Presumably they are destroyed by collisions.

Another aspect of the concentration of aphelia to Jupiter's orbit is the concentration of values of ω for comets toward 0° and 180° (Porter, 1963).

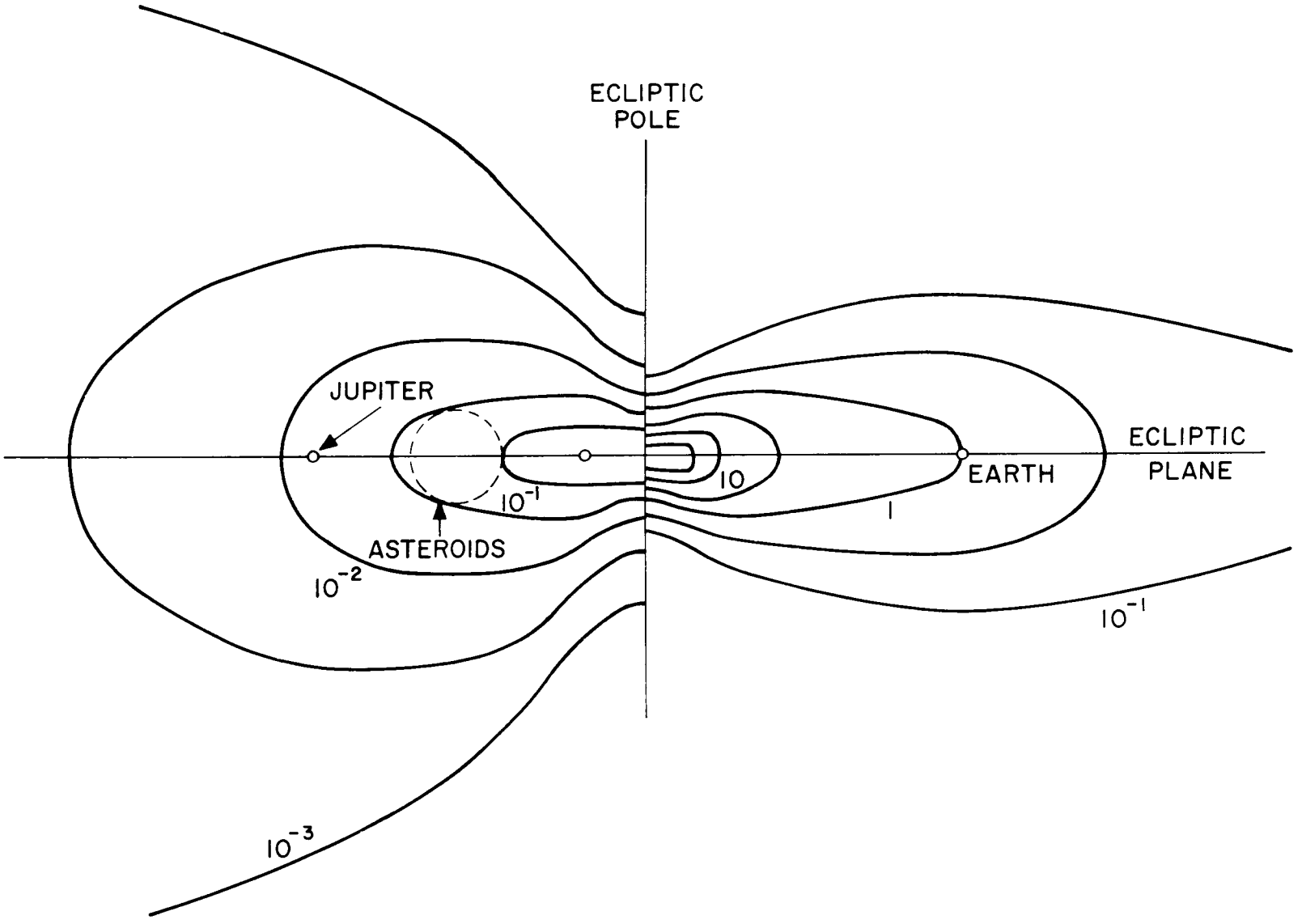

Figure 5. Relative space density of radio meteors.

Meteors may be expected to show some such concentration of values of ω, partly because of initial capture by Jupiter, and partly because the regression of the nodes under later Jupiter perturbations is not at uniform speed. As Moulton (1914) remarked, and as Whipple (1950) showed specifically for Comet Encke, the rate of change of ω is faster when ω is near 90° or 270° than when ω is near 0° or 180°.

The effect on space density of a concentration of values of ω near 0° and 180° is to shrink the density distribution far from the sun to low latitudes, because the meteors are then near their aphelia, which are near the ecliptic. I have discussed (Southworth, 1967) the mean space distribution when the orbits evolve under the Poynting-Robertson effect and ω is concentrated in this way. The conclusion reached there is that, at greater distances from the sun than two or three times the mean of the original perihelion distances, the distribution of latitudes will be compressed toward the ecliptic. Nearer the sun, the distribution of latitudes will reflect the distribution of inclinations without bias. Figure 4 clearly shows that the distribution of latitudes of radio meteors is broader near the sun, confirming the argument stated above. The spread in latitude in the innermost curve reflects a broad distribution of inclinations, and helps to confirm that the orbits are comparable to those of short-period comets.

7. COMPARISON WITH ZODIACAL CLOUD

Figures 3 and 4 also show curves of density distribution derived from observations of the zodiacal light (Southworth, 1967). When they were derived it was assumed for convenience that the latitude distribution was independent of distance from the sun. Thus each latitude curve in Figure 3 is necessarily a blending of latitude curves appropriate to different distances. All the information came from distances between 0.5 and 2 a.u., but while the low latitudes were mostly seen in the neighborhood of the earth, the high latitudes were mostly observed nearer the sun. Moreover, the region nearer the sun seems to have been contaminated by extra strong light. Thus the zodiacal-cloud curve could be plausibly reconciled with the meteor curves: they agree at low latitudes near the earth; they agree at higher latitudes nearer the sun; and the zodiacal curve is probably wrong at the highest latitudes.

The radial distribution of density fitted to the zodiacal light has been drawn in Figure 4 so as to intersect the low-latitude meteor curve at the earth. (This does not imply anything about their absolute densities.) The zodiacal distribution is appreciably steeper than the meteor distributions. It is not certain that the difference is statistically significant, because the zodiacal light was nearly as well fitted by radial distributions almost exactly matching those of the meteors. Nonetheless, the difference supports the hypothesis made above that meteors are eliminated by collisions (or other processes) as well as by the Poynting-Robertson effect. Since the zodiacal particles spiral in faster and have less cross section for collisions, they will be more concentrated to the sun than are the meteors.

8. CONCLUSIONS

The relative space density, in the range 0.1 to 10.0 a.u. from the sun, of meteors in the mass range 10^{-3} to 10^{-4} g, has been computed. It shows a broad maximum near the ecliptic plane, and a deep minimum near the ecliptic poles.

There is little evidence for an asteroidal origin for these meteors. Planetary perturbations and collisional destruction appear important in their evolution.

9. REFERENCES

BRIGGS, R. E.

1962. Steady-state space distribution of meteoritic particles under the operation of the Poynting-Robertson effect. Astron. Journ., vol. 67, pp. 710-723.

ELFORD, W. G.

1964. Calculation of the response function of the Harvard Radio Meteor Project Radar System. Harvard Radio Meteor Project Res. Rep. No. 8, October 1964.

HAWKINS, G. S., AND UPTON, E. K. L.

1958. The influx rate of meteors in the earth's atmosphere. Astrophys. Journ., vol. 128, pp. 727-735.

MOULTON, F. R.

1914. An Introduction to Celestial Mechanics. Macmillan Company, New York, 437 pp.

ÖPIK, E. J.

1951. Collision probabilities with the planets and the distribution of interplanetary matter. Proc. Roy. Irish Acad., vol. 54A, pp. 165-199.

PORTER, J. G.

1963. The statistics of comet orbits. In The Moon, Meteorites, and Comets, ed. by B. M. Middlehurst and G. P. Kuiper, Univ. of Chicago Press, Chicago, Illinois, pp. 550-572.

SOUTHWORTH, R. B.

1964. The size distribution of the zodiacal particles. Ann. N. Y. Acad. Sci., vol. 119, pp. 54-67.

1967. Phase function of the zodiacal cloud. Smithsonian Astrophys. Obs. Spec. Rep. No. 239, pp. 47-74.

VERNIANI, F., AND HAWKINS, G. S.

1964. On the ionizing efficiency of meteors. Astrophys. Journ., vol. 140, pp. 1590-1600.

WHIPPLE, F. L.

1950. A comet model. I. The acceleration of comet Encke. Astrophys. Journ., vol. 111, pp. 375-394.

ORBITAL DISTRIBUTION OF METEORS OF LIMITING MAGNITUDE +6 OBSERVED FROM THE SOUTHERN HEMISPHERE

Carl S. Nilsson

ABSTRACT

A radio survey of orbits of meteors of limiting magnitude +6 was carried out at Adelaide, South Australia, during 1961. Each orbit has been weighted for observational and astronomical selection, and the distributions of 1900 orbits are compared to those of other surveys, particularly to those of the faint photographic survey of McCrosky and Posen (1961). The distributions for stream orbits and sporadic orbits are given separately.

The two most noteworthy distributions are those with perihelion distance and longitude of perihelion. The latter shows evidence of Jupiter alignment for the sporadic meteor orbits, which, however, still does not differentiate between an asteroidal or cometary source.

ORBITAL DISTRIBUTION OF METEORS OF LIMITING MAGNITUDE +6 OBSERVED FROM THE SOUTHERN HEMISPHERE

Carl S. Nilsson

1. INTRODUCTION

This paper presents the orbital distributions of 1900 meteors detected during a radio survey of meteor orbits carried out at Adelaide, South Australia, during 1961. Several surveys of this type have been undertaken in the Northern Hemisphere at varying magnitudes. Davies and Gill (1960) measured the orbits of over 2000 meteors of limiting radio magnitude +8; McCrosky and Posen (1961) analyzed the trails of 2500 meteors of limiting magnitude +3 photographed simultaneously from two camera stations; and Hawkins (1962) has extended radio measurements of meteor orbits to magnitude +10. Kascheyev, Lebedinets, and Lagoutin (1960) have also made a similar radar survey of meteor orbits of a limiting magnitude of about +7, but none of these northern surveys has been able to include radiants south of declination -20°. Our observations extend to meteors of radio magnitude +6 and include both overdense and underdense meteor trails. Our results will be briefly compared to those of the northern surveys mentioned above.

This work was supported in part by grant NSR 09-015-033 from the National Aeronautics and Space Administration.

2. OBSERVATIONAL TECHNIQUE

The radio equipment consists of a combination of CW and radar on 27 mc/sec; the CW transmitting power was only 300 w, and this limited the survey to meteors giving rise to line densities greater than 3×10^{13} electrons/m. This limit corresponds to a radio magnitude of about +6 (McKinley, 1961). The equipment has been described in detail by Weiss and Elford (1963). One feature of the system is that not only are the velocity and trail orientation measured for each meteor, but also the actual positions of the three specular reflection points are uniquely determined. The heights of each reflection point are measured to ± 2 km.

We have corrected the apparent reflection-point positions for wind shear from the measures of Doppler drift at each reflection point. Also, having measured the antenna radiation patterns, we are able to determine the electron line density at each reflection point. Thus, assuming a certain vaporization theory, the mass of each meteor could be calculated. A more complete description of the observational method, data processing, geocentric corrections, and accuracy of results has been published previously (Nilsson, 1964).

Weighting against selection effects is of the greatest importance in the attempt to derive real distributions of meteor orbits in space, so I shall briefly describe the weights applied to these data.

First, there are the selection factors inherent in the radio method of observation. Electron line density depends heavily on meteor velocity, the relationship probably being of the form

$$q_{max} \propto v_{max}^{\eta} \quad , \tag{1}$$

where the subscript refers to the point of maximum ionization. The value of η has been variously determined to be between 3 and 5; and the most recent work (Verniani and Hawkins, 1964) confirms the value 4.0 chosen to weight the orbits of this survey.

Because of the location of the observing station, certain radiant declinations are more favored than others; from the known equipment parameters it has been possible to calculate directly the expected echo rate as a function of declination. This is shown in Figure 1. The observed diurnal-rate variations of various showers have been used to verify the equipment response as a function of radiant position, and each orbit has been weighted according to the declination of its radiant.

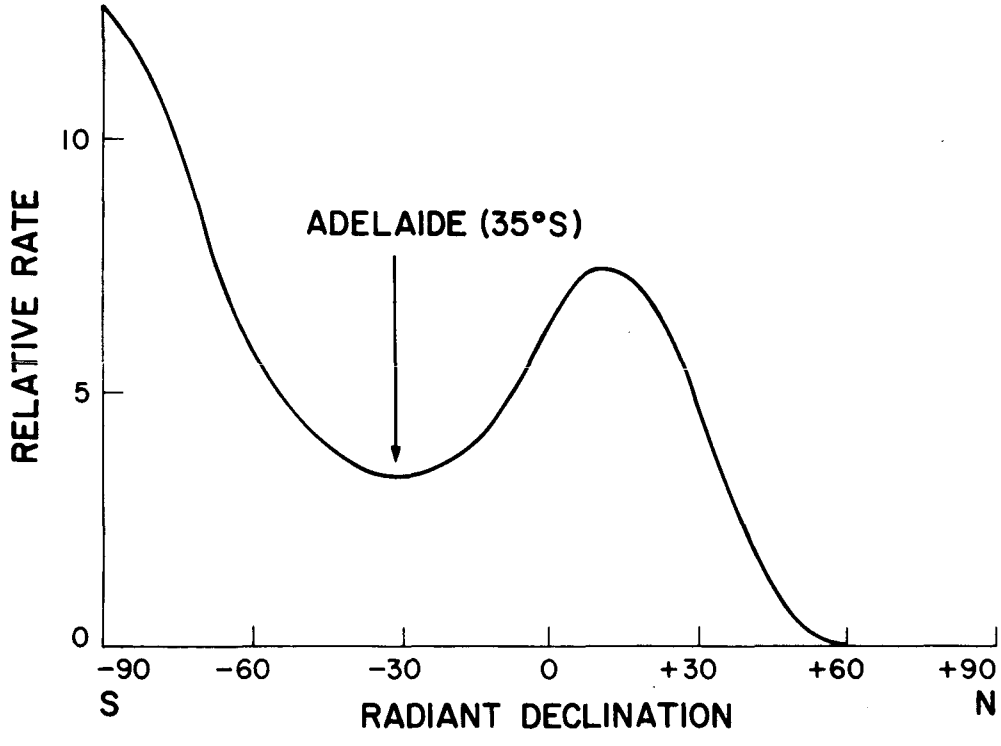

Figure 1. The calculated meteor-echo rate for the Adelaide equipment as a function of radiant declination.

Some other selection factors have also been considered: Certain hours of observation were more frequently interrupted than others, and there was

some dependence of the number of echoes reduced on the Fresnel diffraction frequency. These factors were included. Whipple (1955) has suggested that rapid diffusion of the ion column of high-altitude meteors inhibits their observation by radio techniques. The height of maximum ionization increases with velocity; hence, the high-velocity meteors will be selectively discriminated against, with a concomitant effect on the orbit distributions. This effect does not seem so serious in practice as theory suggests. The velocity distribution in Figure 2 does not differ markedly from the faint photographic meteor-velocity distribution found by McCrosky and Posen (1961). From the classical vaporization theory (Weiss, 1959), we expect that the atmospheric density at the height of maximum ionization ρ_{max} will be given by

$$\rho_{max} \propto \cos \chi \cdot V_\infty^{-2} \quad , \tag{2}$$

where χ is the zenith angle of the radiant. From a study of the distributions of echo heights of the meteors observed at Adelaide, it was found (Nilsson, unpublished) that the exponent of V_∞ in (2) was about -1.1 rather than -2. This held for the slow meteors as well as for the fast ones, and is consistent with the results of Greenhow and Hall (1960), who found the exponent of V_∞ in (2) to be between -1.0 and -1.5. Thus the height of maximum ionization does not vary as markedly with velocity as theory suggests.

Finally, there is the astronomical weighting factor, which involves the probability that a meteor of given orbital elements will collide with the earth. Fortunately, all the meteor distributions shown here from various radio and photographic surveys have used the same factor, the original derivation of which is due to Öpik (1951):

$$W \propto \frac{V_g \sin i}{V_\infty^2} \cdot \left(\frac{2}{r} - \frac{1}{a} - \frac{p}{r^2} \right)^{1/2} \quad , \tag{3}$$

where W is the weight, V_g is the geocentric velocity of the meteor, V_∞ is the velocity at the top of the atmosphere, i is the inclination of the orbit, r is the sun-earth distance, a is the semimajor axis, and $p = a(1 - e^2)$.

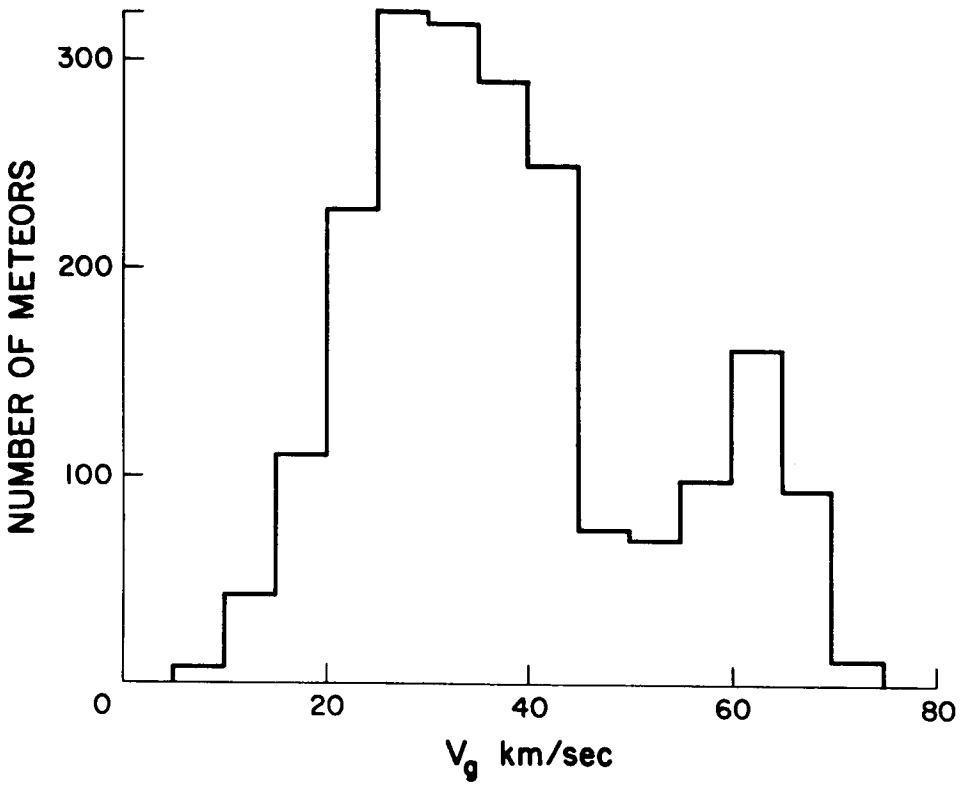

Figure 2. The observed distribution with geocentric velocity V_g for all meteors.

3. DISTRIBUTIONS OF ORBITAL ELEMENTS

The distributions are presented as double histograms, the shaded area representing the contribution due to meteor streams, both major and minor. By analyses of orbit associations (Nilsson, 1964), about 29% of the weighted total of orbits can be significantly associated into groups of three or more orbits. The top histogram, in each case, represents all the meteors observed in the survey; the lower one represents the sporadic, or unresolvable, background; and the shaded area in between shows the contribution of all the streams. Figure 2 shows the unweighted distribution with geocentric velocity V_g of 2040 meteor velocities observed at Adelaide. The observed values of velocity have been corrected for retardation through the earth's atmosphere, for diurnal motion of the observer, and for the earth's gravitational attraction. This distribution is consistent with those of other surveys, the modal value being about 30 km/sec. It is the only Adelaide radio-survey distribution presented here that has not been weighted for selection, as it is more useful for comparison in this form.

A comparison of various distributions with the reciprocal semimajor axis $1/a$ is given in Figures 3(a) to 3(e). The distributions are arranged in order of decreasing brightness and clearly show a steady increase in the proportion of short-period orbits as we proceed to fainter magnitudes. Negative values of $1/a$ signify orbits that have been calculated to be hyperbolic. In view of the known experimental error of the order of 0.1 in $1/a$, no significant number of hyperbolic orbits were found in the Adelaide data, shown in Figure 3(c). This distribution appears to fit quite consistently between the faint photographic survey of McCrosky and Posen (1961) at limiting magnitude +3 and the radio survey of Davies and Gill (1960) at limiting magnitude +8. The similarity of the latter distribution with that of the Harvard Radio Meteor Project (Southworth, unpublished) is quite noticeable.

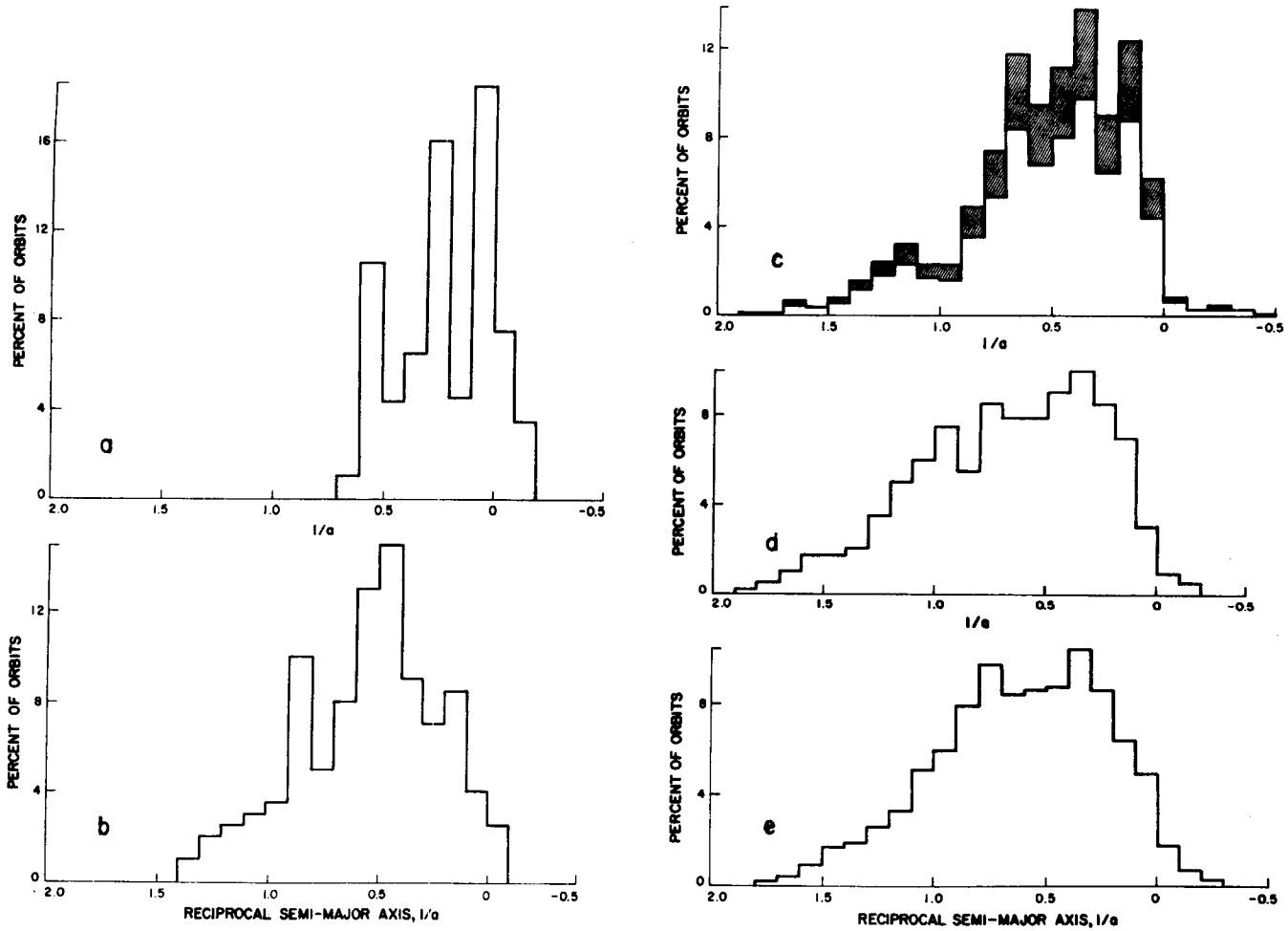

Figure 3. Distributions with reciprocal semimajor axis 1/a for various meteor surveys in order of limiting magnitude: (a) bright photographic survey, 144 meteors (Whipple, 1954, from McCrosky and Posen, 1961); (b) faint photographic survey, 2529 meteors (from McCrosky and Posen, 1961); (c) Adelaide radio survey, about 1900 meteors; (d) Jodrell Bank radio survey, 2510 meteors (from Davies and Gill, 1960); (e) Harvard radio survey, about 12,500 meteors (Southworth, unpublished).

As Davies and Gill allowed for observational selection in quite a different manner from Southworth, this suggests that the distributions with 1/a are not very sensitive to observational weighting.

Figure 4 shows the distribution with eccentricity; it is of normal appearance and shows the usual tendency for streams to have high eccentricities.

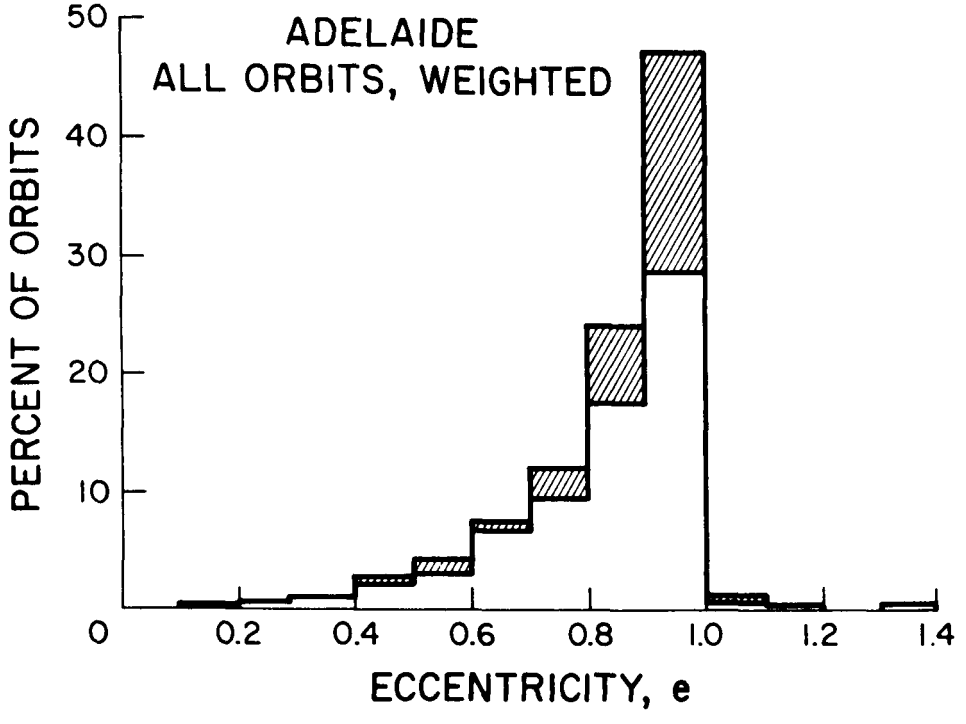

Figure 4. The distribution with eccentricity e.

Two distributions with inclinations are given in Figure 5 for the Adelaide data. In Figure 5(a), for all values of eccentricity, we can see that the streams are generally, but not entirely, concentrated in direct orbits within 40° of the ecliptic plane. Figure 5(b) gives the distribution with inclinations for the 130 orbits for which $e < 0.5$. It seems to be of the same form as that for all values of eccentricity, although the median value of inclination for the low-eccentricity orbits is 50°, compared to 36° for all the orbits. This difference is brought about by the stream content of the orbits with $e > 0.5$; the median values of

inclination for the sporadic content are the same for each distribution, viz., 42°. There are a few minor associations of orbits at high inclinations, the most noticeable being the Puppid stream at 70°. This stream, of low eccentricity, belongs to the class of orbits described by Hawkins (1962) as "toroidal."

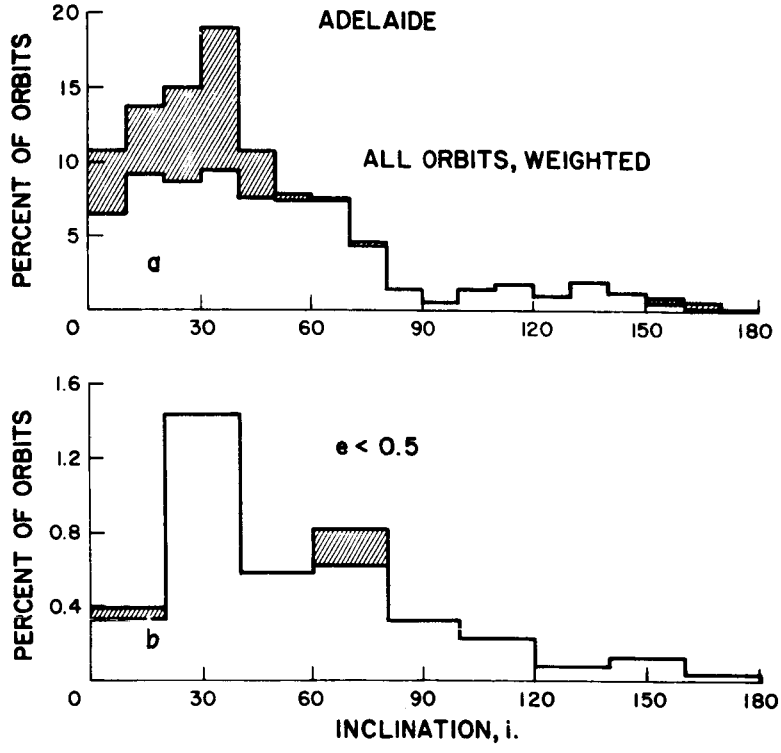

Figure 5. Distributions with inclination i for (a) all orbits, (b) orbits with e < 0.5.

The distribution with perihelion distance for the Adelaide data, given in Figure 6(d), is quite different from that obtained by other surveys. Figure 6(a) shows an observed distribution for 369 comets with perihelia < 1.9 a.u., compiled by McCrosky and Posen (1961) from the Baldet and De Obaldia catalog. From a study of absolute brightness as a function of perihelion distance, McCrosky and Posen concluded that the distribution was reasonably true out to 1 a.u. It seems obvious, however, that the peak at 1 a.u. is due to

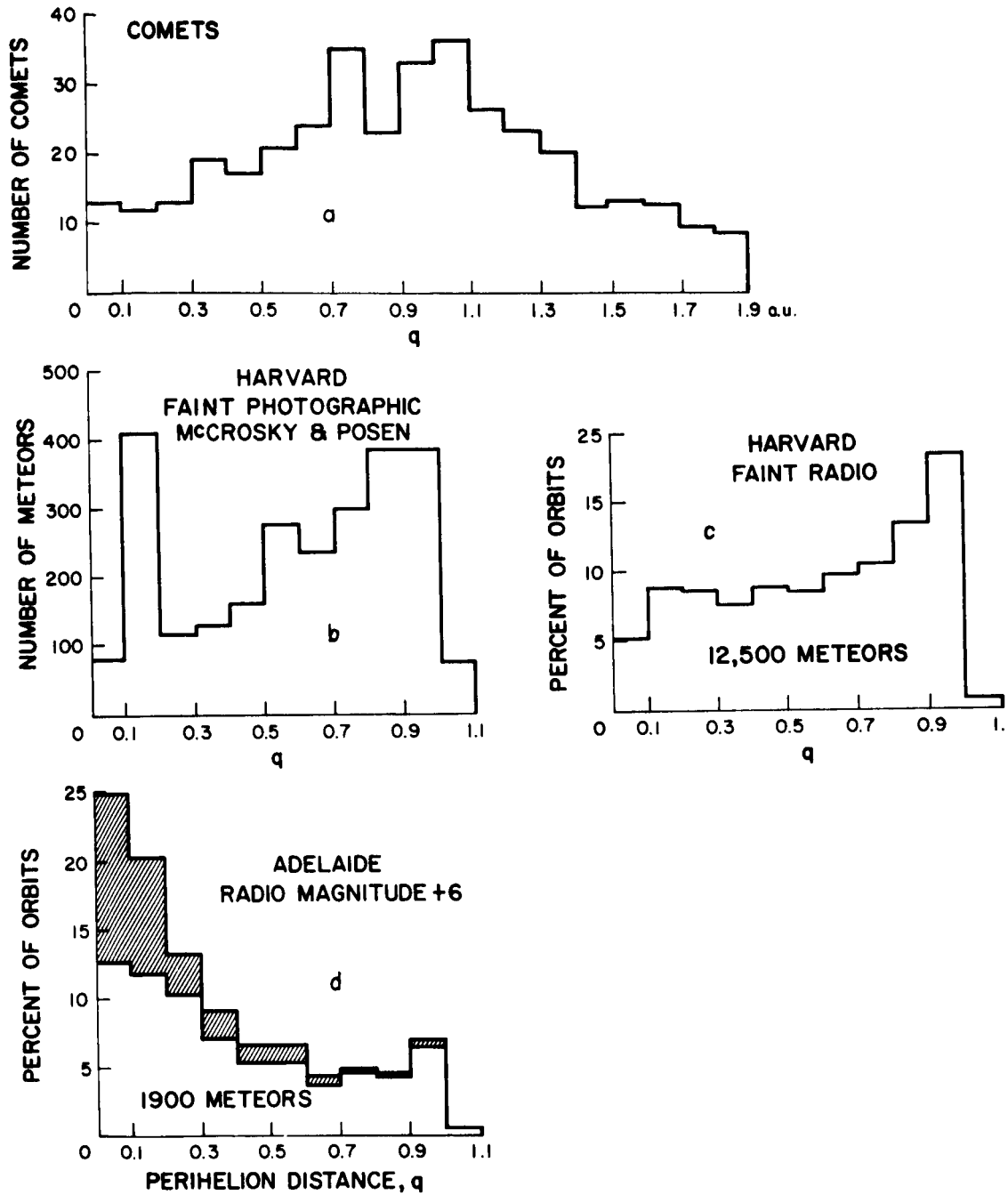

Figure 6. Distributions with perihelion distance q: (a) the distribution for 369 comets with $q < 1.9$ a.u. (from McCrosky and Posen, 1961); (b) faint photographic survey (from McCrosky and Posen, 1961); (c) Harvard radio survey (Southworth, unpublished); (d) Adelaide radio survey. The shaded portion shows the contribution of streams.

observational selection. The distribution for faint photographic meteors is certainly similar out to 1 a.u., and it is supported by the Harvard Radio Meteor data shown in Figure 6(c). The Adelaide data, in contrast with the above, show a marked decrease in weighted numbers as the perihelion distance increases out to 1 a.u. The stream contributions are quite marked at small perihelion distances, corresponding to orbits of moderate size and high eccentricities. Incomplete separations of stream orbits are not responsible for this major difference between surveys, as the other distributions contain both sporadic and stream orbits, so we can simply compare the distributions for all the meteors observed. It thus appears that the Adelaide survey observed more short-period high-eccentricity orbits than the other surveys, and it will be interesting to see if this distribution is confirmed by any other surveys around limiting magnitude +6.

Figure 7 shows the distribution with aphelion distance. This distribution, of course, is strongly influenced by the fact that a meteor orbit must cross that of the earth to be observed. Hence $q < 1.0$ and $q' > 1.0$ a.u. for all observed orbits, and the bulk of the orbits have aphelia between the orbits of Mars (1.5 a.u.) and Jupiter (5.2 a.u.). This suggests that we may be able to detect the influence of Jupiter on the aphelion alignment of the low-inclination members of these orbits, such as is observed for the short-period comets and the asteroids. The latter two sets of bodies both show pronounced maxima in number against longitude of perihelion around 13°, the longitude of perihelion of Jupiter's orbit. This can be clearly seen in Figure 8(a) (McCrosky and Posen, 1961) and Figure 8(b) (Porter, 1952).

Jacchia and Whipple (1961) and McCrosky and Posen have looked for signs of this alignment in their data, shown in Figures 9(a) and 9(b), respectively, but without success. If a sufficient number of comets, or asteroids, are sources of these meteors, we should expect to see a similar distribution for meteors, since the longitude of perihelion is not perturbed very quickly.

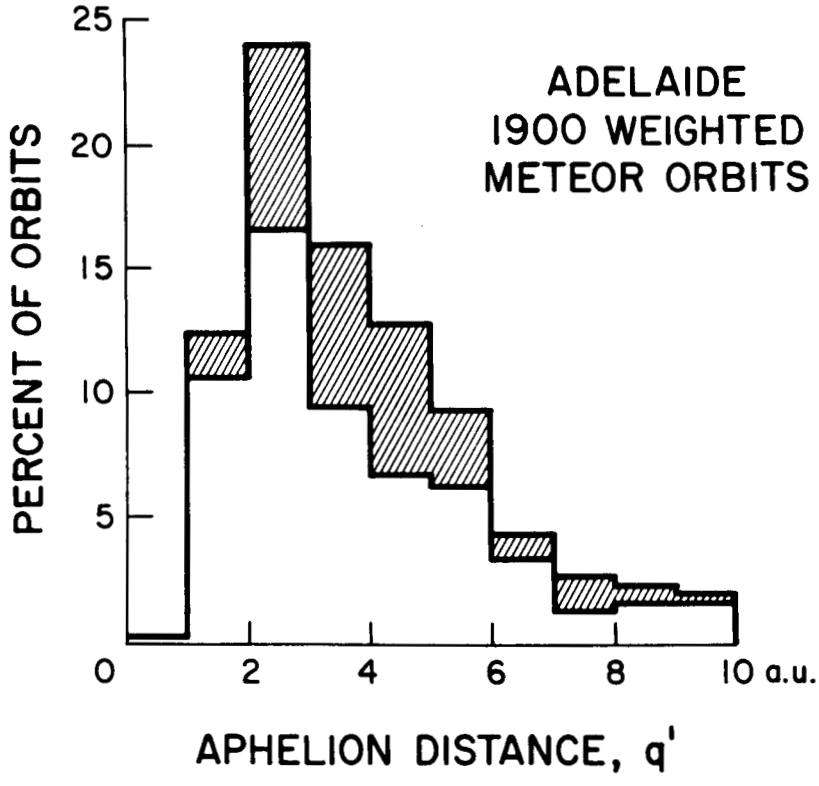

Figure 7. The distribution with aphelion distance q'.

McCrosky and Posen suggested that the bright meteor distributions could be explained if only relatively few comets that approach close to the earth's orbit were responsible for most of the meteor population. Thus, the distribution with longitude of perihelion would vary from time to time, depending on the particular sources at hand. The perihelion longitudes of the six close-approach comets satisfying their conditions of observation for the Northern Hemisphere do, in fact, lie near the maxima of the bright-meteor distribution. These longitudes are marked by arrows underneath the abscissa in Figure 9(a). There appears to be little correlation, however, with the distribution for the faint photographic meteors shown in Figure 9(b). The Adelaide data are rather instructive in this study. The orbits selected are those within 30° of the ecliptic plane with aphelia between 3 and 5 a.u. from the sun. It can be seen from Figure 9(c) that the total distribution for all orbits shows a maximum-to-minimum range similar to the bright meteor

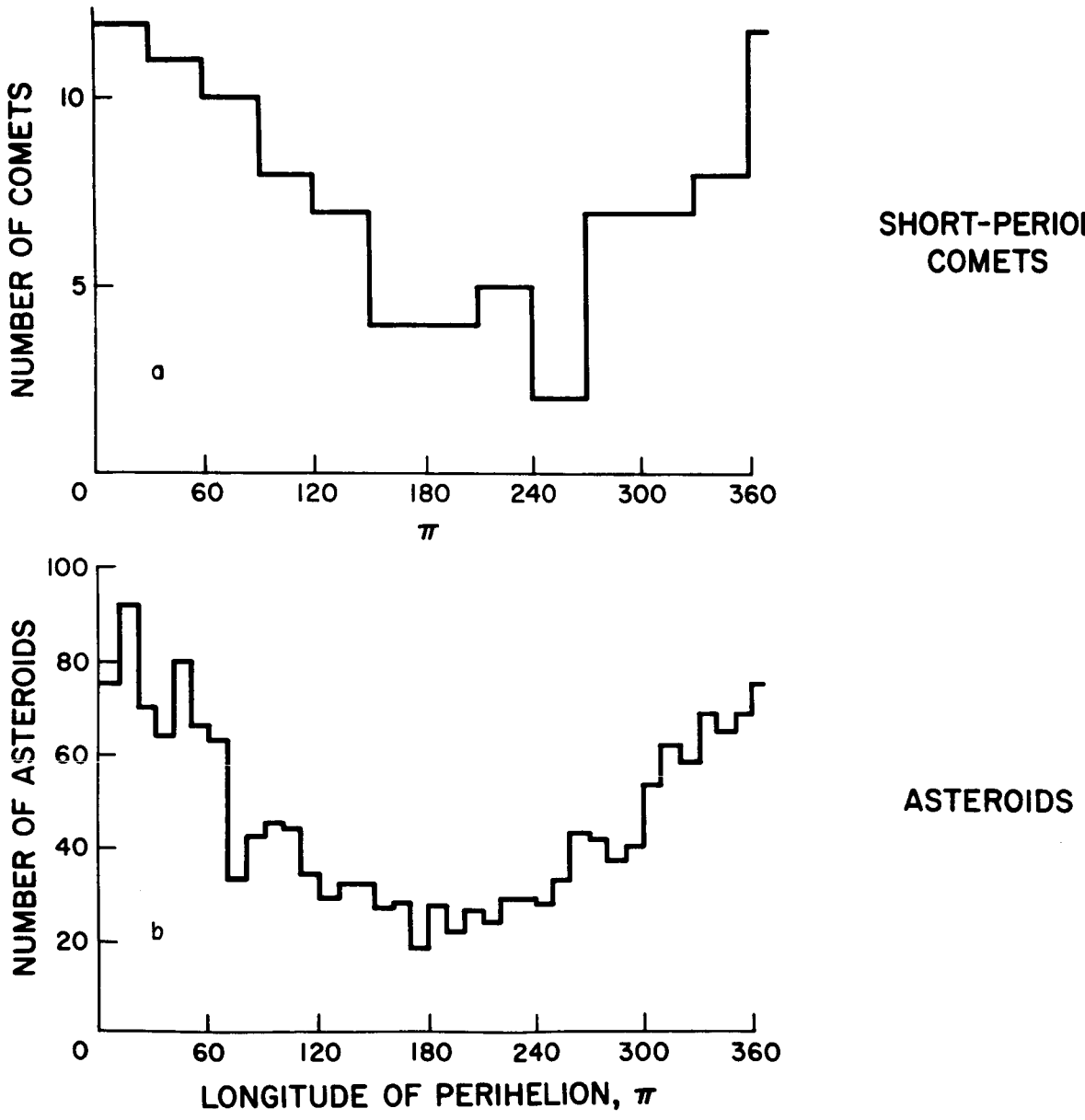

Figure 8. Distributions with longitude of perihelion π, for (a) short-period comets (Porter, 1952); (b) asteroids (McCrosky and Posen, 1961).

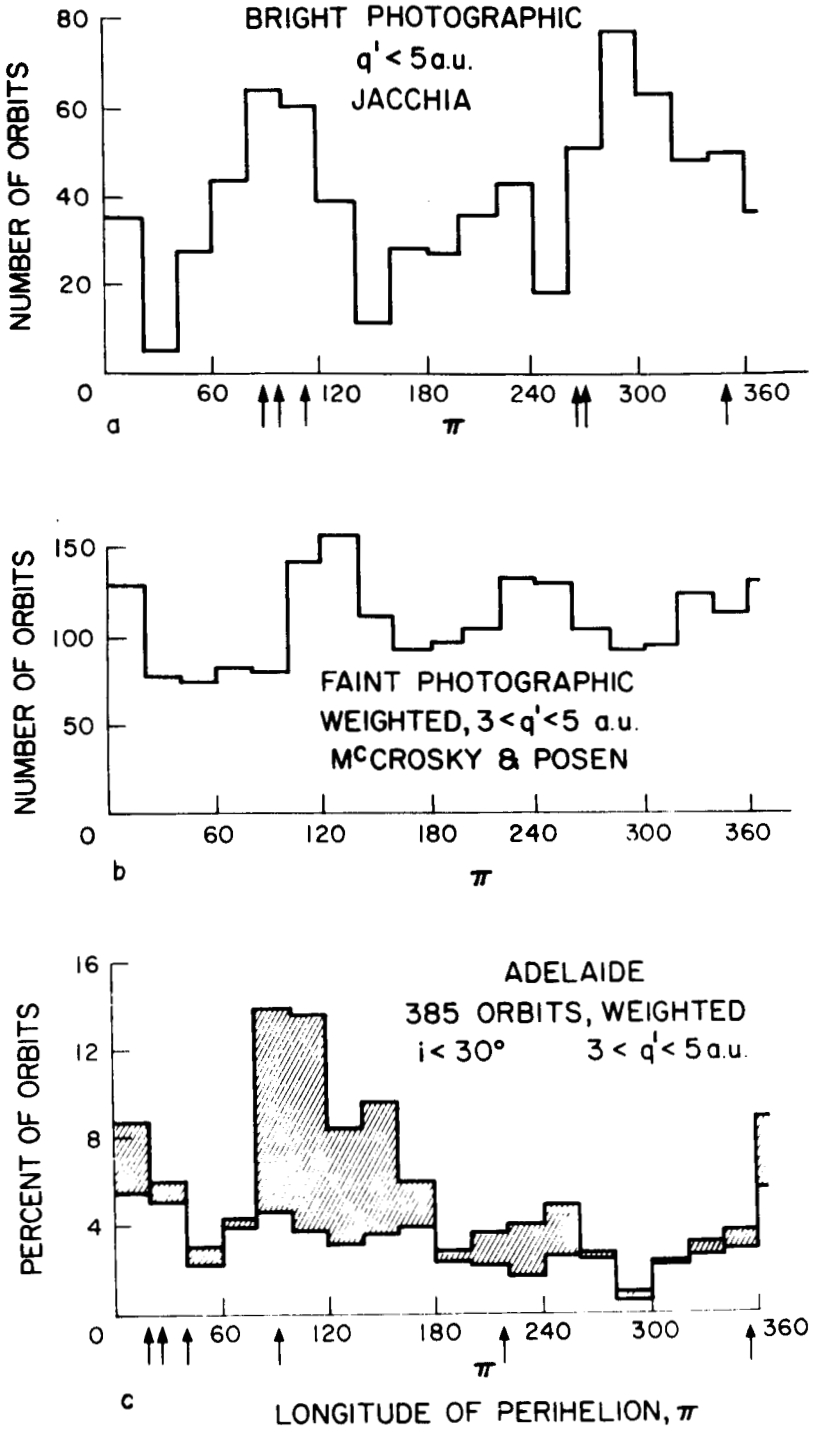

Figure 9. Distributions with longitude of perihelion π, for (a) bright photographic meteors reduced by Jacchia (from McCrosky and Posen, 1961); (b) faint photographic meteors (from McCrosky and Posen, 1961); (c) Adelaide radio meteors.

distribution, although there is only one pronounced peak, not two. The streams are heavily concentrated in the region $70° < \pi < 180°$. Observations were made reasonably uniformly throughout the year, so this concentration is real, at least for 1961. When the stream orbits are subtracted, however, the remaining sporadic distribution does indeed show a simple maximum near the expected longitude of 13°. This could either show the original alignment, consistent with short-period cometary injection, for example, or it could be the result of aphelion capture by Jupiter from some other original distribution. In the latter case, longer meteor lifetimes are required, as this alignment would probably take at least approximately 10^5 years to eventuate.

For completeness, I have included in Figure 9(c) the longitudes of the six short-period comets from Porter's (1952) list that closely approach the earth's orbit and could give rise to meteor radiants visible in the Southern Hemisphere. These, not unexpectedly, are grouped near 13° and do not correlate with the total maximum between 70° and 180°. There is, thus, little support from the Adelaide data for the suggestion that these particular comets determine the total distribution with longitude of perihelion. Other classes of comets, such as the long-period comets that have more random distributions with longitude of perihelion, may indeed contribute a significant proportion of the meteor population.

Whipple (1954) has introduced an empirical comet-asteroid criterion K, defined by

$$K = \log_{10}\left[\frac{a(1+e)}{1-e}\right]^{-1} , \qquad (4)$$

which is positive for most comet orbits and negative for most asteroid orbits. This index is thus quite helpful in any discussion of the general characteristics of meteor orbits and their origin, and it is interesting to see how the orbits are distributed with respect to this criterion. Figure 10 gives the distribution for the Adelaide data. Most of the orbits have $K > 0$, particularly

those associated with streams, but a significant proportion have $K < 0$. This proportion appears to increase as fainter magnitudes are considered. Whipple's (1954) analysis of bright meteors showed 6% with $K < 0$; McCrosky and Posen (1961) found 26% of their faint photographic meteors to have orbits for which $K < 0$. From the Adelaide data, about 22% of the observed numbers of orbits have $K < 0$, but only 17% of all the weighted orbits have $K < 0$.

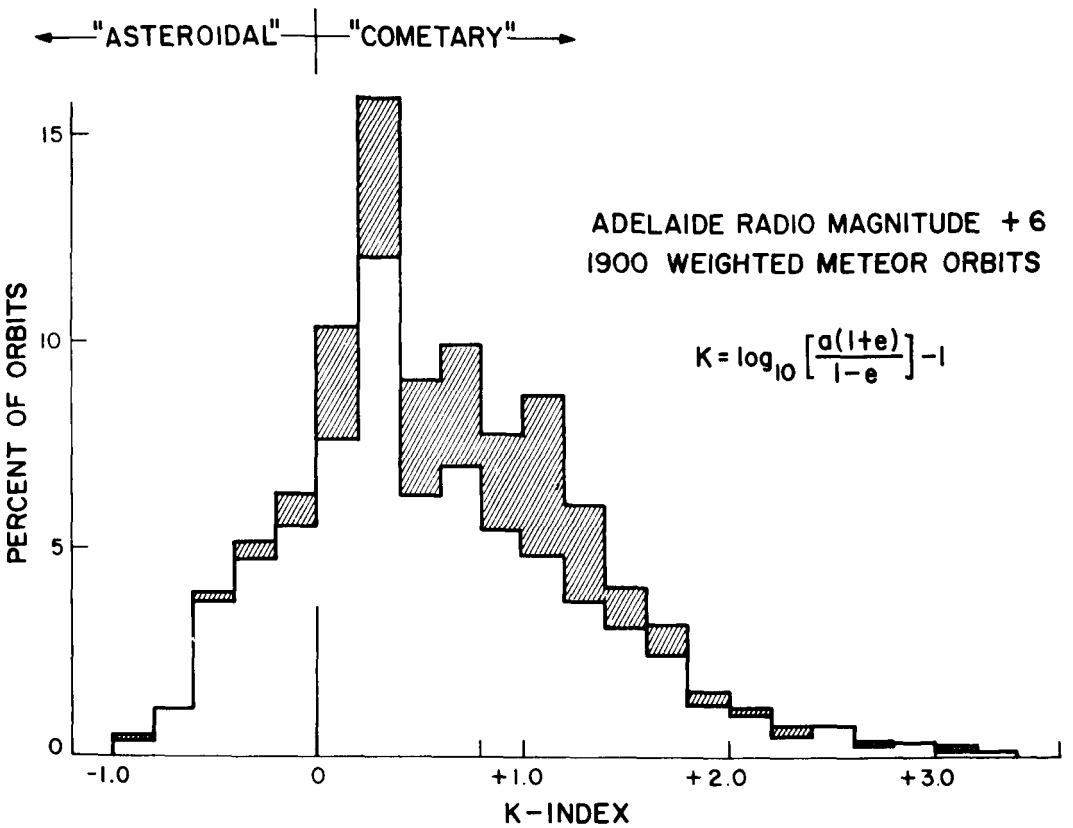

Figure 10. Distribution of Adelaide data with K index.

The proportion is greater, however, if streams are excluded; about 21% of the weighted sporadic orbits have $K < 0$. It is surprising that this figure is a little less than that found for the faint photographic meteors, in view of the fainter limiting magnitude of the Adelaide data, but further comments on this are better left until figures from other surveys are available.

It remains to look at the distributions of the orbits for which $K < 0$. By definition, they will be smaller and of lower eccentricity than those for which $K > 0$. This is obvious in Figures 11(a) and 11(b). The distribution with inclination is shown in Figure 11(c). The orbits are predominantly direct with inclinations < 70°; however, the distribution does not drop between 0° and 20°, as do the two distributions in Figure 5 for orbits with all values of K. The distribution can be described quite well by a simple cosine law out to 90° inclination. Now, both the short-period comets and the asteroids are generally confined to within 30° of the ecliptic plane. The distribution of stream meteors, however, does not show a maximum until 30° and extends out to 60°. If the stream meteors mostly originate from the short-period comets, then perturbations must have extended the distribution with inclination out and away from the ecliptic. The distribution in Figure 11(c) for the "asteroidal" orbits seems to indicate, therefore, that either the source, or the age, or both, of at least some of these meteors is different. In fact, they may well be asteroidal in origin.

Figure 11(d) shows the distribution with perihelion distance for these orbits. By definition of K, we have excluded orbits with $e > 0.9$, so it is not surprising to see that the peak at small perihelion distance shown in Figure 6(e) has disappeared, and that the distribution for the asteroidal orbits is essentially flat out to 1.0 a.u.

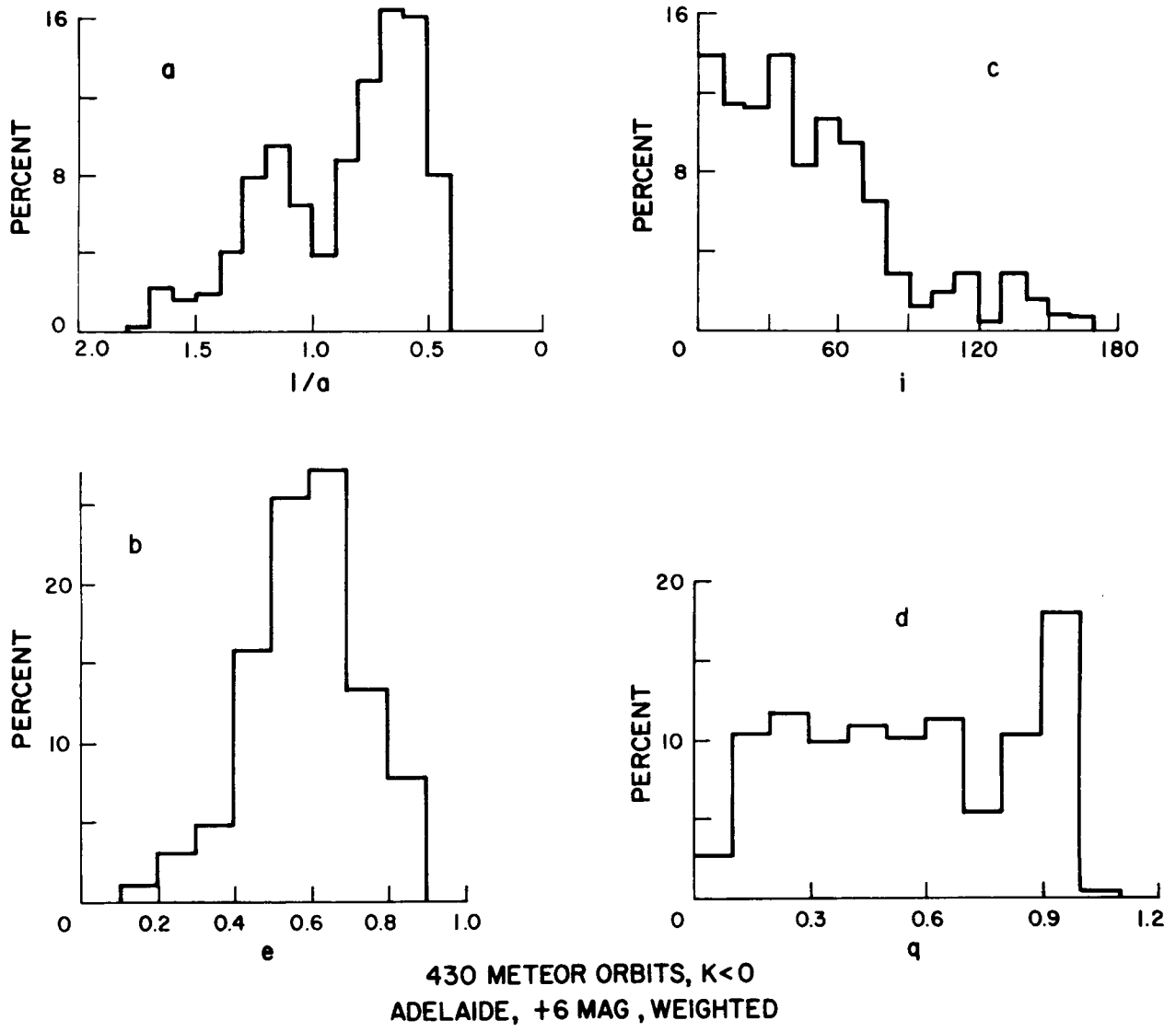

Figure 11. Distributions of all Adelaide meteor orbits for which $K < 0$ with (a) reciprocal semi-major axis $1/a$; (b) eccentricity e; (c) inclination i; (d) perihelion distance q.

4. ACKNOWLEDGMENTS

This survey was carried out at the University of Adelaide, first under the direction of Professor L. G. H. Huxley and later under Professor J. H. Carver. The author particularly wishes to acknowledge the guidance of Dr. W. G. Elford, University of Adelaide, and the late Dr. A. A. Weiss, CSIRO, Sydney, who jointly supervised the project. Finance for the survey was provided by the Radio Research Board of Australia and a University Research Grant. The author was supported by a General Motors-Holden Pty, Ltd., Post Graduate Research Fellowship and a CSIRO Senior Research Studentship.

This paper was written during the author's tenure at the Harvard College Observatory and the Smithsonian Astrophysical Observatory, Cambridge, on the Radio Meteor Project under the coordination of Dr. G. S. Hawkins.

The author also thanks Dr. R. B. Southworth for valuable assistance and the use of unpublished data.

5. REFERENCES

DAVIES, J. G., AND GILL, J. C.

1960. Radio echo measurements of the orbits of faint sporadic meteors. Monthly Notices Roy. Astron. Soc., vol. 121, pp. 437-462.

GREENHOW, J. S., AND HALL, J. E.

1960. The variation of meteor heights with velocity and magnitude. Monthly Notices Roy. Astron. Soc., vol. 121, pp. 174-182.

HAWKINS, G. S.

1962. Radar determination of meteor orbits. Astron. Journ., vol. 67, pp. 241-244.

JACCHIA, L. G., AND WHIPPLE, F. L.

1961. Precision orbits of 413 photographic meteors. Smithsonian Contr. Astrophys., vol. 4, pp. 97-129.

KASCHEYEV, B. L., LEBEDINETS, U. N., AND LAGOUTIN, M. F.

1960. Meteory. Sbornik Stotei No. 1, U. I. Lenin Polytechnic Inst., Kharkov.

McCROSKY, R. E., AND POSEN, A.

1961. Orbital elements of photographic meteors. Smithsonian Contr. Astrophys., vol. 4, pp. 15-84.

NILSSON, C. S.

1964. A Southern Hemisphere radio survey of meteor streams. Australian Journ. Phys., vol. 17, pp. 205-256.

1967. Unpublished work.

ÖPIK, E. J.

1951. Collision probabilities with the planets and the distribution of interplanetary matter. Proc. Roy. Irish Acad., vol. 54A, pp. 165-199.

PORTER, J. G.

1952. Comets and meteor streams. Chapman and Hall Publ. Co., London.

SOUTHWORTH, R. B.

1967. Unpublished work.

VERNIANI, F., AND HAWKINS, G. S.

1964. On the ionizing efficiency of meteors. Astrophys. Journ., vol. 140, pp. 1590-1600.

WEISS, A. A.

1959. Theory of the radio-echo meteor height distribution in a non-isothermal atmosphere. Australian Journ. Phys., vol. 12, pp. 54-64.

WEISS, A. A., AND ELFORD, W. G.

1963. An equipment for combining geophysical and astronomical measurements of meteors. Proc. Inst. Radio Engrs. Australia, vol. 24, pp. 197-203.

WHIPPLE, F. L.

1954. Photographic meteor orbits and their distribution in space. Astron. Journ., vol. 59, pp. 201-217.

1955. The physical theory of meteors. VII. On meteor luminosity and ionization. Astrophys. Journ., vol. 121, pp. 241-249.

BIOGRAPHICAL NOTES

FRED L. WHIPPLE, named Director of the Smithsonian Astrophysical Observatory in 1955, oversees the research of more than 55 scientists engaged in the study of stellar interiors, the upper atmosphere, meteoritics, celestial mechanics, geodesy, and related fields. He also directs SAO's field programs, including the 12 astrophysical observing stations, the Prairie Network, and the Radio Meteor Project.

Dr. Whipple attended Occidental College and received the A.B. and Ph. D. degrees from the University of California in 1927 and 1931, respectively. Before joining the staff of the astronomy department at Harvard University in 1931, he held various teaching and research appointments at the University of California, Stanford University, and Lick Observatory.

Dr. Whipple's previous affiliations also include the chairmanship of the Department of Astronomy, Harvard University, 1949 to 1956; the chairmanship of the Committee on Concentration in the Physical Sciences, Harvard University, 1947 to 1949; and research associate, Radio Research Laboratory, 1942 to 1945, in charge of the development of an antiradar device. He is currently Professor of Astronomy at Harvard University.

Dr. Whipple is the recipient of two presidential commendations: the Presidential Certificate of Merit for the development of "Confusion Reflectors" used extensively in World War II, and the Distinguished Federal Civilian Service Award for the conception and development of an optical satellite-tracking system.

His own research has resulted in the development of methods to measure photographically the speeds and decelerations of meteors and to compute the orbits of comets and asteroids, and in the conception of the "dirty snowball theory" to explain the nature of comets. Other areas of investigation include interplanetary dust, the moon, and the origin of the solar system.

RICHARD B. SOUTHWORTH received the B.A. degree from Swarthmore College in 1950, and the M.A. and Ph.D. degrees from Harvard University in 1960 and 1961, respectively.

Prior to his association with SAO, Dr. Southworth held research assistantships at Massachusetts Institute of Technology and Harvard College Observatory.

His investigations at SAO since his appointment as staff physicist in 1961 cover meteors, comets, and the zodiacal cloud.

CARL S. NILSSON received the B.Sc. and Ph.D. degrees from the University of Adelaide, Australia, in 1955 and 1963, respectively.

Before joining the staff at SAO, Dr. Nilsson was a research associate at the Goddard Space Flight Center, Maryland.

Since he came to SAO in 1966, his work has been directed toward problems in total flux of extraterrestrial material into the earth's atmosphere and the orbital distributions of the meteors in the solar system. He is also principal investigator for micrometeoroid experiments on the OGO-2 and OGO-D satellites.

NOTICE

This series of Special Reports was instituted under the supervision of Dr. F. L. Whipple, Director of the Astrophysical Observatory of the Smithsonian Institution, shortly after the launching of the first artificial earth satellite on October 4, 1957. Contributions come from the Staff of the Observatory.

First issued to ensure the immediate dissemination of data for satellite tracking, the reports have continued to provide a rapid distribution of catalogs of satellite observations, orbital information, and preliminary results of data analyses prior to formal publication in the appropriate journals. The Reports are also used extensively for the rapid publication of preliminary or special results in other fields of astrophysics.

The Reports are regularly distributed to all institutions participating in the U. S. space research program and to individual scientists who request them from the Publications Division, Distribution Section, Smithsonian Astrophysical Observatory, Cambridge, Massachusetts 02138.